THESIS FOR THE DEGREE OF DOCTOR OF PHILOSOPHY

Complete methane oxidation over alumina and zeolite supported palladium for emission control

IDA FRIBERG

Department of Chemistry and Chemical Engineering

CHALMERS UNIVERSITY OF TECHNOLOGY

Gothenburg, Sweden 2020

Complete methane oxidation over alumina and zeolite supported palladium for emission control
Ida Friberg

ISBN 978-91-7905-305-5

Doktorsavhandlingar vid Chalmers tekniska högskola
Ny serie nr. 4772
ISSN 0346-718X

Department of Chemistry and Chemical Engineering
Chalmers University of Technology
SE-412 96 Gothenburg
Sweden
Telephone + 46 (0)31-772 1000

Printed by Chalmers Reproservice
Gothenburg, Sweden 2020

Complete methane oxidation over alumina and zeolite supported palladium for emission control

Ida Friberg

Department of Chemistry and Chemical Engineering
Chalmers University of Technology, Gothenburg 2020

Abstract

The use of methane-based fuels, such as natural gas and biogas, gives lower emissions of for instance carbon dioxide (CO_2) and particulate matters compared to traditionally used liquid fossil fuels. However, the exhaust gases contain significant levels of unburnt methane (CH_4) residuals, which are desirable to minimize since CH_4 has a high global warming potential. This can be accomplished by completely oxidizing the CH_4 remains to CO_2 and water using a catalytic converter. Palladium-based catalysts provide high CH_4 oxidation activity, however, low temperatures and exposure to deactivating compounds, such as water vapor and sulfur dioxide (SO_2), are challenging. It is however possible to optimize the catalytic properties by a careful selection of the support material which the palladium (Pd) is dispersed upon. Therefore, Pd supported on different materials, more specifically zeolites, alumina (Al_2O_3) and barium (Ba) promoted Al_2O_3, have been investigated in this thesis under various conditions using catalytic activity measurements combined with detailed characterization.

The results show that zeolite supported Pd is a promising candidate for the future CH_4 oxidation catalyst. The use of zeolites with high silicon content significantly improved the CH_4 oxidation activity in the presence of water vapor, which is ascribed to limited hydroxyl formation on the hydrophobic zeolite surface. In addition, the formation of ion-exchanged Pd^{2+} species is minimized in zeolites with low aluminum content. The formation of ion-exchanged Pd^{2+} species and Pd sintering appear to be important deactivation routes of Pd/zeolites, especially upon treatment at high temperatures and in the presence of water vapor. Zeolite supported Pd is also generally sensitive to SO_2, however, the regeneration after SO_2 poisoning is easier compared to for Pd/Al_2O_3. Hence, two major challenges for Pd/zeolite materials are stabilization of dispersed Pd particles and sulfur poisoning.

The catalytic properties can be altered by the addition of promoters, which was tested by adding Ba to Pd/Al_2O_3. It was found that a content of up to 2 wt.% Ba in Pd/Al_2O_3 does not provide electronic promotion of the Pd, however, the Ba addition improves the catalytic activity in the presence of water vapor and facilitates regeneration after water deactivation.

Whilst methane oxidation typically is tested under lean conditions, it was here also evaluated under stoichiometric and rich conditions for Pd/Al_2O_3. The presence of water vapor and SO_2 caused substantial deactivation under stoichiometric conditions. Treatment of Pd/Al_2O_3 under rich conditions resulted in severe deactivation, due to reduction of active PdO into less active metallic Pd. Regeneration under stoichiometric conditions was difficult due to poor Pd re-oxidation.

Keywords: *methane oxidation, water deactivation, sulfur poisoning, regeneration, hydrothermal aging, stoichiometric, Pd/zeolite, Pd/Al_2O_3, Ba*

Acknowledgements

This work is performed at Chemical Engineering and Competence Centre for Catalysis, Chalmers University of Technology, Gothenburg, Sweden, during the period August 2015 to June 2020.

The Swedish Research Council is gratefully acknowledged for the financial support. The Swiss Light Source (SLS) at the Paul Scherrer Institute is gratefully acknowledged for the granted beamtime at the SuperXAS beamline.

I would also like to thank:

My main supervisor Louise Olsson for all your encouragement, support and understanding. I am grateful to have been given the opportunity of doing my PhD in your research group and for the independence and freedom I had in my work.

My co-supervisor Nadezda Sadokhina for all your guidance, help, patience, especially when I was a new PhD student, and all fun moments we have had together.

Davide Ferri, Oliver Kröcher, Maarten Nachtegaal and all co-workers at the Paul Scherrer Institute (PSI) for the warm welcome and for making my time in Switzerland enjoyable. I would also like to thank you for the help with my experiments and the things I learnt during my visit.

My office mates: Kunpeng, Xavier and Rojin, for all the discussions and everyday fun at the office.

Stefan Gustafsson, Ludvig De Knoop and Lars Ilver for your help with TEM and XPS measurements.

Malin Larsson, Anna Oskarsson, Mattias Zetterberg and Ximena Rozo Sevilla for your help with the administrative and practical work at the division.

Lasse Urholm and Lennart Norberg for all your help in the reactor lab.

My current and past co-workers at KCK and KART for all fun, discussions and valuable advices in the labs.

All my friends, within and outside of Chalmers, for being there for me and for the great times we have shared.

Lastly, a very special thanks to my family and Fredrik for being supportive of me. This would never have been possible without you.

List of publications

I. The effect of Si/Al ratio of zeolite supported Pd for complete CH_4 oxidation in the presence of water vapor and SO_2
I. Friberg, N. Sadokhina, L. Olsson
Applied Catalysis B: Environmental 250 (2019) 117-131.

II. Structure and performance of zeolite supported Pd for complete methane oxidation
I. Friberg, A. H. Clark, N. Sadokhina, G. J. Smales, J. Woo, X. Auvray, D. Ferri, M. Nachtegaal, O. Kröcher, L. Olsson
Submitted

III. Hydrothermal aging of Pd/LTA monolithic catalyst for complete CH_4 oxidation
I. Friberg, A. Wang, L. Olsson
Catalysts 10 (2020) 517.

IV. Complete methane oxidation over Ba modified Pd/Al_2O_3: The effect of water vapor
I. Friberg, N. Sadokhina, L. Olsson
Applied Catalysis B: Environmental 231 (2018) 242-250.

V. Deactivation of Pd based catalysts for methane oxidation under rich, stoichiometric and lean conditions
I. Friberg, N. Sadokhina, L. Trandafilovic, G. Smedler, U. Nylén, M. Olofsson, L. Olsson
In manuscript

Contribution report

Paper I

I synthesized the catalyst samples, performed the catalyst characterization (except for STEM and ICP), conducted the flow reactor experiments, interpreted the results together with my co-authors and was responsible for writing the manuscript.

Paper II

I synthesized the catalyst samples, participated in XAS data collection, performed other catalyst characterization (except for SAXS, STEM and ICP), interpreted the results together with my co-authors and was responsible for writing the manuscript.

Paper III

I synthesized the catalyst samples (except for zeolite synthetization), performed the catalyst characterization (except for XRD, STEM and ICP), conducted the flow reactor experiments, interpreted the results together with my co-authors and was responsible for writing the manuscript.

Paper IV

I synthesized the catalyst samples, performed the catalyst characterization (except for STEM and ICP), conducted the flow reactor experiments, interpreted the results together with my co-authors and was responsible for writing the manuscript.

Paper V

I was responsible for writing the manuscript and interpreted the results together with my co-authors.

List of abbreviations

BBU	Basic Building Unit
BET	Brunauer, Emmet and Teller
BJH	Barrer, Joiyner and Halenda
CBU	Composite Building Unit
CEM	Controlled Evaporator and Mixer
DRIFTS	Diffuse Reflectance Infrared Fourier Transform Spectroscopy
EDX	Energy Dispersive X-ray Spectroscopy
EXAFS	Extended X-ray Absorption Fine Structure
FT	Fourier Transform
FTIR	Fourier Transform Infrared Spectroscopy
HC	Hydrocarbon
ICP-SFMS	Inductively Coupled Plasma Sector Field Mass Spectrometry
IR	Infrared
LCF	Linear Combination Fitting
MFC	Mass Flow Controller
MS	Mass Spectrometer
QEAXFS	Quick-EXAFS
SAR	Silica to Alumina Ratio (molar ratio SiO_2/Al_2O_3)
SAXS	Small-Angle X-ray Scattering
SDA	Structure Directing Agent
STEM	Scanning Transmission Electron Microscopy
TEM	Transmission Electron Microscopy
TPD	Temperature Programmed Desorption
TPO	Temperature Programmed Oxidation
TPR	Temperature Programmed Reduction
TWC	Three Way Catalyst
WAXS	Wide-Angle X-ray Scattering
XANES	X-ray Absorption Near Edge Structure
XAS	X-ray Absorption Spectroscopy
XPS	X-ray Photoelectron Spectroscopy
XRD	X-ray Diffraction

Contents

1 Introduction

1.1 Catalytic emission control

Energy obtained from combustion of different fuels is a cornerstone in maintaining the high standard of today's modern society, both when it comes to transportation, heating and industrial production. However, the generated exhaust gases contain air pollutants, which negatively influence both the local and the global environment. The major pollutants include carbon monoxide (CO), nitrous oxides (NO_x), hydrocarbons (HC), sulfur oxides (SO_x) and particulate matters (PM). Exhaust gas after treatment with catalytic converters is one main strategy to reduce the emissions of these compounds. Currently used catalytic converters consist of a catalyst washcoated honeycomb structured monolith, which converts toxic gases and pollutants into less harmful substances. The catalytic converter is typically placed near the engine's exhaust manifold and consists of multiple units with different functions. For the automotive sector, the three-way catalyst, with the feature to oxidize CO and HC as well as to reduce NO_x compounds, was launched in 1979 [1]. Today all newly produced passenger cars with combustion engines are equipped with catalytic exhaust gas after treatment units with increased complexity in order to meet the strict international emission standards.

1.2 Methane utilization and emission

The use of methane-based fuels, such as natural gas and biogas, has steadily grown during the last decades. The small-scale use of natural gas has been going on for a long time whereas the large-scale use started first in the end of the 1920s, when pressure-resistant pipelines of sufficiently high quality were developed and enabled for efficient transportation of the fuel. Natural gas is a fossil fuel which is extracted from the underground and is nowadays attractive amongst others due its relatively low market price. It contains about 75-98% methane (CH_4) together with smaller contents of for example nitrogen (N_2), ethane (C_2H_6) and carbon dioxide (CO_2) [2]. A more sustainable alternative to natural gas is biogas which is produced from a biological feedstock. Biogas typically contains 50-75% CH_4, 25-50% CO_2 and 2-8% of other gases such as water vapor, N_2, oxygen (O_2), ammonia (NH_3), hydrogen (H_2) and sulfur compounds. To facilitate the usage of biogas it can be upgraded to biomethane which has the same standard as natural gas and can be used in the same applications [3]. It is also possible to reduce the net carbon emissions by partially mix the fossil natural gas with biogas-based fuel. Furthermore, the use of biogas can be facilitated by utilizing the existing infrastructure of

natural gas. A significant advantage by shifting to CH_4-based fuels from the traditionally used liquid fossil fuels, *i.e.* diesel and gasoline, is that the low C/H ratio of the CH_4 molecule results in approximately 20% lower CO_2 emissions compared to an equivalent gasoline car [2]. The combustion of natural gas also generates exhaust gases with lower levels of CO, NO_x, SO_x, non-methane HC and PM compared to diesel and gasoline [2, 4]. It should also be noted that the potential generation ground-level ozone, as a secondary pollutant, is limited since the highly stable CH_4 molecule is less prone to react with NO_x to form ozone compared to non-methane HC [2]. The major pollutant generated from natural gas combustion is unburned CH_4 residuals. The atmospheric concentration of CH_4 increased during the 20th century, and despite the fact that the level has been close to constant during the last two decades it is still around 150% higher than the pre-industrial levels in 1750 [5]. Although the average residence time of a CH_4 molecule in the atmosphere is relatively short, approximately 10-12 years [2, 5], the global warming potential of CH_4 is ca. 28 times higher than CO_2 over a period of 100 years [5]. Thus, the negative environmental impact of for instance natural gas vehicles can be significantly reduced by removing the remains of unburnt CH_4 from the exhaust gases. This can be accomplished by complete oxidation of the CH_4 to CO_2 and H_2O. To realize this in practice, a catalytic converter is required since the concentration of the remaining CH_4 (ca. 400-1500 ppm [6]) and the temperature (ca. 450-550°C [6]) are not high enough for this reaction to occur spontaneously with a desired rate.

Catalysts for complete CH_4 oxidation are typically composed of palladium (Pd) supported on porous metal oxides with high surface areas, such as γ-Al_2O_3. However, since the CH_4 molecule is the smallest of all hydrocarbons, it has the highest activation energy barrier for breakage of C-H bond. Consequently, high temperatures are required to oxidize the CH_4, but the simultaneous development of more efficient combustion engines will likely result in lower temperatures of the generated exhaust gases. This results in a demand of catalytic materials which are efficient for CH_4 abatement at low temperatures. Another challenge is to maintain high activity in the presence of catalyst poisons and deactivating compounds. Although Pd/Al_2O_3 provides high CH_4 oxidation activity in the absence of catalyst poisons under laboratory conditions, the CH_4 conversion drops significantly when exposed to real exhaust gases containing water vapor [6] and sulfur compounds [7]. The water vapor, which constitutes ca. 10-15% of the exhaust gases generated from natural gas combustion [6], is produced in the CH_4 combustion reaction and is therefore inevitable. Sulfur compounds are only present as traces in the exhaust gases, however, even tiny amounts of sulfur can result in severe deactivation of Pd-based catalysts [7]. Consequently, it is important, to design the catalyst so that it can maintain high activity also in the presence of pollutants, like water vapor and sulfur.

1.3 Objectives

The objective of this thesis is to provide knowledge and understanding of the complex relations between the many underlying factors influencing the performance of Pd-based CH_4 oxidation catalysts. The work has especially focused on the properties of the support material, the exposure to deactivating compounds and the catalytic performance under various conditions.

The possibility to substitute the traditionally used Al_2O_3 support with different types of zeolites was investigated in **Paper I**-**III**. The main objectives of **Paper I** and **Paper II** were to correlate the catalytic activity to different types of Pd species and to the exposure to water vapor and SO_2. **Paper III** concerns hydrothermal aging of zeolite supported Pd and how this impacts the performance. The possibility to enhance the CH_4 oxidation activity in the presence and absence of water vapor by an addition of Ba promotor to Pd/Al_2O_3 was examined in **Paper IV**. Finally, the aim of **Paper V** was to investigate stoichiometric CH_4 oxidation in the presence of water vapor and SO_2. Various characterization techniques have been applied in combination with catalytic activity measurements in order to investigate the complex relation between the CH_4 oxidation activity, the palladium and the support material under different thermal and gaseous conditions.

2 Heterogeneous catalysis for complete CH_4 oxidation

The terms "*catalysis*" and "*catalytic force*" were presented by J.J. Berzelius already in 1835. However, the major knowledge and understanding of catalysis have been acquired during the last century, amongst many reasons due to the development of various advanced experimental techniques, such as spectroscopic techniques, and lately also computational methods. A catalyst increases the rate of reaction by providing an alternative reaction path with lower activation energy compared to the uncatalyzed reaction, without being consumed itself. The change in free energy is the same with and without catalyst. Hence, the catalyst has no impact on the thermodynamics but only on the kinetics of the reaction. Catalysis can be divided into three sub-groups, namely homogenous, heterogenous and bio catalysis. Bio catalysis referrers to biological reactions which are accelerated by biocatalysts, commonly enzymes. Catalytic processes where both the catalyst and the reactants are of the same phase, *i.e.* gas, liquid or solid, are called homogenous catalysis and the opposite to this is denoted heterogenous catalysis. Homogenous catalysis is commonly encountered in many industrial processes for chemical production. Heterogenous catalysis is also common within chemical process industry and one famous example of heterogenous catalysis is the Haber-Bosch process for the production of NH_3 from N_2 and H_2 [1]. Another category of heterogenous catalysis is environmental catalysis for exhaust gas cleaning, recognized as catalytic converters in the exhaust outlet of engines and combustion units. This category includes for instance selective catalytic reduction (SCR) of NO_x, diesel oxidation catalysts (DOC) for oxidation of CO, HC, PM and NO and CH_4 oxidation catalysts. The latter is used for CH_4 abatement of the exhaust gases generated from combustion of CH_4-based fuels and aims to oxidize the unburnt residuals of CH_4, according to the following reaction:

$$CH_4 + 2O_2 \rightarrow CO_2 + 2H_2O$$

Exhaust gases from a typical natural gas vehicle contain around 400-1500 ppm CH_4, 10-15% H_2O and 15% CO_2 and have temperatures of approximately 450-550˚C [6]. The goal of using a CH_4 oxidation catalyst is to oxidize as much as possible of the CH_4 under these conditions, but also to oxidize as much as possible during the warm-up of the catalyst.

2.1 Catalyst formulations

Heterogeneous catalysts for exhaust gas after treatment are typically composed of nanoparticles of a catalytically active metal distributed on a support material with high surface area. However, zeolite-based materials, where the active metal is ion-exchanged with zeolite framework, are also common. The most thoroughly investigated catalytic system for CH_4 abatement is palladium supported on alumina, *i.e.* Pd/Al_2O_3. However, numerous combinations of noble metals, promoters, additives and support materials have been investigated over the years.

2.1.1 Noble metals

Palladium has the highest activity for complete CH_4 oxidation [6], hence Pd-based catalysts are the most commonly investigated catalytic system for this purpose. Under lean conditions, *i.e.* in O_2 excess, the active phase for CH_4 oxidation is PdO or PdO-Pd at moderate temperatures [8-11] and metallic Pd at high temperatures [12]. In diluted O_2, PdO is stable at temperatures up to around 700-800˚C, where it decomposes into metallic Pd [13, 14]. However, the PdO reduction is easier accomplished when CH_4 is admixed [15]. The CH_4 oxidation over Pd catalysts has commonly been described with kinetic models based on the Langmuir-Hinshelwood-Hougen-Watson [16-19] or the Mars-van Krevelen [20-22] rate expressions in the literature, although the exact mechanism is uncertain. The abstraction of the first hydrogen atom from the CH_4 molecule, *i.e.* C-H activation, is considered to be the rate limiting step under lean conditions in the absence of water vapor [23, 24].

In addition to palladium, platinum-based catalysts have been extensively investigated for CH_4 oxidation. Under lean conditions, Pd-based catalysts provide higher CH_4 oxidation activity than platinum-based catalysts [25-27]. Platinum-based catalysts have been shown to have an advantage for CH_4 oxidation under rich conditions, *i.e.* O_2 deficient conditions [26], and are normally preferred for the oxidation of higher HC [28]. Many research studies concern CH_4 oxidation over bi-metallic PdPt catalysts. However, although it has been observed that PtPd catalyst can provide higher CH_4 oxidation activity than mono-metallic Pd catalysts [29, 30], several authors have also reported the opposite or a more complex relation between Pt promotion and the CH_4 oxidation activity [13, 30-32]. Nevertheless, it appears that an addition of Pt may be beneficial to maintain higher CH_4 oxidation activity over time [29, 30] and after various aging procedures [32, 33] as well as to mitigate noble metal sintering [29, 34, 35] and deactivation by SO_2 poisoning [36]. However, some uncertainty regarding this bi-metallic systems may have arisen from the use of different Pt/Pd ratios, which highly influences the catalytic properties [31, 32].

2.1.2 Support materials

Metal oxides

Most commonly, different kind of metal oxides with high surface areas are used as support materials for CH_4 oxidation catalysts. One of the most extensively investigated support materials is γ-Al_2O_3 [25, 37, 38], which is stable at temperatures up to around 1000˚C [39]. The support material is not inert but on the contrary it highly influences the catalytic performance.

As an example of the influence from the Pd-support interactions, supports with higher basicity yield larger PdO/Pd ratio [40, 41]. It is suggested that supports with moderate acidity provides the optimal PdO/Pd ratio for CH_4 oxidation [41]. Support materials with high oxygen storage capacity facilitate the PdO formation and therefore also the CH_4 oxidations activity [9]. Furthermore, several literature reports have shown that the choice of support has a crucial effect on tolerance to water vapor [6] and sulfur compounds [7]. Therefore, support modification, either by using completely different materials in terms of structure and composition or by adding promoters, is a strategy that can be employed in order to obtain desired catalytic properties. This have resulted in numerous studies concerning alternative support materials for Pd-based CH_4 oxidation catalysts, for example other metal oxides, such as ZrO_2, CeO_2 and SiO_2, zeolites and perovskites [6, 25, 28, 37, 38].

Zeolites

Aluminosilicates zeolites are three-dimensional frameworks composed out of Al, Si and O atoms. The basic building units (BBU) are TO_4 tetrahedrons, where the central T-atom is either Al or Si. The BBU:s are assembled into polyhedral composite building units (CBU) via shared oxygen atoms. The entire zeolite framework is then periodically constructed out of the specific CBU:s. The faces of the CBU:s consist of rings with n T-atoms (n-rings) and are normally referred to as pores, or more specifically cages for $n \leq 6$ or cavities for $n > 6$ and the cavities with infinite extension are denoted channels [42]. Moreover, depending on the size of the cavities and channels, the zeolite frameworks are divided into narrow pore (n=8), medium pore (n=10) and wide pore (n=12) zeolites, with crystallographic diameters of 0.35-0.45, 0.45-0.60 and 0.60-0.80 nm, respectively [43]. The alumina BBU, *i.e.* AlO_4, has a negative net charge which is balanced out by a cation. When the cation is a proton (H^+), this is a Brønsted acid site. It is also common with for instance alkali metal ions. However, the cation is mobile and can be ion-exchanged with another cation [43]. Examples of zeolites often used in environmental catalysis are ZSM-5, beta, SSZ-13, SAPO-34, zeolite Y, LTA and mordenite.

One of the most important structural parameters for the zeolite framework is the SiO_2/Al_2O_3 ratio (SAR). An increased SAR of the zeolite framework is reflected by lower acidity, ion-exchange capacity and cation concentration as well as higher hydrophobicity and thermal stability [43]. For zeolite supported Pd, an increased SAR results in enhanced tolerance to water vapor due to the high hydrophobicity of the zeolite, formation of larger Pd particles as a result of lower acidity [44] and less ion-exchanged Pd^{2+} species [45].

Highly siliceous zeolites can be produced using post-synthesis dealumination methods, since the range of SAR, which is possible to obtain via direct synthesis, often is limited. Commonly used dealumination methods are hydrothermal dealumination, alumina extraction by chemical agents and substitution of alumina framework with silicon. The suggested pathway for extraction of alumina with acids is shown in Figure 2.1. [46]. Using this method, different degree of dealumination can be obtained by adjusting the time, temperature, pH and type of acid [47-52], although also the type of zeolite framework and synthesis conditions influence how easily the zeolite can be dealuminated [50]. However, extensive dealumination may result in loss of thermal stability, crystallinity, and other structural defects [46].

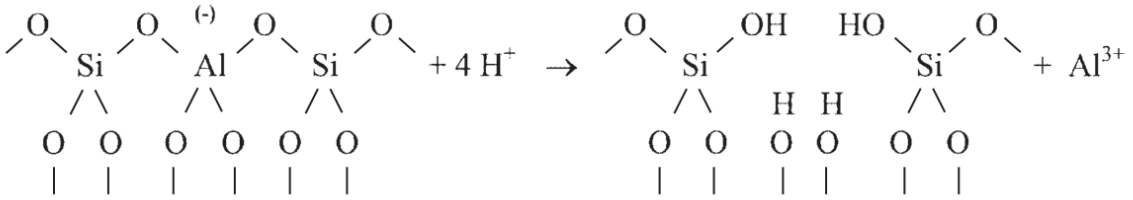

Figure 2.1. Suggested pathway for dealumination of zeolites with acids. Image from Beyer [46].

2.1.3 Promoters

In general, there are two groups of promoters: structural and electronic promoters. The structural promoters serve as dispersion enhancers for the metal particles [53] whereas the electronic promoters alter the chemisorptive bond strength of adsorbents by virtue of electron density modifications of the active metal surface, electrostatic interactions and/or blockage of surface sites [54-58]. Alkali and alkaline earth metals are commonly employed as electropositive promoters in catalysts for reactions which benefit from the increased chemisorptive bond strength between the electronically promoted metal surface and electro accepting adsorbents (*e.g.* oxygen and carbon monoxide) and/or the weakened bond strength for electro donating adsorbents (*e.g.* hydrogen) [53, 58]. For instance, there are several examples in the literature where an addition of alkali /alkaline earth metals promoters to Pd based catalysts has been reported to increase the PdO/Pd ratio and result in higher stability of the PdO [59-63].

2.2 Catalyst deactivation

Loss of activity and/or selectivity is referred to as catalyst deactivation and can result from either mechanical, chemical or thermal processes. There are two types of mechanical deactivation: fouling and attrition/crushing. The former one refers to the deposition of gaseous compounds onto the catalyst surface, which potentially can cause pore blockage and/or entire or partial encapsulation of the active metal particles and the latter one is a result of physical abrasion resulting in loss in catalytic material [64]. One example of fouling is surface coke formation, which occurs for instance when Pd-based catalysts are provided with CH_4 in the absence of O_2 at high temperatures [13, 14]. Moreover, there are three types of chemical deactivation mechanisms: poisoning, volatilization of catalyst material and formation of inactive catalytic material due to chemical reactions between solid-solid and/or solid-vapor compounds. The first mentioned, *i.e.* catalyst poisoning, is attributed to the chemisorption of gaseous compounds (catalyst poisons) resulting in loss of active sites and/or altered electron density or geometry. The second chemical deactivation process, volatilization of catalyst material, results from reactions between the catalyst material and certain compounds, which produce volatile species with resulting loss of catalytic material. Lastly, the third cause of chemical deactivation, is formation of inactive compounds due to reactions between of the catalytic material and solid or gaseous compounds. Treatment at high temperatures may result in thermal deactivation because of sintering of metal particles and support material and/or

transformation of the active catalyst into inactive material. The degree and rate of sintering is also highly influenced by other factors, such as gas composition, addition of promoters and type of metal/support material. For example, the presence of water vapor normally accelerates the sintering process [64].

2.2.1 Water deactivation

Water vapor, which typically constitutes around 10-15% of the exhaust gases from natural gas vehicles [6], is one of the major contributors to chemical deactivation of Pd-based catalysts for CH_4 oxidation. The exposure to water vapor results in formation of surface hydroxyls which cause the deactivation by (*i*) blockage of active PdO sites [65] and (*ii*) decreased surface oxygen mobility resulting in less Pd re-oxidation and consequently less PdO sites [66, 67]. The negative impact of water vapor on the catalytic activity is most pronounced at low temperatures and levels out at higher temperatures [65]. However, the catalytic activity can be completely or partly regenerated by water desorption from the catalyst surface at high temperatures [68-70]. Two water deactivation routes [17, 71] have been distinguished: (*i*) rapid formation of hydroxyls which cause an immediate deactivation and can be desorbed under mild conditions and (*ii*) slow formation of hydroxyls with higher energy barrier which result in accumulative water deactivation over time and are more difficult to desorb and therefore may require more complex regeneration treatments. Moreover, excess of O_2 has been reported to facilitate the hydroxyl formation [14], *i.e.* the water deactivation becomes more significant under lean conditions than under stoichiometric and rich conditions. The water deactivation of Pd-based materials can be mitigated by a careful selection of the support material, for instance highly hydrophobic zeolites [44] or other more complex zeolites [72, 73].

2.2.2 Sulfur poisoning

Next to water vapor, gaseous sulfur containing compounds is another group of catalyst poisons which significantly impedes the CH_4 oxidation over Pd-based catalysts. The SO_2 concentration prior to the catalyst unit is typically around 0.5-1 ppm and originate from the natural gas itself and/or from added odorants [74]. Although the SO_2 concentration is very low it is highly relevant since substantial deactivation occurs even at SO_2 concentrations less than 1 ppm [7]. Based on SO_2 and H_2S poisoning experiments, the main reason for the deactivation under lean conditions has been ascribed to the formation of surface sulfates [75-80]. It should be noted the deactivation mechanism is similar for H_2S and SO_2 under lean conditions, since H_2S easily converts to SO_2 under lean conditions [77, 78]. The simultaneous presence of water vapor and SO_2 results in formation of more $PdSO_4$, which thus accelerates the sulfur deactivation. The reason for this is decreased spill-over of sulfur species from the Pd to the support material and/or the opposite, increased spill-over from the support material to Pd [75, 81].

The type of support material highly affects the degree and rate of SO_2 poisoning and possibility to regenerate the catalytic activity. Lampert et al. [7] observed that Pd supported on sulfating support material, *i.e.* with high sulfur storage capacity such as Al_2O_3, have lower sulfur deactivation rate since the support material acts as a sulfur sink and thereby suppresses the

formation of $PdSO_x$ species. However, Pd supported on non-sulfating materials, *i.e.* with low sulfur storage capacity such as SiO_2, is easier to regenerate due to the low sulfur spill-over from the support material to the PdO [7].

Partial or complete regeneration of the catalytic activity after sulfur poisoning is however possible by thermal decomposition of the formed sulfur species at high temperatures [7, 74]. Arosio et al. [74] observed partial regeneration of Pd/Al_2O_3 under lean conditions at temperatures from 750˚C and complete regeneration was observed after treatment at 900˚C. This is similar to the results from Lampert et al. [7], where a small sulfur release from the Pd/Al_2O_3 was recorded under lean conditions at 650˚C but most sulfur remained. However, Arosio et al. [74] also observed a markedly enhanced regeneration in rich gas feed, as the Pd/Al_2O_3 then could be partially regenerated already at 550˚C and close to complete regeneration was obtained at 600˚C. According to these findings, rich conditions and high temperatures provide the highest degree of sulfur regeneration.

2.2.3 Hydrothermal aging

The simultaneously exposure to high temperatures and water vapor during a longer period is often referred to as hydrothermal aging. Hydrothermal aging typically changes the catalytic performance due to deactivation by one or several mechanisms. Sintering of the active metal and/or the support material is common as it generally is accelerated at high temperatures and in the presence of water vapor [64]. For zeolite supported Pd, hydrothermal aging has been reported to facilitate the formation of ion-exchanged Pd species [82, 83]. Different support materials show different tolerance to hydrothermal aging. γ-Al_2O_3 is stable up to around 1000°C whereas it transforms into other alumina phases at higher temperatures [39]. The hydrothermal stability of zeolites depends on the structure and composition. Hydrothermal aging of zeolite-based catalysts may result in dealumination, *i.e.* Al migration from the zeolite framework, and structural collapse [84, 85]. Zeolite SSZ-13 is known to have high hydrothermal stability [84, 85] and has consequently been extensively investigated, above all for SCR applications. However, it has recently been shown that zeolite LTA provides even higher hydrothermal stability [86, 87] and is therefore a good option for future catalytic support material.

3 Experimental section

3.1 Catalyst synthesis

3.1.1 Palladium deposition on supports

The palladium was deposited on the support materials by impregnation with diluted Pd precursor solution. For **Paper I-III** and **Paper V**, the Pd was added to the support material using the incipient wetness impregnation method whereas the samples used in **Paper IV** were prepared by the wet impregnation method accompanied by freeze drying.

Incipient wetness impregnation method (Paper I-III and Paper V)

For this method, the impregnation was performed using the volume of Pd precursor and solvent (water) equal to the total pore volume of the support material. The impregnation solution was prepared from $Pd(NO_3)_2$ precursor and a proper volume of milliQ water. The solution was added dropwise to the support material (Al_2O_3 or zeolite) and was thereafter divided evenly with a spatula. Subsequently, the wet catalyst powder was dried in an oven at 80˚C overnight, followed by calcination at 550˚C for 2 h. Note that the samples in **Paper I-II**, had a Pd loading of 1 wt.% and the samples in **Paper III-IV** and **Paper V** were loaded with 2 wt.% and 3.8 wt.% Pd, respectively.

Wet impregnation method (Paper IV)

For this method, an excessive volume of solvent (water) was used for the impregnation. More detailed, this was accomplished by first suspending the support powder (Al_2O_3) in milliQ water. The pH of the slurry was adjusted to 4 with dilute HNO_3 followed by addition of the Pd precursor, *i.e.* aqueous $Pd(NO_3)_2$. The pH was thereafter adjusted and stabilized at 2. Subsequently, the entire slurry was frozen with liquid nitrogen and dried under vacuum for a prolonged period to ensure complete sublimation of the water. The dry powder was calcined for 2 h at 550˚C in oven. Note that a Pd loading of 2 wt.% was used for the samples prepared with this method in **Paper IV**.

3.1.2 Addition of Ba promoter

Three promoted Pd/Al_2O_3 samples, studied in **Paper IV**, were doped with 0.5, 1 and 2 wt.% Ba, respectively. The proper amount of $Ba(acetate)_2$ was dissolved in milliQ water and added

to an agitated suspension of as prepared Pd/Al_2O_3 (2 wt.% Pd) and milliQ water. The pH was stabilized at around 8 using weak NH_3 solution. Finally, the slurries were frozen with liquid nitrogen and dried under vacuum using a freeze drier. The Ba promoted Pd/Al_2O_3 powders were thereafter calcined at 550˚C for 2 h.

3.1.3 Preparation of support materials

γ-Al_2O_3 support

For the samples in **Paper IV** and **Paper V**, Al_2O_3 was used as support material. However, Pd/Al_2O_3 was also included as a reference sample in **Paper I** and **Paper III**. The Al_2O_3 powder was pre-calcined at 700˚C for 2 h prior to Pd deposition, with exception for **Paper V** where the calcination temperature was 900°C.

SSZ-13 support

The zeolite H-SSZ-13 supports, used for **Paper I-II**, were synthesized from zeolite H-Y under basic conditions and at high pressure based on the method described by McEwen et al. [88] and Olsson et al. [89]. Concisely, a mixture containing dilute NaOH, sodium silicate solution, powder of zeolite H-Y and structure directing agent (SDA) TMAAI (tricyclo[3.3.1.13,7]decan-1-aminium,N,N,N-trimethyl-,hydroxide) were evenly stirred at room temperature before it was divided into Teflon-lined autoclaves. The autoclaves were transferred into a 140˚C oven and kept under those conditions for 6 days. The autoclaves were thereafter cooled down to room temperature. A centrifuge was used to separate the liquids from the solids and to thoroughly wash the solids with milliQ water. The powder was thereafter dried at room temperature followed by calcination for 8 h at 550˚C (heating ramp: 0.5˚C/min).

In total, two different batches of SSZ-13, with different SAR, were synthesized according to this procedure. For the first batch, zeolite H-Y (SAR=80) was used as supplied for the synthesis and for the second sample, dealuminated zeolite H-Y (see detailed description of the dealumination procedure below) was used in order to produce SSZ-13 with higher SAR. The final SAR of the synthesized SSZ-13 zeolites were 43 and 52, respectively. The incipient wetness method was applied to deposit 1 wt.% Pd on each of the two SSZ-13 supports.

Beta support

In total three different zeolite H-beta supports, with SAR of 40, 511 and 969, were prepared and studied for **Paper I-II**. The two latter beta supports with higher SAR were obtained by dealumination of commercial zeolite H-beta (see detailed description of the dealumination procedure below). The beta support with SAR=40 was calcined at 500˚C for 5 h in order to change from ammonia to hydrogen cationic form but otherwise used as supplied. A Pd loading of 1 wt.% was deposited with the incipient wetness impregnation method on each of the beta supports.

LTA support

The LTA support used in **Paper III** was synthesized according to the procedure described by Wang et al. [86]. Briefly, the SDA was synthesized from 1,2-dimethyl imidazole, 4-methylbenzyl chloride and chloroform. After synthesis an anion-exchange resin was used to convert the SDA into its hydroxide form. The zeolite synthesis was made from a gel consisting

of SDA, tetramethylammonium hydroxide, HF, SiO_2, Al_2O_3 and H_2O which after preparation was put in an agitated Teflon-lined autoclave at 175°C for 96 h. Finally, the zeolite was dried and calcined in air at 100°C and 600°C, respectively [86].

Zeolite dealumination

Zeolite supports with high SAR were prepared by extracting parts of the alumina from the zeolite framework with oxalic acid. In brief, the zeolite powder was added to a 3 M or 1.5 M oxalic acid solution at 70˚C during vigorous agitation. The slurry was kept under those conditions for 16 h or 7 days. Thereafter, the liquid phase was separated by centrifugation and the zeolite powder was washed multiple times with milliQ water followed by drying at 80˚C in an oven. Possible traces of remaining oxalic acid were removed thermally by 5 h of calcination at 500˚C.

Two dealuminated samples were prepared from zeolite H-beta (original SAR = 300). For both cases, 3 M oxalic acid solution was used and the dealumination time was 16 h or 7 d which resulted in final SAR of 511 and 969, respectively. The SSZ-13 zeolite was not dealuminated as synthesized, but instead was zeolite H-Y (original SAR = 80) dealuminated in 1.5 M oxalic acid solution for 16 h prior to the synthesis of zeolite SSZ-13. The SSZ-13 synthesis procedure was otherwise identical to the description above.

3.1.4 Monolith washcoating

All catalyst powders were washcoated onto cordierite honeycomb monoliths prior to catalytic activity test in the flow reactor. Boehmite binder (γ-AlO(OH)) was used to improve the adherence of the washcoat. The washcoat slurries used for **Paper I-III** were prepared with 90 wt.% liquids (1:1 ethanol to water) together with 10 wt.% solids (1:19 binder to catalyst powders). The weight of washcoat applied on the monoliths (Ø=15 mm, L=20 mm, 400 cpsi) was 300 ± 5 mg and 250 ± 5 mg washcoat for **Paper I-II** and **Paper III**, respectively. For the samples in **Paper IV**, the washcoat slurries consisted of 80 wt.% liquids (1:1 ethanol to water) together with 20 wt.% solids (4:1 catalyst powder to binder) and 500 ±10 mg of washcoat was applied on each monolith (Ø=21 mm, L=20 mm, 400 cpsi). The same washcoat slurry proportions were used for **Paper V**, however smaller monoliths were used (Ø=15 mm, L=20 mm, 400 cpsi) and the weight of applied washcoat was 300 ± 5 mg.

The washcoating procedure was the same for all studies. The monoliths were dipped into the agitated washcoat slurry followed by drying at 90˚C during continuous rotation, to ensure equally divided washcoat layers. This was repeated several times until the desired washcoat loading was reached. Subsequently, the washcoated monoliths were calcined for 2 min at 500˚C (600°C for **Paper V**) with heat gun and for 2 h at 500˚C (600°C for **Paper V**) in a muffle oven.

3.2 Characterization methods

3.2.1 N_2 physisportion

The surface area and pore volume of solids, such as supported catalysts, are commonly estimated by physisorption measurements, typically using N_2 or other inert gases. The specific

surface area of the solid can be calculated using the BET-method which was introduced in 1938 by Brunauer, Emmett and Teller [90]. The BET-equation (1) describes the volume of the first monolayer (V_0) in relation to the adsorbate volume (V_a), and the relative pressure (ratio of the equilibrium pressure to the saturation pressure of the adsorbate, P/P_0).

$$\frac{P}{V_a(P_0-P)} = \frac{1}{cV_0} + \frac{(c-1)}{cV_0}\frac{P}{P_0} \quad (1)$$

The straight line obtained by plotting $P/V_a(P_0-P)$ against P/P_0 enables determination of V_0 from the slope $(c-1)/cV_0$ and the y-axis intersection $1/cV_0$. The BET method is based on a number of assumptions: (*i*) equal adsorption and desorption rate for all layers, (*ii*) the adsorption sites are equivalent in the first monolayer, (*iii*) the adsorptions sites of the molecules in the $(n+1)^{th}$ layer are the molecules in the n^{th} layer, (*iv*) there are no interactions between the adsorbates, (*v*) the conditions for adsorption and desorption are the same for all layers $n>1$, (*vi*) the adsorption energy equals the condensation energy for all layers $n>1$ and (*vii*) $n\rightarrow\infty$ when $P=P_0$, *i.e.* at the saturation pressure [1]. This method provides a good estimation of the surface area for macroporous[1] and many mesoporous[2] materials but is misleading for microporous materials[3] [91], such as many zeolites, since such small pore volumes limit the multi-layer formation and results in capillary condensation [1, 92]. Nevertheless, BET surface measurements of zeolite-based materials are anyway frequently reported in the literature for comparative reasons, but these should not be interpreted as the physical surface area but rather to be proportional to the pore volume [92].

Commonly used methods for pore size estimation based on physisorption data are the method presented by Barrer, Joiyner and Halenda (BJH method) and the t-plot method. The BJH method is suitable for pore size estimation of mesoporous materials as it accounts for capillary condensation based on the Kelvin equation. The t-plot method can be used to determine the volume of micropores based on the plot of V_a against the statistical thickness t of the adsorbed layer [91].

A TriStar 3000 instrument was used to measure the N_2 physisorption used to estimate the surface area and pore size volume in **Paper I** and **Paper III**. All samples were degassed in N_2 at 240˚C for 4 h prior to the measurement.

3.2.2 Inductively coupled plasma sector field mass spectrometry (ICP-SFMS)

The elemental composition of the samples used in **Paper I-III** was analyzed with ICP-SFMS in order to determine the SAR and the content of Pd and Na. In this method, inductively coupled plasma is used to ionize the sample, which compositions thereafter is qualitatively and quantitatively determined with high accuracy using a mass spectrometer (MS). The ICP-SFMS analysis was performed by ALS Scandinavia.

[1] Macroporous: pore diameter > 50 nm
[2] Mesoporous: 2 nm < pore diameter < 50nm
[3] Microporous: pore diameter < 2 nm

3.2.3 Temperature programmed reduction (TPR) and oxidation (TPO)

The temperature of reduction can be obtained by heating the pre-oxidized sample under reducing gas conditions, for example in diluted H_2 or CH_4. The temperature where the reducing agent is consumed corresponds to the temperature of reduction. The temperature of oxidation can be retrieved in the same way but by starting with a pre-reduced sample which is heated in an oxidizing gas mixture, commonly diluted O_2. The TPO and TPR experiments can provide essential insights about support-metal interactions, oxidation state etc. In **Paper I**, the TPO and TPR were employed in order to study how the zeolite supports and the SAR influence the Pd oxidation/reduction properties, but also to see whether the Pd exists in particle form or as ion-exchanged Pd^{2+} species in the zeolite framework. For **Paper IV**, TPO and TPR were conducted to elucidate whether the addition of Ba promoter could alter the surface electron density of the Pd and thus influence the oxidation state of the Pd. In both studies, the TPO and TPR were followed after pre-reduction in H_2 or pre-oxidation in O_2 at 500˚C, respectively. Thereafter the samples were cooled down to room temperature before the O_2 was introduced for the TPO or the CH_4 added to the feed for the TPR. The temperature was subsequently ramped (10˚C/min) up to 600˚C (**Paper I**) or 700˚C (**Paper IV**) in O_2 or CH_4. The TPO/TPR sequences were performed with scanning differential calorimeter (Sensys DSC, Setaram) and the outlet gases were monitored with a mass spectrometer (MS, Hiden HPR-20 QUI MS). The inlet gas flow was regulated by multiple MFC:s (Mass Flow Controller, Bronkhorst).

3.2.4 Temperature programmed desorption (TPD)

This characterization method relies on temperature dependent desorption of previously adsorbed probe molecules. The number of desorbed molecules and the desorption temperature provide information about the number of adsorption sites and the how strongly the adsorbate is attached to the adsorption site. One concrete example is NH_3-TPD which is commonly used to qualitatively and quantitively estimate the acidity of catalyst material together with the strength and type of acid sites [93-95]. This was performed on the zeolite supported Pd samples in **Paper II**, first by NH_3 adsorption in 500 ppm NH_3 at 100°C for 2 h. Thereafter the temperature was ramped (10°C/min) to 500°C in Ar while the desorbed NH_3 was detected in the outlet gases.

3.2.5 Diffuse reflectance infrared Fourier transform spectroscopy (DRIFTS)

Infrared (IR) spectroscopy can be used to identify chemisorbed species on the catalyst surface. It is also a common method to elucidate the different catalyst sites by studying the adsorption of specific probe molecules, such as CO or NO. The analysis can be performed either in transmission or diffuse reflectance mode. The latter one is commonly referred to as DRIFTS. The technique is based on detecting the absorbance of IR of specific frequencies associated to the transition between vibrational energy levels of certain chemisorbed surface compound [1]. For the DRIFTS experiments herein presented, a Vertex 70 spectrometer (Bruker) equipped with liquid nitrogen cooled MCT detector was used. The sample was loaded in a stainless steel reaction chamber (Praying Mantis, High Temperature Reaction Chamber), the inlet gas flow was supplied by multiple MFC:s (Bronkhorst) and the water vapor was provided from a CEM (Controlled Evaporator and Mixer, Bronkhorst) system.

The DRIFTS analysis in **Paper I** was performed to study the ion-exchanged Pd^{2+} species in the zeolite supported samples using NO as a probe molecule. For this experiment, the fresh powder samples were first calcined at 600˚C for 2 h in air followed by degreening and pre-treatment in the DRIFTS cell. The degreening was performed at 550˚C by first reducing the samples in 2 vol.% H_2 (30 min) followed by CH_4 oxidation in 500 ppm CH_4, 8 vol.% O_2 and 2 vol.% H_2O (60 min). The pre-treatment consisted of reduction in 2 vol.% H_2 (30 min) and oxidation in 8 vol.% O_2 (30 min), also at 550˚C. The samples were thereafter cooled in Ar to 80˚C where the background spectra were acquired. Subsequently, the samples were provided with 1000 ppm NO and the IR absorbance spectra herein presented were collected after 60 min. The DRIFTS cell was equipped with CaF_2 windows.

In the third paper, **Paper III**, DRIFTS was also combined with NO adsorption in order to detect ion-exchanged Pd^{2+} species. This was done for degreened (600°C) and hydrothermally aged (900°C) catalyst powder. The samples were pre-treated in the DRIFTS cell at 550°C in 2 vol.% H_2 (30 min) followed by 8 vol.% O_2 (30 min) and cooling in 8 vol.% O_2 to 80°C. The NO adsorption was performed with 200 ppm NO at 80°C for 60 min. The spectra were corrected with the background acquired at 80°C in Ar prior to the introduction of NO and CaF_2 windows were used.

For **Paper IV**, DRIFTS was used to study the adsorption/desorption of water on oxidized catalyst samples. This was done in order to elucidate whether the addition of Ba promotor influences the rate and/or degree of hydroxylation/dehydroxylation and/or the type of formed hydroxyl species. Note that the samples were degreened and pre-treated in the flow reactor prior to loading in the DRIFTS cell. The samples were also pre-treated for 60 min in 2 vol.% O_2 at 550˚C in the DRIFTS cell immediately before the experiments and the background spectrum was acquired in the end of this step. The DRIFTS spectra herein presented were recorded while the samples were provided with a gas feed containing 2 vol.% O_2 and 1 vol.% H_2O for 2 h followed 3 h in 2 vol.% O_2, also at 550˚C. It should also be noted that the sample powder was diluted with 10 wt.% KBr and that CaF_2 windows were used.

3.2.6 NaCl-titration

NaCl titration is a method developed by Ogura et al. [96] for estimating the amount of ion-exchanged Pd^{2+} in Pd/zeolite samples. The general principle is to add the Pd/zeolite to an agitated NaCl solution at an elevated temperature and keep it under those conditions for some time and thereby replace the Pd^{2+} cations on the zeolite acid Brønsted sites with Na^+ ions. This procedure may be repeated multiple times to improve the ion-exchange. The difference in Pd content of sample treated in NaCl solution and fresh catalyst powder, measured by ICP, is assumed to equal the amount of ion-exchanged Pd^{2+} in the fresh sample. This method was applied in **Paper II** where the cation exchange was repeated two times in 0.1 M NaCl solution at 80°C.

3.2.7 Transmission electron microscopy (TEM)

With this type of spectroscopy, it is possible to acquire high resolution images of the specimen down to the nanometer scale. In this way, essential information can be obtained about the chemistry, morphology and crystallography of the sample. For this technique the sample is bombarded with electrons. The electrons will then either get scattered by the sample atoms or pass straight through the sample without any interactions. The scattered electrons will follow a path with certain angular deviation compared to the path of the incident electrons. Hence, the structural information of the sample can be determined based on the non-uniform electron distribution after the interactions with the specimen. Thick samples are non-transparent due to the higher proportion of backscattered electrons, thus only thin samples can be analyzed with TEM [97].

The images herein presented were acquired with a FEI Titan 80–300 microscope, equipped with probe Cs-corrector and high-angle annular dark-field (HAADF) detector. The microscope was operated in scanning mode (STEM, Scanning Transmission Electron Spectroscopy) with a voltage of 300 kV. The obtained STEM images were used to analyze the potential changes in Pd particle size and shape due to different treatment and different support material (**Paper I-III**) and due to the addition of Ba promoter (**Paper IV**).

3.2.8 Energy-dispersive X-ray spectroscopy (EDX)

Energy-dispersive X-ray spectroscopy (EDX) is commonly used to obtain quantitative and qualitative information of elemental composition in a particular area of the sample. For the samples in **Paper IV**, EDX was used to investigate the distribution of Ba in the promoted samples and was performed with a FEI Titan 80–300 microscope, *i.e.* the same instrument as for the TEM analysis (Section 3.2.7). This technique relies on the excitation of inner shell electrons of the sample atoms as the specimen is bombarded with electrons. Another electron from an outer shell of the atom will fill the resulting core hole and the excess energy is released either as an Auger electron or as an X-ray. The EDX detector records the number and element characteristic energy of the X-rays emitted in the latter case [97].

3.2.9 X-ray photoelectron spectroscopy (XPS)

This X-ray based technique provides valuable information about the quantitative and qualitative elemental composition of the top surface layer (approximately < 10 nm) and the chemical nature, including the oxidization state of the atomic species. In brief, the sample is irradiated with a monochromatic X-ray beam with high energy under vacuum. This results in ejection of photoelectrons from the sample atoms. The characteristic binding energy of these photoelectrons can be determined based on their kinetic energy, which is recorded by the detector [98]. In **Paper IV**, XPS was used to analyze whether Ba promotion of Pd/Al_2O_3 influences the oxidation state of the Pd. The analysis was performed with a Perkin Elmer PHI 5000C ESCA system equipped with monochromatic Al Kα X-ray source with the binding energy of 1486.6 eV. For reference, the C1s with a binding energy of 284.6 eV was used.

3.2.10 X-ray powder diffraction (XRD) and X-ray scattering

XRD is an X-ray based characterization method, which is used to study the structures of crystalline matters. There is a large number of different applications for XRD, for instance it can serve as a tool to determine whether the correct crystalline zeolite structure was generated during synthesis [42]. The sample is placed between the X-ray source and the detector, which are separated by an angle of 2θ. The incident X-rays will be scattered by the atoms in the sample. The spacing of the atomic planes can be obtained using the information from the constructively interfering scattered X-rays, recorded by the detector, by applying Bragg's law [99]. The samples used for **Paper I** and **Paper III** were analyzed with XRD in order to study the Pd particles and the zeolite structure after synthesis, dealumination treatment and hydrothermal aging. The diffraction patterns for **Paper I** were collected with a Siemens D5000 diffractometer. The 2θ increment was set to 0.03˚ for SSZ-13 zeolites and to 0.02˚ for the beta zeolites. For **Paper III** a BrukerAXS D8 advanced diffractometer was used with an 2θ increment of 0.02°.

Small-angle X-ray scattering (SAXS) is a similar method. However, SAXS relies on the interference of X-rays scattered by larger blocks (typically 20-1000 Å) of uniform material. This is different from XRD, or wide-angle X-ray scattering (WAXS), where wider 2θ angles are used and the recorded X-ray interference is a result of X-ray scattering by the atoms in small unit cells, typically < 20 Å. In practice, SAXS is performed with a small angle between the detector and the X-ray source, $\sin 2\theta/\lambda < 0.1$ Å^{-1} [100]. One example of application for SAXS is to estimate size distribution of particles in catalyst materials, which was made in **Paper II** for Pd particles supported on different support materials.

3.2.11 X-ray absorption spectroscopy (XAS)

XAS is an element specific method to characterize the local neighborhood and the oxidation state of the absorbing atom. Briefly, the sample is bombarded by X-rays of a narrow energy span. Parts of the X-rays get absorbed by the sample, which is described by Lambert-Beer's law (2),

$$\mu t = ln\left(\frac{I_o}{I}\right) \qquad (2)$$

where the absorption coefficient (μ) is expressed by the sample thickness (t), the intensity of the incident X-ray beam (I_o) and the intensity of transmitted X-rays (I) [101]. The X-ray absorption causes excitation or ejection of a core electron which leaves an empty core hole. Hence, the X-ray absorption will increase when the energy of the incident X-rays equals the binding energy of the core electron. This sudden increase of the X-ray absorption is called the absorption edge. The filling of the created core hole by an electron from a higher energy level results in either emission of a fluorescence photon or ejection of an Auger electron. The X-ray absorption is often quantified by comparing the intensity of the transmitted X-rays to the incident X-rays as in equation (2). This was done for the measurements in **Paper II**. However, the absorption can also be quantified by measuring the emitted fluorescence or ejected Auger electrons. The absorption spectrum is obtained by repeating this procedure for different energies of the incident X-ray beam around the absorption edge. Normally a synchrotron X-ray source

is used for the XAS measurements because of its high brilliance and tunable energy. The XAS spectrum is divided into (*i*) the X-ray absorption near edge structure (XANES) region, which stretches up to ca. 50 eV above the edge and is commonly used to determine the oxidation state of the absorbing atoms, and (*ii*) the extended X-ray absorption fine structure (EXAFS) region which constitutes the energy region above the XANES region and contains information about the local structure around the absorbing atoms. The recorded XAS spectra are first normalized and background subtracted, thereafter the detailed XANES and EXAFS analysis can be performed [102].

The XAS measurements in **Paper II** were performed at the SuperXAS beamline [103] at the Swiss Light Source (SLS), Switzerland, using the Quick-EXAFS technique (QEXAFS) for collection of highly time-resolved data. In brief, the X-rays from a superbend magnet were collimated by a Pt-coated mirror, monochromatized by a channel-cut Si(111) crystal monochromator and focused by a Pt-coated toroidal mirror. The oscillating monochromator allows for rapid energy scans, *i.e.* high frequency XAS spectra collection, which is suitable for operando experiments. In **Paper II** a spectra collection rate of 1 Hz was used.

The operando XAS experiments in **Paper II** were performed with alternated rich (CH_4/Ar) and lean (CH_4/O_2/Ar) pulses at different temperatures. The recorded XAS spectra were analyzed to observe changes in Pd oxidation state and Pd speciation.

X-ray absorption near edge spectra (XANES)

The XANES spectra can provide information of the oxidation state of the absorbing atom, however it is also sensitive to the coordination environment. XANES spectra are often analyzed using fingerprint methods, *i.e.* by comparison of the sample spectrum to other calculated or recorded data [102]. For instance, the oxidation state of a Pd-based sample can be estimated by linear combination fitting (LCF) of PdO and Pd^0 standards, which was done in **Paper II**. The processing of XANES spectra, including the LCF analysis, was performed with the ProQEXAFS data processing software [104].

Extended X-ray absorption fine structure (EXAFS)

The EXAFS region of the absorption spectrum gives information of the local environment around the absorbing atoms including the distances and coordination numbers to the nearest neighbors. The Fourier transformed EXAFS spectra can be described by the EXAFS equation [102]

$$\chi(k) = S_0^2 \sum_i N_i \frac{f_i(k)}{kR_i^2} \sin(2kR_i + \delta_i(k))\, e^{-2R_i/\lambda(k)} e^{-2\sigma_i^2 k^2} \quad (3)$$

where the photoelectron wave vector (k) is expressed as

$$k = \frac{2\pi}{\lambda} = \sqrt{\frac{2m_e(E-E_0)}{\hbar^2}} \quad (4)$$

The parameters in the EXAFS function ($\chi(k)$), described in equation (3) and (4), are the amplitude reduction factor (S_0^2), distance between the absorbing atom and the scattering atom (R), coordination number (N), backscattering amplitude function ($f(k)$), phase shift function ($\delta(k)$) photoelectron mean free path ($\lambda(k)$), Debye-Waller factor or mean square radial

displacement (σ^2), electron mass (m_e), incident X-ray energy (E), adsorption edge energy (E_0) and reduced Planck constant ($\hbar$) [102]. The values of S_0^2, R, σ^2 E_0 and N are obtained by fitting the EXAFS equation to the Fourier transformed EXAFS spectra of the sample.

Fitting of the Fourier transformed (k-range 3.0-10.25 Å) and k^2-weighted Pd k-edge EXAFS spectra in **Paper II** was performed using the Demeter software package [105]. Fitting of the first Pd-Pd shell of Pd^0 foil yielded the S_0^2, which was used for all scattering paths. The value of σ^2 for the Pd-Pd shell was also extracted from the Pd^0 fit using the Debye model and the Debye temperature of 274 K. Three scattering paths (Pd-O, Pd-(O)-Pd1 and Pd-(O)-Pd2) were fitted to the spectra of PdO. The values of σ^2 and ΔR of these scattering paths were determined by fitting fully oxidized samples at respective experiment temperature.

3.3 Catalytic activity measurements in flow reactor

3.3.1 Flow reactor setups

Monolith plug flow reactor

The catalytic activity of the washcoated monolith samples was tested in a flow reactor. All the monoliths were wrapped in quartz wool prior to insertion into the quartz tube in order to minimize by-pass gas flow. The quartz tube holding the sample was surrounded by a heating coil and covered with insulation. The temperature was measured and controlled by a thermocouple positioned 10 mm upstream from the monolith and an Eurotherm system. In addition, a second thermocouple was placed centrally in the monolith and the CH_4 conversion data herein presented is associated to this latter temperature. An illustration of the sample compartment of the reactor setup is shown in Figure 3.1. The inlet gas flows were controlled by multiple MFC:s (Bronkhorst) and the water vapor used in the experiments was obtained from a CEM (Controlled Evaporator and Mixer, Bronkhorst) system. Moreover, the outlet gases were detected and monitored by a Fourier transformed infrared (FTIR) spectrometer (MKS MultiGas 2023 HS).

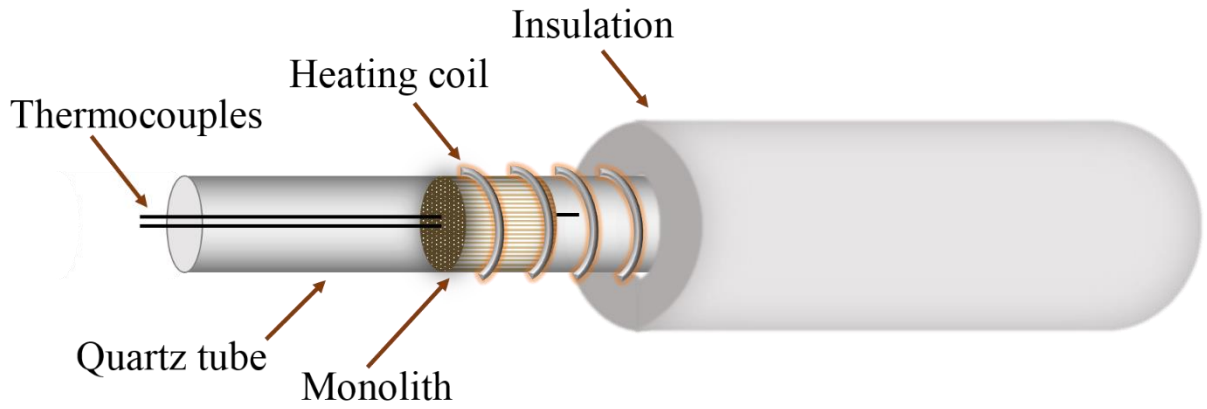

Figure 3.1. Illustration of the sample compartment of the reactor setup. Gas flow direction is from right to left.

Note that the sizes of the monoliths differed for the studies. For **Paper I-III** and **Paper V** the monolith size was Ø=15 mm/L=20 mm and for **Paper IV** it was Ø=21 mm/L=20 mm. The total gas flow was therefore also different in the different studies. The gas hourly space velocity was 13 600 h^{-1} in **Paper I-III**, 30 000 h^{-1} in **Paper IV** and 20 400 h^{-1} in **Paper V**. Figure 3.2 shows a washcoated monolith.

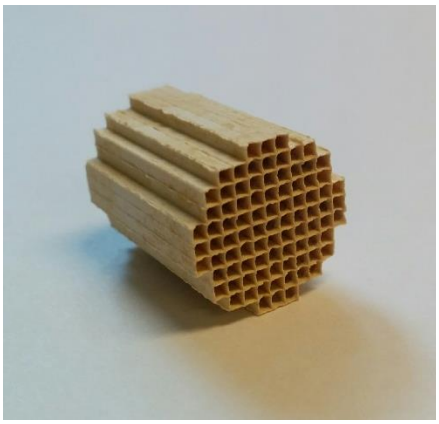

Figure 3.2. Washcoated monolith

Powder plug flow reaction cell for operando XAS measurements

The activity tests for **Paper II** were performed in a plug flow reactor equipped with graphite windows for simultaneous XAS and catalytic activity measurements [106]. The temperature was regulated using a thermocouple placed centrally in the sample powder bed. The reactor cell was loaded with about 25 mg of catalyst powder sample, sieved in the range 100-150 μm, between two quartz wool plugs. The total gas flow was 70-100 mL/min.

3.3.2 Outlet gas detection

The contents of the outlet gases were analyzed with either FTIR or mass spectroscopy (MS). For both methods the recoded data was calibrated based on measurements of known gas concentrations.

Fourier transform infrared spectroscopy (FTIR)

This method relies on the same principle as DRIFTS (Section 3.2.5), *i.e.* the IR absorbance associated to transitions between vibrational energy levels of the analyzed molecules [1]. Whilst DRIFTS is used to study the molecules adsorbed on a solid surface, the FTIR technique can also be used to analyze molecules in gas phase. However, one drawback is that it cannot detect molecules without dipole moment, such as H_2, O_2, N_2 and Ar.

Mass spectrometry (MS)

An MS operates by ionizing and fragmenting the sample, *i.e.* the outlet gas molecules for this application, and then separate these fragments based on their mass/charge ratio. The mass spectrometer provides the relative abundance of the fragments with the same mass/charge ratio [107] which can be translated into the concentration of a specific gas by calibration based on known gas concentrations. One drawback is that fragments consisting of different atoms can

have the same mass/charge ratio and different molecules can be split into the identical fragments, which can make it difficult to distinguish between certain compounds.

3.3.3 Degreening and pre-treatment procedures

The washcoated samples were degreened once and pre-treated before each activity experiment. The degreening procedure consisted of alternated rich and lean steps in the presence of water vapor in order to stabilize the catalyst. The subsequent pre-treatment steps served to remove potential adsorbates from the surface.

More detailed, the degreening procedure, which was the same for **Paper I** and **Paper III-IV** except for the maximum temperature (600˚C for **Paper I** and **Paper III** and 700˚C for **Paper IV**), was performed in the following steps: (*i*) reduction at 500˚C in 2 vol% H_2 (30 min), (*ii*) CH_4 oxidation at 700/600˚C in 500 ppm CH_4, 8 vol.% O_2 and 5 vol.% H_2O (60 min), (*iii*) reduction at 700/600˚C in 2 vol.% H_2 and 5 vol.% H_2O (20 min), (*iv*) repetition of step *ii*. The degreening procedure used in **Paper V** was identical to that of **Paper IV**, except for that the feed gas consisted of 500 ppm CH_4, 500 ppm NO, 300 ppm CO, 8 vol.% O_2 and 5 vol.% H_2O in step (*ii*) and (*iv*). For **Paper II**, the degreening was performed at 450°C in (*i*) 2 vol.% H_2 (20 min), (*ii*) 1000 ppm CH_4 and 2 vol.% O_2 (10 min), (*iii*) 2 vol.% H_2 (10 min) followed by repetition of step (*ii*).

The samples in **Paper I**-**III** and **Paper IV**-**V** were pre-treated at 600-700°C in 1-2 vol.% H_2 for 30-60 min followed by 8 vol.% O_2 for 30-60 min. For **Paper II**, the pre-treatment consisted of 2 vol.% O_2 for 20 min at 450°C.

3.3.4 Catalytic activity tests

The catalytic activity of the degreened and pre-treated catalysts was measured in different gas feed mixtures and at different temperatures. The activity in **Paper I** and **Paper III-IV** was typically tested under lean conditions in the absence of water vapor in 500 ppm CH_4 and 8 vol.% O_2 (referred to as dry reaction feed) and in the presence of water vapor in 500 ppm CH_4, 8 vol.% O_2 and 5 vol.% H_2O (referred to as wet reaction mixture). The samples in **Paper II** were analyzed in the absence of water vapor in 1000 ppm CH_4 and 2 vol.% O_2. **Paper V** focused on stoichiometric CH_4 oxidation and the activity was therefore typically tested in 500 ppm CH_4, 1000 ppm O_2 and 5% H_2O (referred to as stoichiometric reaction mixture) More details about respective catalytic activity test will be presented together with the results in the forthcoming sections.

4 Zeolite supported palladium for complete CH_4 oxidation

Traditional methane oxidation catalysts are typically composed out of Pd nanoparticles supported on metal oxides with high surface area, commonly Al_2O_3. Most of the available studies concerning CH_4 oxidation catalysts focus on such materials and the major challenges are water deactivation [6] and sulfur poisoning [7]. Potential alternatives to the metal oxide support materials are zeolites. Whilst the knowledge of how Pd/zeolite materials are impacted by sulfur compounds is poor, it has been shown that zeolite supported Pd can provide high and stable CH_4 oxidation activity in the presence of water vapor [44, 72, 73, 108]. Hence, zeolite supported Pd is a promising candidate for future CH_4 abatement catalyst. However, more knowledge is needed to understand the complex relation between the Pd, zeolite support material and different thermal and gaseous conditions. Therefore, **Paper I - III** concern different kinds of zeolite-based Pd catalysts with focus on how the type of zeolite support and its properties influence the CH_4 oxidation activity under dry and wet conditions, in the presence of SO_2 and after hydrothermal aging.

4.1 Catalytic properties in the absence of catalyst pollutants

This section concerns the catalytic performance under dry conditions, *i.e.* in the absence of water vapor, which was investigated in **Paper I** and **Paper II**. The aim has been to correlate the type of zeolite support and the formed Pd species to the oxidation-reduction behavior of the Pd and the CH_4 oxidation activity. Various characterization methods were used, STEM, DRIFTS, TPO, TPR, SAXS, NaCl-titration, XANES and EXAFS in combination with catalytic activity measurements. To simplify, the following denotations of the samples will be used: Pd/Al_2O_3-"PdAl", Pd/beta (SAR=40)-"PdB40", Pd/beta (SAR=511)-"PdB511", Pd/beta (SAR=969)-"PdB969", Pd/SSZ-13 (SAR=43)-"PdS43" and Pd/SSZ-13 (SAR=52)-"PdS52". It should be noted that the same samples were tested in both **Paper I** and **Paper II**, however the degreening and pre-treatment procedures were different (see Section 3.3.3) which contributed to differences in the catalytic performance. Briefly, the samples in **Paper I** were degreened at 600°C in the presence of water vapor and pre-treated at the same temperature. For **Paper II**, the degreening and pre-treatment were performed at 450°C in the absence of water vapor. To make it clear, the samples tested in **Paper I** and **Paper II** will be noted with index I and II, respectively.

4.1.1 Palladium species formed in zeolite supports

The nature of the Pd is more complex using zeolites as support materials compared to traditional metal oxide supports, such as Al_2O_3. For Pd/zeolite materials, the Pd can exist both as particles within or outside the pores and/or as ion-exchanged Pd^{2+} species, whereas solely Pd particles are formed on Al_2O_3. There are many underlying factors influencing the Pd speciation in Pd/zeolite materials. The ratio of ion-exchanged Pd^{2+} to Pd particles increases with lower Pd loadings [45, 96, 109]. The use of zeolites with high Al content generally facilitates the formation of small Pd particles and/or ion-exchanged Pd^{2+} [44, 110-113]. It has also been reported that the formation isolated Pd^{2+} is hampered in small pore zeolites due to low Pd mobility [83, 109]. Ion-exchanged Pd^{2+} species are formed relatively easy in zeolites with H^+ as nominal cation form, whereas Pd particle formation is favored on zeolites exchanged with alkali metals, such as Na^+ [114]. Another major factor influencing the Pd speciation is the conditions the Pd/zeolite material has been treated under. Hydrothermal aging facilitates the formation of isolated Pd^{2+} sites and/or Pd sintering [45, 82, 83]. It is also generally accepted that the Pd can rearrange reversibly between large particles under rich conditions and smaller particles and/or isolated Pd^{2+} species under lean conditions [109, 112, 114]. Hence, several factors control the complex nature of the Pd supported on zeolites, which means that the choice of zeolite support and treatment of the catalyst highly affect the catalytic properties.

Palladium particle size

The Pd particles size in $PdB511_I$ and $PdB40_I$ in **Paper I** was investigated with STEM before and after the activity tests and the acquired images are displayed in Figure 4.1. Note that the activity tests included both exposure to water vapor and SO_2. It should also be emphasized that ion-exchanged Pd^{2+} species cannot be detected by STEM, but only Pd particles. For $PdB40_I$ (Figure 4.1a and 4.1b), the major fraction of the Pd particles were well dispersed with approximate diameters of < 6 nm, however, in addition to a few larger Pd particles. By contrast, larger and less dispersed Pd particles with diameters of around 5-20 nm were observed in the $PdB511_I$ sample (Figure 4.1c and 4.2d). This confirms that a higher SAR results in the formation of larger Pd particles which previously has been suggested by Okumura et al. [44].

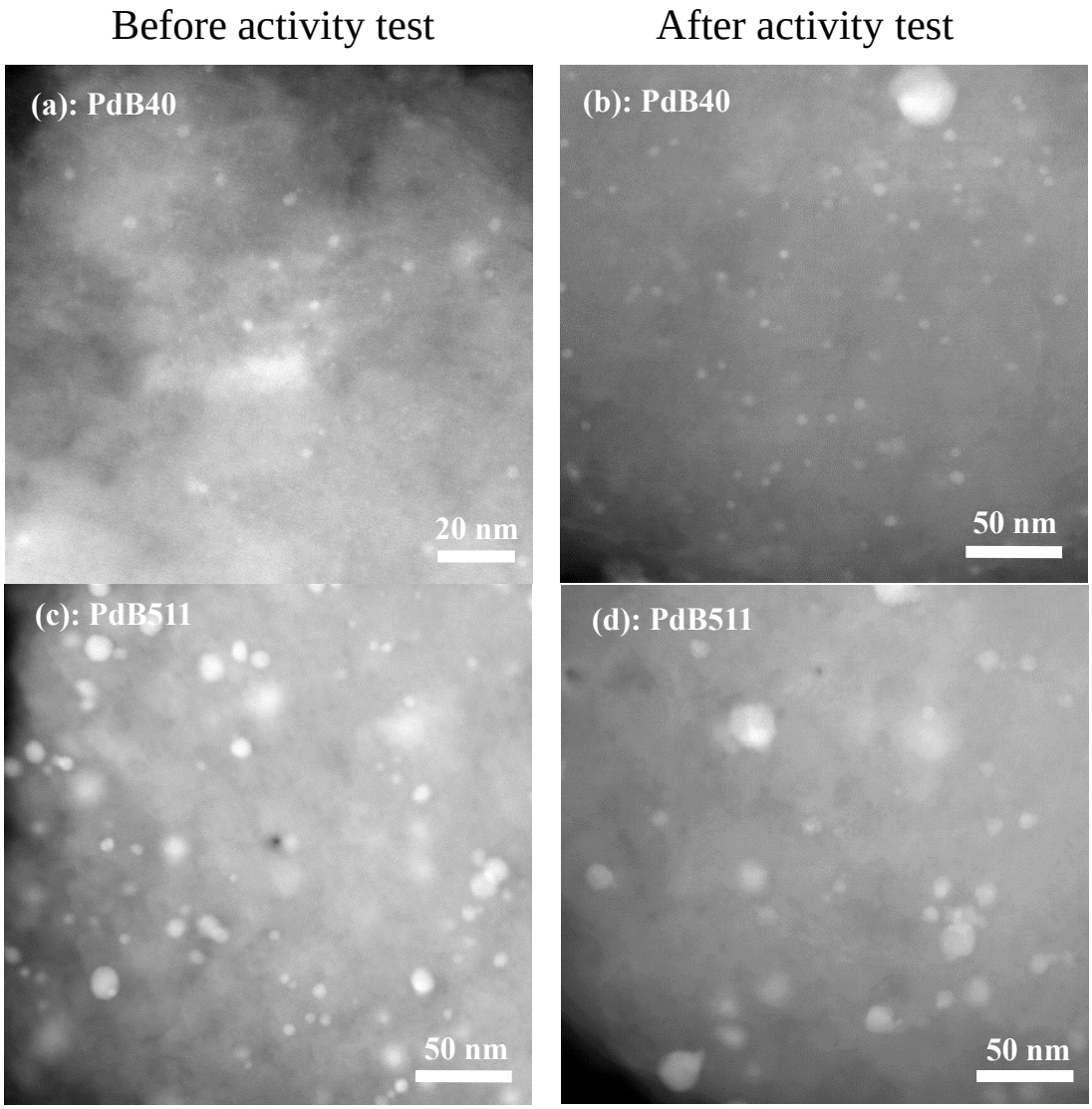

Figure 4.1. STEM images of $PdB40_I$ (a-b) and $PdB511_I$ (c-d). Figure (a) and (c) represent samples degreened at 600°C in the presence of water vapor, prior to the activity tests in **Paper I**, whereas the images in (b) and (c) were acquired after the activity tests (including exposure to water vapor and SO_2).

The particle size of the samples in **Paper II** were also investigated with STEM and SAXS. The particle size distribution of $PdB511_{II}$, $PdB40_{II}$ and $PdS43_{II}$ estimated with SAXS is displayed in Figure 4.2 and Table 4.1. It can be seen that the Pd particle radius was widely spread with an average radius of 9.4 nm for $PdB511_{II}$. The wide particle size distribution is likely a result of weak support-Pd interactions because the of the highly siliceous B511 support. $PdB40_{II}$ exhibited a bimodal particle size distribution, with many large Pd particles (average radius 22.7 nm) together with a lower number of small particles (average radius 3.8), the total average radius was 18.4 nm. This is very different from the $PdS43_{II}$ sample, where the majority of the particles were small and well dispersed (total average radius 5.0 nm). The formation of small Pd particles in $PdS43_{II}$ may be a result of strong zeolite-Pd interactions due to the strong acidity of the S43 zeolite.

By comparing the particles in Figure 4.1 and Figure 4.2 it appears that the high temperature degreening in the presence of water vapor in **Paper I** facilitated the formation of small Pd particles in $PdB40_I$. By contrast, $PdB40_{II}$ mainly contained larger particles in addition to a low number of small particles after the degreening at lower temperatures and in the absence of water vapor (**Paper II**). However, it should also be noted that use of different characterization methods (STEM and SAXS) may cause some differences.

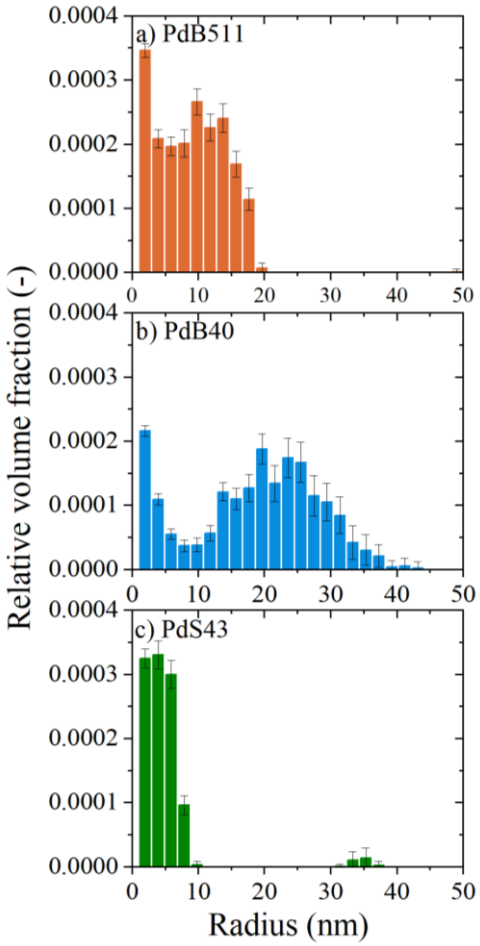

Figure 4.2. Palladium particle radius distribution from SAXS measurements after degreening, pre-treatment and 10 rich-lean cycles at 360°C for a) $PdB511_{II}$, b) $PdB40_{II}$ and c) $PdS43_{II}$.

Table 4.1. Palladium particle radius determined from SAXS measurements and portion of Na^+ exchangeable Pd estimated with NaCl-titration for $PdB511_{II}$, $PdB40_{II}$ and $PdS43_{II}$, **Paper II**.

	Total average radius (nm)	Average radius of particles <10 nm (nm)	Average radius of particles >10 nm (nm)	Portion of Pd exchangeable with Na^+ (%)
$PdB511_{II}$	9.4 ± 0.5	5.4 ± 0.1	14.0 ± 0.1	4
$PdB40_{II}$	18.4 ± 0.2	3.8 ± 0.1	22.7 ± 0.2	13
$PdS43_{II}$	5.0 ± 0.6	4.2 ± 0.0	27.2 ± 14.1	2

Ion-exchanged Pd^{2+} species

The ion-exchanged Pd^{2+} were studied with NO adsorption combined with DRIFTS, TPO and TPR in **Paper I**, whereas NaCl-titration was used for the same purpose in **Paper II**.

The samples in **Paper I** were degreened and pre-treated in the DRIFTS cell at 550°C and in the presence of water vapor (Section 3.2.5) followed by cooling in Ar prior to the NO adsorption at 80°C in 1000 ppm NO. The DRIFTS spectra displayed in Figure 4.3 were collected after 60 min exposure to this gas mixture. Exposure of NO to Pd/zeolite samples results in formation of nitrosyl groups on the isolated Pd species. The nitrosyl groups on Pd^{2+} absorb IR in the in the wavenumber region 1800-1881 cm^{-1} [82, 115-118]. $PdB40_I$, $PdS43_I$ and $PdS52_I$, but not $PdB511_I$, exhibited clear peaks in this wavenumber region, thus confirming the presence of ion-exchanged Pd^{2+}. The reason for the absence of Pd^{2+} species in $PdB511_I$ is the lack of acid Brønsted sites in the siliceous B511 zeolite. It should also be noted that it is not possible to demonstrate the presence of Pd particles with this method due to low NO adsorption on PdO particles [82, 96, 119].

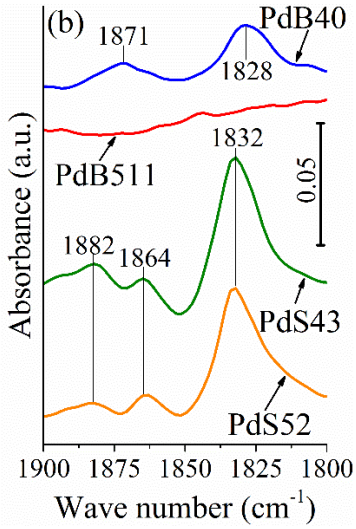

Figure 4.3. DRIFTS spectra acquired after 60 min of exposure to 1000 ppm NO at 80°C. From top to bottom: $PdB40_I$ (blue), $PdB511_I$ (red), $PdS43_I$ (green) and $PdS52_I$ (orange).

Further insights about the nature of the Pd of the samples in **Paper I** were obtained with TPR and TPO. Analysis by TPR and TPO can provide essential information regarding the Pd oxidation and reduction properties. In addition, TPR can be used to detect and distinguish between Pd^{2+} species and Pd particles since the reduction temperature is lower for Pd particles than for monodispersed Pd species [120, 121].

The TPR patterns for the beta and SSZ-13-based samples are displayed in Figure 4.4. For all the samples, the first negative CH_4 consumption peak represents the reduction of the PdO particles with corresponding production of CO_2 and H_2O. There were differences between the samples in the amount of CH_4 consumed in this first reduction peak, but also small differences in the temperature of reduction. The largest CH_4 oxidation peak was observed for $PdB511_I$ at around 223˚C. This shows that $PdB511_I$ had a high content of PdO. The fact that no ion-exchanged Pd^{2+} species were detected with NO-DRIFTS (Figure 4.3) supports the interpretation that this peak of $PdB511_I$ corresponds to the reduction of PdO particles. By contrast, the first

CH_4 consumption peak at 214˚C for $PdB40_I$ was much smaller and an additional weak peak at 305˚C was observed. The first and latter mentioned peaks are assigned to PdO particles and ion-exchanged Pd^{2+}, respectively. The similar trend was reflected by the SSZ-13 supported samples. Interestingly, $PdS43_I$ showed almost no CH_4 consumption in the temperature range corresponding to PdO particle reduction. On the other hand, $PdS52_I$ expressed two peaks corresponding to reduction of particles (216˚C) and Pd^{2+} species (≈ 287˚C).

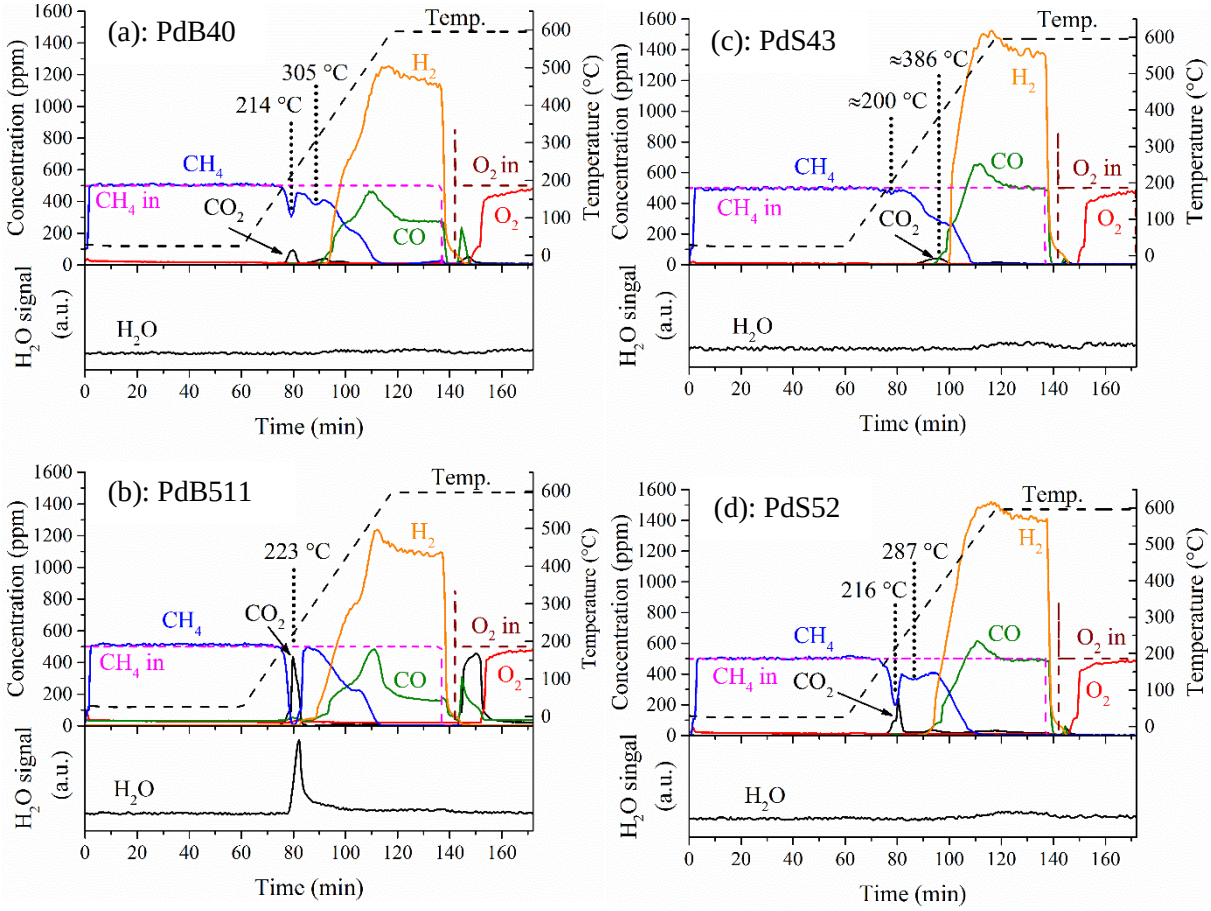

Figure 4.4. Temperature programmed reduction (TPR) for a) $PdB40_I$, b) $PdB511_I$, c) $PdS43_I$ and d) $PdS52_I$.

The TPO results in Figure 4.5, agree well with the TPR results (Figure 4.4) of the same samples. A sharp singlet O_2 consumption peak was expressed by $Pd511_I$. Both the DRIFTS and the TPR results (Figure 4.3 and Figure 4.4) showed that all Pd existed as particles in $Pd511_I$ which suggests that the sharp peak at 359˚C corresponds to the oxidation of Pd particles. By comparison, a much shallower and wider O_2 consumption peak with minima at higher temperature (454˚C) was exhibited by $PdB40_I$. For this sample, the existence of both PdO particles and isolated Pd^{2+} species was confirmed with STEM, DRIFTS and TPR (Figure 4.1, 4.3 and 4.4). The reason for this may be that the Pd^{2+} species are oxidized at higher temperatures, which results in the broadly shaped peak for $PdB40_I$ which corresponds to the oxidation of both particles and ion-exchanged Pd^{2+}. The SSZ-13 supported samples show the same trend as the beta-based samples. A sharp peak centered at around 386˚C with a clear asymmetry of O_2 consumption towards higher temperatures was exhibited by $PdS52_I$. Using the same reasoning as for the beta samples, this means that the sample contains a large fraction

of Pd particles in addition to Pd^{2+} species, which were oxidized at a higher temperature. The $PdB43_I$ sample consumed most O_2 at around 456˚C, which indicates that most of the Pd was ion-exchanged with the zeolite framework. However, both $PdS43_I$ and $PdS52_I$ also showed a decreased O_2 concentration at 600˚C meaning that these samples were difficult to oxidize completely.

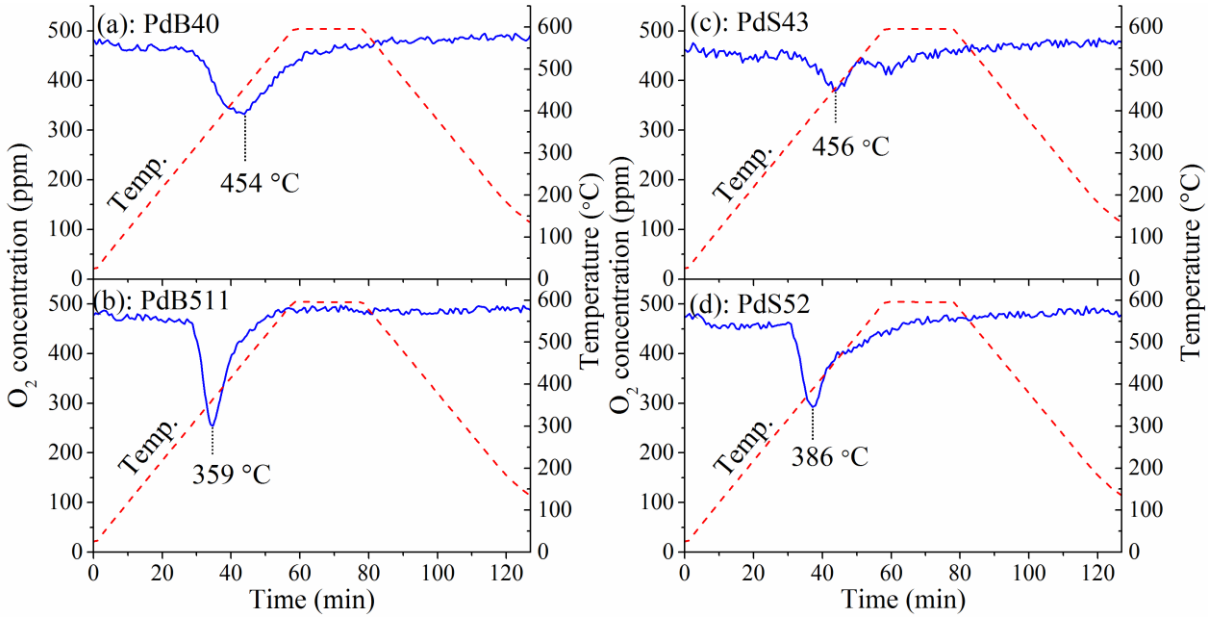

Figure 4.5. Temperature programmed oxidation (TPO) for a) $PdB40_I$, b) $PdB511_I$, c) $PdS43_I$ and d) $PdS52_I$. The blue solid lines represent the O_2 concentration and the red, dashed lines the sample temperature.

To summarize the characterization of the samples in **Paper I**, the TEM, DRIFTS, TPR and TPO analysis showed that $PdB511_I$ contained almost exclusively Pd in particle form, whereas the other zeolite supported samples ($PdB40_I$, $PdS43_I$ and $PdS52_I$) contained both Pd particles and isolated Pd^{2+} species. In addition, the particles in $PdB511_I$ were larger than the particles on $PdB40_I$. The ratio of monoatomic Pd^{2+} species to Pd particles appears to increase with decreasing SAR which most likely is a result of the higher ion-exchange capacity and the high acidity which facilitates stabilization of dispersed Pd particles. The ion-exchanged Pd^{2+} species have considerably higher oxidation and reduction temperatures than Pd in particle form. It was also shown that the use of siliceous zeolites results in more Pd accessible for oxidation and reduction, based on the higher O_2 and CH_4 consumption in the TPO and TPR, respectively.

For **Paper II** the content of ion-exchanged Pd^{2+} was quantified by NaCl-titration and the results are shown in Table 4.1. Whilst no or very little of the Pd in $PdB511_{II}$ and $PdS43_{II}$ was exchangeable with Na^+, about 10% of the Pd in $PdB40_{II}$ was removed by the NaCl-titration. This means that $PdB40_{II}$ contained more exchanged Pd species. Thus, it appears that the higher Al content compared to $PdB511_{II}$ and the larger zeolite pores compared to $PdS43_{II}$ resulted in the formation of more ion-exchanged Pd^{2+} in $PdB40_{II}$. It has previously been suggested that larger pore size facilitates Pd mobility and thereby the formation isolated Pd species [83, 109]. Moreover, it is not surprising that ion-exchanged Pd^{2+} was found in $PdS43_I$ but not in $PdS43_{II}$. Exposure to high temperatures and water vapor has previously been associated to the formation

of ion-exchanged Pd^{2+} species in Pd/SSZ-13 [82, 83]. Hence, the higher temperatures and/or presence of water vapor caused the formation of isolated Pd^{2+} species in $PdS43_I$, whereas the dry pre-treatment at 450°C did not have this effect on $PdS43_{II}$.

4.1.2 Methane oxidation activity in the absence of catalyst pollutants

Activity measurements were performed in order to correlate the catalytic activity to the characterization of the formed Pd species. The CH_4 oxidation activity in the absence of water vapor (dry) and SO_2 is discussed in this section. Prior to the testing, all the samples were degreened and pre-treated according to the protocols in Section 3.3.3.

The dry activity of the samples in **Paper I** was tested by ramping the temperature up and down between 150°C and 600°C in dry reaction mixture (500ppm CH_4 and 8% O_2). There were large differences in the catalytic activity amongst the samples based on the CH_4 conversion shown in Figure 4.6, and the $T_{50\%}$ (temperature of 50% CH_4 conversion) in Figure 4.7. The $T_{50\%}$, for the heating and the cooling ramp, increased in the following order: $PdAl_I$ < $PdB969_I$ < $PdB511_I$ < $PdB40_I$ < $PdS52_I$ < $PdS43_I$. Thus, the highest activity was obtained for the Al_2O_3 supported sample, but the highly siliceous beta samples ($PdB969_I$ and $PdB511_I$) yielded $T_{50\%}$ values in about the same range. The beta supported samples had generally lower $T_{50\%}$ than the SSZ-13-based samples. It is also clear that an increased SAR enhanced the dry CH_4 oxidation activity and resulted in lower $T_{50\%}$. In addition, it also appears that the hysteresis between the heating and cooling ramp decreased with higher SAR. This is particularly evident for the $PdB969_I$, where almost no hysteresis was observed. There are however many possible reasons for this hysteresis. All the samples were thoroughly degreened at 600˚C under alternating rich/lean conditions and in the presence of water vapor. Thus, it seems unlikely that additional sintering of the Pd particles would be responsible for the observed hysteresis. Another potential explanation would be that the produced water vapor in CH_4 oxidation reaction would suppress the catalytic activity, but since the levels of produced water vapor are very low, this is neither considered as a reasonable explanation. The most reasonable explanation is that differences in the oxidation state of the Pd during different parts of the experiment is responsible for the hysteresis. It was also shown with TPR and TPO (Figure 4.4 and Figure 4.5) that the temperature of reduction and oxidation is highly correlated to the SAR of the zeolite support. Hence, it may be that the oxidation state is more stable for the Pd supported in zeolites with high SAR, whereas it changes progressively during the temperature ramped reaction cycle resulting in more pronounced hysteresis for the samples based on zeolites with lower SAR. From the characterization and activity results in **Paper I**, we suggest that the generally increased CH_4 oxidation with higher SAR of the zeolite results from:

i. more Pd particles in relation to ion exchanged Pd^{2+}, which was shown with TPR, TPO and NO-DRIFTS (Figure 4.3, 4.4 and 4.5).
ii. formation of more active PdO, which was observed from the higher oxygen consumption in the TPO and the higher CH_4 consumption in the TPR.
iii. decreased oxidation and reduction temperature due to the higher amount of Pd particles in comparison to ion-exchanged Pd^{2+} species.

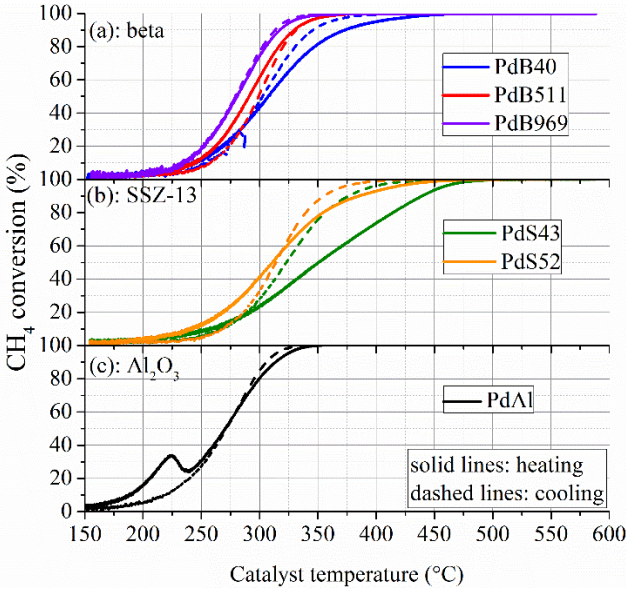

Figure 4.6. Temperature programmed catalytic activity test in dry reaction mixture (500 ppm CH_4 and 8 vol.% O_2), **Paper I**. Solid lines represent heating and dashed lines cooling for a) the beta supported samples (blue: $PdB40_I$, red: $PdB511_I$, purple: $PdB969_I$), b) SSZ-13 supported samples (green: $PdS43_I$, orange: $PdS52_I$) and c) $PdAl_I$ (black).

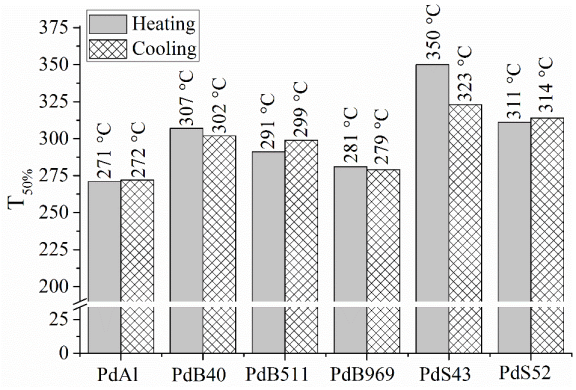

Figure 4.7. Temperature of 50% conversion ($T_{50\%}$) corresponding to the temperature programmed catalytic activity test in dry reaction mixture shown in Figure 4.6, **Paper I**. Solid bars represent heating and checked bars cooling.

Oxidation-reduction behavior of zeolite supported palladium

Operando-XAS experiments were performed in order to correlate the formed Pd species on different zeolite supports to the oxidation-reduction behavior and the CH_4 oxidation activity of the catalysts. The CH_4 oxidation activity was first tested isothermally under lean conditions for 30 min. This was followed by in total 10 rich (CH_4, 1 min) and lean (CH_4 and O_2, 9 min) pulses at the same temperature. The sequence was repeated at different temperatures (360, 330, 300 and 270°C).

The samples exhibited different level of CH_4 conversion during the 30 min of isothermal activity test under lean conditions at 360°C. $PdB511_{II}$ and $PdS43_{II}$ expressed about the same level of CH_4 oxidation activity, which was higher than that of $PdB40_{II}$ (Figure 4.8). Linear combination fitting (LCF) of XANES spectra, using PdO and metallic Pd references, showed that all the samples were completely oxidized at the end of this 30 min sequence. This means that other factors besides the Pd oxidation state also influence the dry CH_4 oxidation activity.

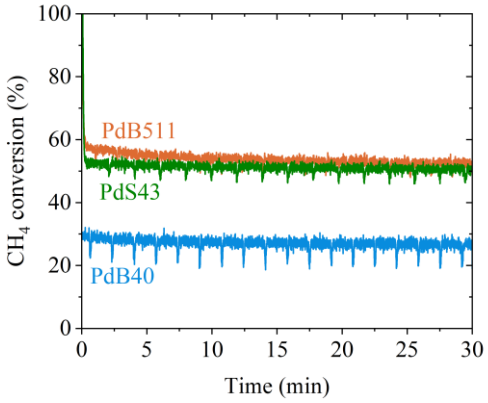

Figure 4.8. Methane conversion during 30 min of lean (1000 ppm CH_4 and 2 vol.% O_2) CH_4 oxidation at 360°C, **Paper II**. From top to bottom, $PdB511_{II}$ (orange), $PdS43_{II}$ (green) and $PdB40_{II}$ (blue).

The Pd^{2+} fraction and the outlet CH_4 concentration during the 9th -10th rich pulse and the 9th lean pulse are shown in Figure 4.9. The time-resolved Pd^{2+} fraction profiles in Figure 4.9a-4.9d show that $PdB511_{II}$ and $PdS43_{II}$ generally were easier to reduce and re-oxidize compared to $PdB40_{II}$, and they also had the highest re-oxidation rate at the beginning of the lean pulse. By contrast, $PdB40_{II}$ could not be reduced at temperatures $\leq$ 300°C, and at higher temperatures, the re-oxidation was both slow and resulted in less Pd^{2+}.

The outlet CH_4 concentration in Figure 4.9e-4.9h shows that the catalytic activity was similar for $PdB511_{II}$ and $PdS43_{II}$ whereas lower CH_4 conversion was recorded for $PdB40_{II}$. It should be noted that the activity was about the same at the end of the lean pulse (with partly oxidized samples) and after 30 min of lean CH_4 oxidation (with completely oxidized samples), compare Figure 4.8 and Figure 4.9e. It has also previously been reported that the CH_4 oxidation activity increases with the Pd oxidation state until a certain level and that further oxidation thereafter gives no additional activity [11, 122]. It appears that the catalytic activity was highest for the samples which were easiest to reduce and re-oxidize. Although the particles were larger in $PdB511_{II}$ than in $PdS43_{II}$ (Figure 4.2), the Pd^{2+} fraction profiles and the CH_4 oxidation activity were similar for these two samples. Hence, small differences in Pd particle size do not seem to influence the catalytic performance much. The formation of ion-exchanged Pd^{2+} and large Pd particles (see NaCl-titration and SAXS characterization, Table 4.1 and Figure 4.2) appears to have hampered the reduction and re-oxidation of the Pd in $PdB40_{II}$ which was accompanied by lower CH_4 oxidation activity. Assuming that the CH_4 oxidation reaction occurs according to the Mars-van Krevelen mechanism, which has been suggested by several studies [24, 123-125], it is not surprising that samples with rapid transitions between reduced and oxidized state upon rich-lean pulses express high CH_4 oxidation activity. Very strong Pd-O interactions would be negative for the CH_4 oxidation reaction as more energy would be required for the O adatoms to react with the CH_4 [24, 126]. Slow formation of PdO may limit the CH_4 oxidation rate due to lack of active PdO phase. However, it is not clear what role the ion-exchanged Pd^{2+} has in the reaction. Another possible reason for the low activity of $PdB40_{II}$ is low number of active PdO sites as large parts of the Pd either formed ion-exchanged Pd^{2+} species or large Pd particles with low dispersion. It has previously been indicated that isolated Pd^{2+} species has lower CH_4

oxidation activity than PdO particles [44, 127], although this has yet to be confirmed in more studies.

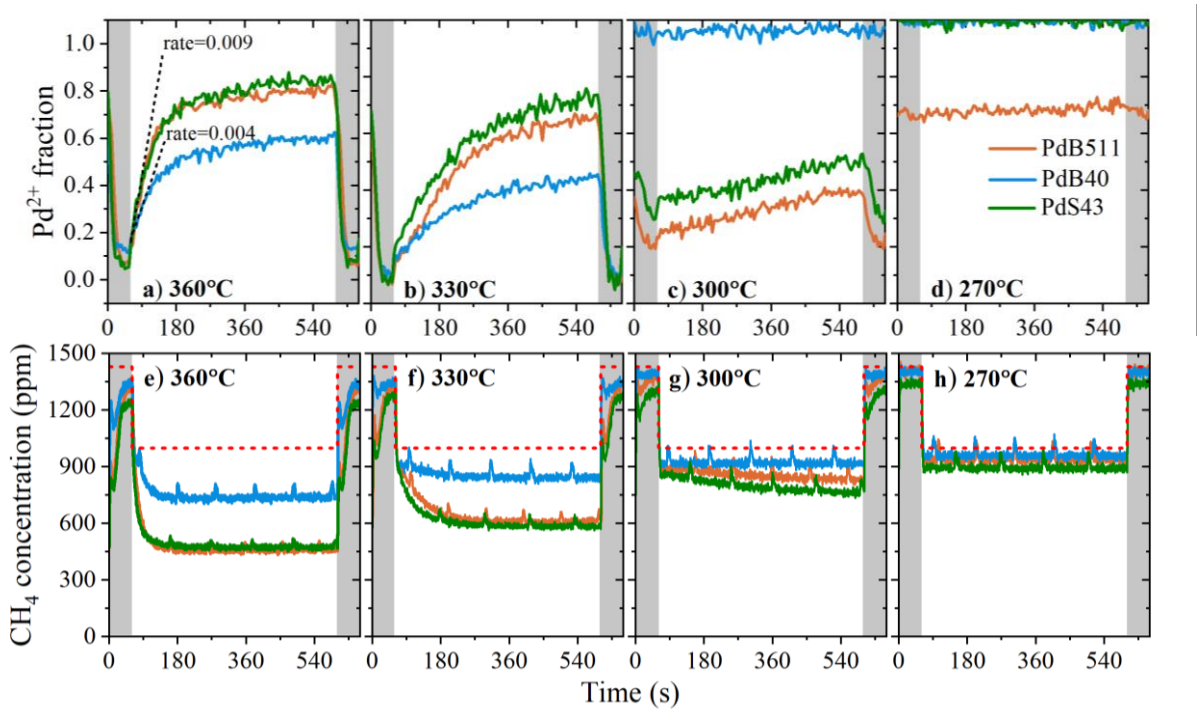

Figure 4.9. Operando XAS data recorded during the rich (CH_4/Ar) and lean (CH_4/O_2/Ar) pulses (9th and 10th rich pulse and 9th lean pulse), **Paper II**. (a-d) Pd^{2+} fraction from LCF of recorded XANES spectra to PdO and Pd^0 reference spectra and (e-h) CH_4 outlet concentration for $PdB511_{II}$ (orange), $PdS43_{II}$ (green) and $PdB40_{II}$ (blue). The sample temperature decreases from left to right, (a, e) 360°C, (b, f) 330°C, (c, g) 300°C and (d, h) 270°C.

The EXAFS spectra seen in Figure 4.10 correspond to the end of the rich and lean pulses. The reduced samples in Figure 4.10a were characterized by intense Pd-Pd peaks at 2.5 Å (phase shift uncorrected) of metallic Pd. Rich pulses at lower temperatures resulted in lower intensity of this peak since the samples only became partially reduced. Fitting of the FT-EXAFS (rich pulse at 360°C) in Figure 4.10a yielded $CN_{Pd\text{-}Pd}$ values of 10.5, 10.0 and 9.5 for $PdB511_{II}$, $PdB40_{II}$ and $PdS43_{II}$, respectively. Hence, it appears that reduction resulted in the formation of large metallic Pd particles. Based on the high $CN_{Pd\text{-}Pd}$ values, these particles are most likely located on the external zeolite surfaces. The FT-EXAFS spectra in Figure 4.10b, (lean pulse 360°C) exhibit peaks at 1.5 Å and 3 Å (phase shift uncorrected), which correspond to the Pd-O and Pd-(O)-Pd scattering paths of PdO, respectively. The Pd-Pd shell of metallic Pd is also contributing to the spectra of the partially oxidized samples. This is probably representing metallic Pd core of large partially oxidized Pd particles.

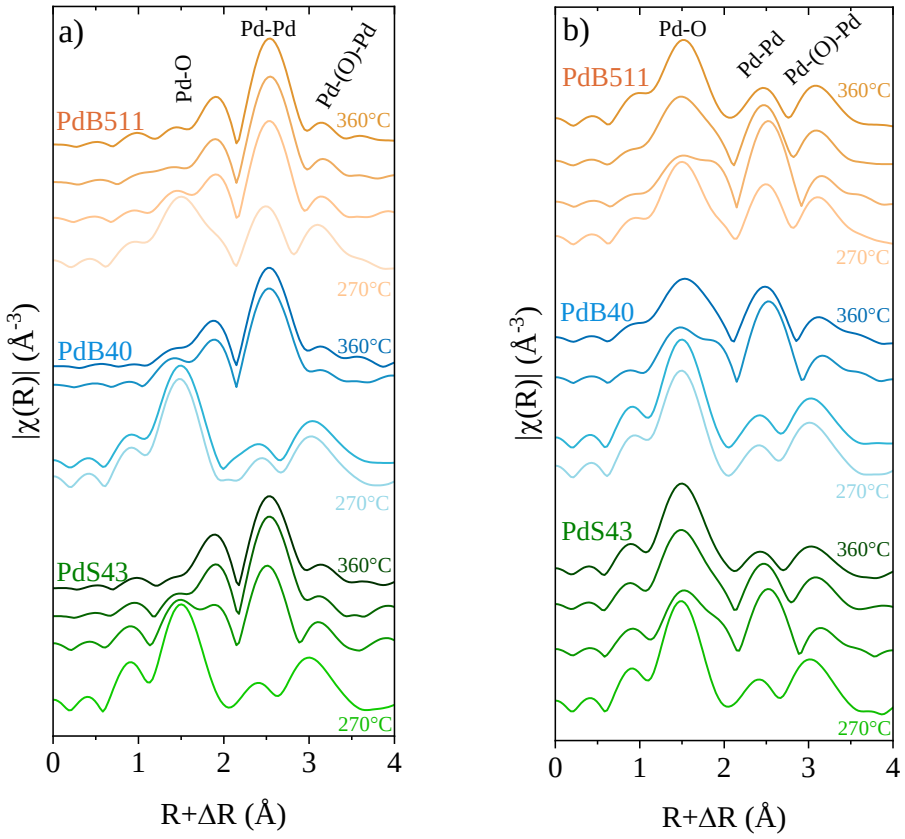

Figure 4.10. Fourier transformed k^2-weighted Pd K-edge EXAFS spectra recorded a) at the end of the rich pulses and b) at the end of the lean pulses, seen in Figure 4.9, for $PdB511_{II}$ (orange), $PdB40_{II}$ (blue) and $PdS43_{II}$ (green), **Paper II**.

The findings in **Paper I** and **Paper II** suggest that PdO particles are more active for CH_4 oxidation than ion-exchanged Pd^{2+} species. Pd/zeolite samples with high number of large Pd particles and isolated Pd^{2+} species were more difficult to reduce and to re-oxidize, which was accompanied with low CH_4 oxidation activity. To maintain high CH_4 oxidation activity it is essential to design the Pd/zeolite catalysts such that the Pd remains as dispersed particles whereas Pd particle agglomeration and formation of ion-exchanged Pd^{2+} are avoided. This can be accomplished by using highly siliceous zeolite supports but is also facilitated for small pore zeolites, such as SSZ-13, as the Pd mobility then will be lower. However, treatment at high temperatures and/or in the presence of water vapor facilitate the formation of isolated Pd^{2+} species also in small pore zeolites which is accompanied by lower CH_4 oxidation activity. Based on the literature, Pd particle stabilization can also be accomplished by forming mesopores in the zeolite support, removal of extra framework alumina [72] and by using zeolites which are fully exchanged with alkali metal ions [72, 73].

4.2 The influence of water vapor and SO_2 on the CH_4 oxidation activity

The CH_4 oxidation was also studied in the presence of water vapor and SO_2 (**Paper I**) which are the major catalyst poisons in the exhaust gases from combustion of CH_4 based fuels. Knowledge of how the catalytic material responds to catalyst poisons is important in order to be able to minimize the deactivating effect and to optimize the regeneration procedures.

4.2.1 The effect of H_2O on the CH_4 oxidation activity

The CH_4 oxidation activity in the presence of water vapor (wet activity) was tested isothermally at 450˚C in **Paper I** and the results are displayed in Figure 4.11. Note that the white areas in this figure represent exposure to a reference wet reaction mixture (500 ppm CH_4, 8 vol.% O_2 and 5 vol.% H_2O), whereas the gas mixture used in the grey areas was different. The grey areas from left to right represent the following modifications of the wet reaction mixture: addition of 500 ppm NO, change to 10 vol.% water vapor and change to 3 vol.% water vapor, respectively.

The $PdAl_I$ sample demonstrated a steady decrease in CH_4 conversion during the entire isothermal activity test sequence. This reflects the typical loss of catalytic activity due to the formation of surface hydroxyl species, which block the active PdO sites [65] and decrease the oxygen mobility between the support material and the Pd and therefore suppress the re-oxidation of Pd [66, 67]. The zeolite supported samples demonstrated not only a marked difference in the initial CH_4 oxidation activity, but also completely different degrees of water deactivation over time. The samples based on highly siliceous zeolites ($PdB511_I$ and $PdB969_I$) showed high and stable CH_4 conversion of around 91-93% and almost no accumulative water deactivation during the first 3 h of exposure to the wet reaction mixture. By contrast, $PdB40_I$ was quickly deactivated during the first hour on stream. Hence, an increased SAR significantly increases the tolerance to water vapor. The same trend was observed for the SSZ-13 supported samples, *i.e.* $PdS52_I$ had higher catalytic activity and less water deactivation compared to $PdS43_I$. We suggest that the high hydrophobicity of the highly siliceous samples results in less hydroxyl formation and water deactivation, which also was suggested by Okumura et al. [44].

After 3 h of experiment, the addition of 500 ppm NO was studied. The addition of NO resulted in suppressed activity for $PdAl_I$, $PdB969_I$ and $PdB511_I$ and slightly enhanced or unchanged activity for $PdB40_I$, $PdS43_I$ and $PdS52_I$. The effect of NO was previously studied by Sadokhina et al. [13] who suggested that the decreased activity was caused by the formation surface compounds which block active sites. However, they also observed a promoting effect when NO was provided together with water vapor. This effect was ascribed to the formation of surface HNO_2 upon the reaction between NO and the hydroxyl species on the surface. Based on the same reasoning, the enhanced activity for $PdB40_I$ upon the introduction of NO may be due to HNO_2 formation because of the high hydroxyl coverage whereas the formation of blocking compounds was favored for the samples with less hydroxyl coverage, *i.e.* $PdAl_I$, $PdB969_I$ and $PdB511_I$. Another interesting observation is that the presence of NO stopped the accumulative water deactivation for all samples. This observation is particularly evident for the $PdAl_I$ sample.

During the last 5 h of experiment in Figure 4.11, the response to different water vapor concentrations was studied by changing the water vapor concentration in steps of 1 h each according to: 5-10-5-3-5 vol.%. All the samples showed an immediate response of higher and lower CH_4 conversion upon the changes to decreased and increased water vapor concentration, respectively. This effect is a result of rapid hydroxylation or dehydroxylation of the catalyst surface. Interestingly, even during this part of the experiment, the $PdB511_I$ and $PdB969_I$ sample did not express any significant accumulative water deactivation, but only the immediate responses to the changes in water vapor concentration. By contrast, the other samples showed

both accumulative deactivation over time and immediate responses to the altered water vapor concentration. Sadokhina et al. [17] have previously suggested that there are two types of hydroxyl species: the first type is responsible for the immediate response and the second type, with higher energy barrier, causes the accumulative water deactivation over time. Thus, almost only the first type of hydroxyl species appears to be formed on the samples based on highly siliceous zeolites ($PdB511_I$ and $PdB969_I$) whereas both hydroxyl types were formed on the other samples. This suggests that an increased hydrophobicity of the zeolite support, *i.e.* increased SAR in this case, impedes the formation of the second type of hydroxyls which is responsible for the accumulative water deactivation.

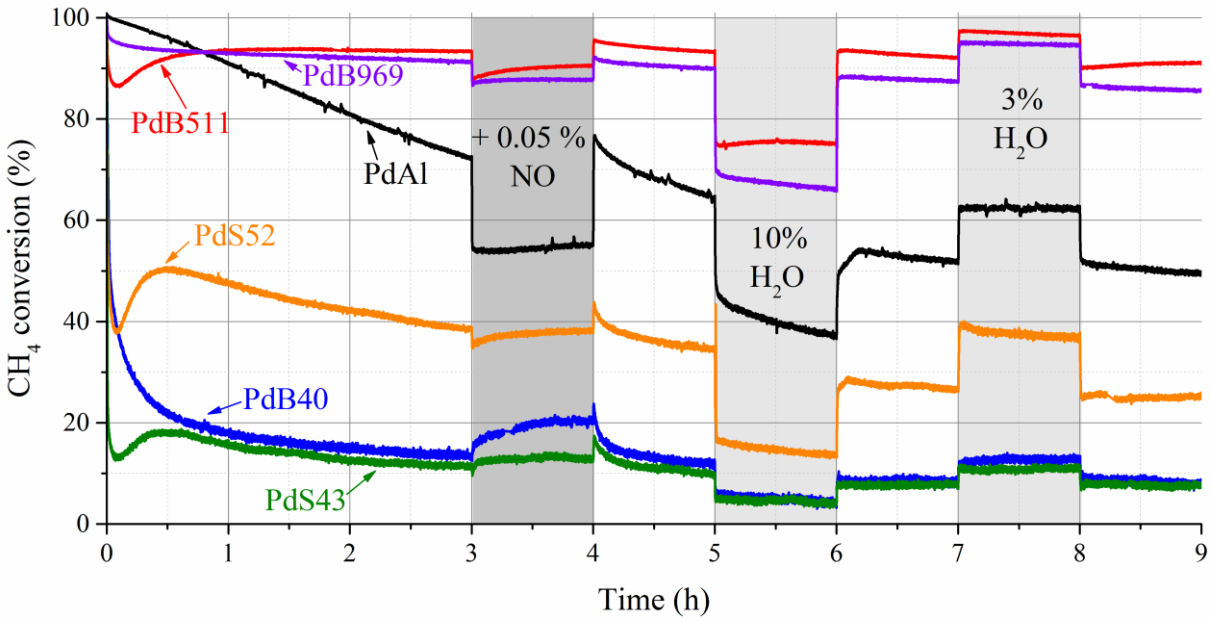

Figure 4.11. Isothermal activity test at 450˚C for $PdB969_I$ (purple), $PdB511_I$ (red), $PdAl_I$ (black), $PdS52_I$ (orange), $PdB40_I$ (blue) and $PdS43_I$ (green). White areas represent wet reaction mixture (500 ppm CH_4, 8 vol.% O_2 and 5 vol.% H_2O). Grey areas from left to right represent: wet reaction mixture + 500 ppm NO; wet reaction mixture but with 10 vol.% H_2O; wet reaction mixture but with 3 vol.% H_2O.

4.2.2 The combined effect of SO_2 and H_2O on the CH_4 oxidation activity

The exhaust gases generated from the combustion of CH_4-based fuels typically contain about 0.5-1 ppm of SO_2 [74], which also is a major catalyst poison. The effect of sulfur was tested by adding 10 ppm of SO_2 to the wet reaction mixture simultaneously as the CH_4 conversion was recorded, see Figure 4.12. To clarify, this experiment followed directly after the experimental sequence shown in Figure 4.11, and the 9th hour is displayed in both Figure 4.11 and Figure 4.12.

The zeolite supported samples expressed a large difference in the SO_2 tolerance compared to $PdAl_I$. The $PdAl_I$ sample showed a slowly progressed deactivation resulting in a linearly decreased CH_4 oxidation during the 4 hours of SO_2 exposure. By contrast, all the zeolite supported samples rapidly lost the majority of the catalytic activity during the first 0.5 h. Hence, the zeolite supported samples were much more sensitive to sulfur than the alumina supported sample. In a previous study, Lampert et al. [7] reported that Pd/SiO_2 deactivates much faster by SO_2 than Pd/Al_2O_3. They suggested that Pd/Al_2O_3 has a higher resistance to SO_2 deactivation

because of the higher SO_2 adsorption on the Al_2O_3 support. The Al_2O_3 support was therefore thought to act as a sulfur sink, thus preventing the formation of $PdSO_x$ species. This may also explain the large differences between the zeolite-based samples and the $PdAl_I$ sample, shown in Figure 4.12, *i.e.* the low SO_2 adsorption on the zeolite supports accelerates the deactivation whereas the high sulfur storage capacity of Al_2O_3 decelerates the deactivation. To confirm this, the sulfur content in SO_2 poisoned samples was measured with ICP-SFMS. The S/Pd ratio was 2.83 and 0.25 for $PdAl_I$ and $PdB969_I$, respectively. This supports the hypothesis that the $PdSO_4$ formation in $PdAl_I$ is impeded due to the high SO_2 adsorption on the Al_2O_3 support whereas the opposite holds for the Pd/zeolite samples.

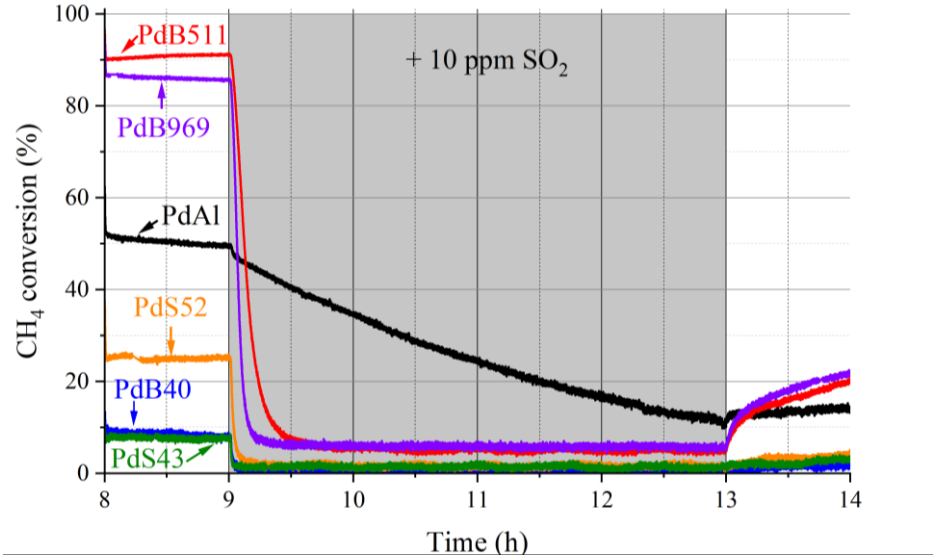

Figure 4.12. Isothermal SO_2 poisoning at 450˚C for $PdB969_I$ (purple), $PdB511_I$ (red), $PdAl_I$ (black), $PdS52_I$ (orange), $PdB40_I$ (blue) and $PdS43_I$ (green). White areas represent wet reaction mixture (500 ppm CH_4, 8 vol.% O_2 and 5 vol.% H_2O). The grey area represents wet reaction mixture + 10 ppm SO_2. Note that the image is the continuation of Figure 4.11.

The possibility to recover the catalytic activity after the SO_2 poisoning was tested with four different regeneration steps. The details for the regeneration steps are given in Table 4.2 and the corresponding CH_4 conversion is shown in Figure 4.13. Note that the regeneration sequence in Figure 4.13 followed directly after the poisoning sequence in Figure 4.12, thus the 14th hour is displayed in both of the figures.

Table 4.2. Regeneration procedures (R1-R4) used in the experiment shown in Figure 4.13.

Regeneration 1 (R1)	Lean regeneration at 600˚C: 1. Heating (20˚C/min) to 600˚C in wet reaction mixture 2. 30 min at 600˚C in wet reaction mixture 3. Cooling (5˚C/min) in wet reaction mixture
Regeneration 2 (R2)	Rich regeneration at 450˚C: 1. 30 min at 450˚C in 500 ppm CH_4 and 5 vol.% H_2O
Regeneration 3 (R3)	Rich regeneration at 600˚C: 1. Heating (20˚C/min) to 600˚C in wet reaction mixture 2. 30 min at 600˚C in 500 ppm CH_4 and 5 vol.% H_2O 3. Cooling (5˚C/min) in wet reaction mixture
Regeneration 4 (R4)	Rich regeneration in H_2 at 600˚C: 1. Heating (20˚C/min) to 600˚C in Ar 2. 5 min temperature stabilization in Ar at 600˚C 3. 30 min at 600˚C in 2 vol.% H_2 and 5 vol.% H_2O 4. Cooling (5˚C/min) in Ar 5. 10 min temperature stabilization in Ar at 450˚C

Already during the first hour after the removal of SO_2 from the inlet feed, *i.e.* in wet reaction mixture at 450˚C, the siliceous beta-based samples ($PdB511_I$ and $PdB969_I$) recovered from 6% to 21% of CH_4 conversion, see Figure 4.13. By contrast, the other samples showed none or only very little recovery during this hour. After the subsequent first regeneration step (R1) at 600˚C under lean conditions, $PdB969_I$ and $PdB511_I$ had regained large part of their activity whereas the other samples only showed a minor increase in catalytic activity. It should be emphasized that water vapor was present in the feed also during the entire regeneration which presumably impeded the activity, especially for $PdAl_I$, $PdB40_I$, $PdS43_I$ and $PdS52_I$. The second regeneration step (R2) was performed at 450˚C under rich conditions, *i.e.* in the absence of O_2. After this step, the SSZ-13 and the Al_2O_3 supported samples obtained activities close to the level before the SO_2 poisoning (compare with Figure 4.12). However, no additional recovery was recorded for the beta supported samples. The third regeneration step (R3) under rich conditions at 600˚C resulted in close to complete regeneration of the $PdAl_I$. The fact that the catalytic activity for $PdAl_I$ was at about the same level as prior to any water vapor or SO_2 exposure (compare with Figure 4.11), indicates that also a large part of the hydroxyls was desorbed during this step. Also, the other samples showed some additional regeneration, but to a lower degree. Furthermore, no significant increase of the CH_4 oxidation activity was recorded for any of the samples after the fourth regeneration step (R4) at 600˚C in H_2 and H_2O. This means that all easily removed sulfur species already were removed in the previous steps.

A general observation from the regeneration sequence was that a large part of the catalytic activity could be regenerated rather easily for the siliceous beta-based samples ($PdB969_I$ and $PdB511_I$). However, it appears to be difficult to completely regenerate these samples. The $PdAl_I$ could almost be completely recovered, however, not as easily as the siliceous beta samples. For the other zeolite supported samples ($PdB40_I$, $PdS43_I$ and $PdS52_I$), it is more difficult to determine whether the lower activity resulted from water and/or sulfur deactivation. However,

it appears that the samples based on highly siliceous zeolites were easier to regenerate than the samples based on zeolites with lower SAR. Lampert et al. [7] also found that the catalytic activity of Pd/SiO_2 could be regenerated more easily compared to Pd/Al_2O_3. Their suggested explanation for this is that the high sulfur storage capacity of the Al_2O_3 support results in more spill-over of sulfur species from the support material to the Pd, which results in formation of more $PdSO_x$ species during the regeneration. Using the same reasoning for the samples herein analyzed, the regeneration of the zeolite supported samples was facilitated by the lesser amount of sulfur species adsorbed on the support material and consequently less sulfur spill-over from the zeolites to the Pd during the regeneration.

To summarize the SO_2 poisoning and regeneration experiments, it is clear that the zeolite supported samples were much more sensitive than Pd/Al_2O_3 to SO_2. We suggest that this is because of the low sulfur storage capacity of the zeolite supports which results in the formation of more $PdSO_x$ species when SO_2 is present in the feed gas. However, large part of the catalytic activity could be regenerated more easily for Pd supported on highly siliceous zeolites, especially in comparison with $PdAl_I$. We suggest that this latter observation is due to low spill-over of sulfur compounds from the support material to the Pd during the regeneration treatment, *i.e.* when SO_2 is not present in feed gas.

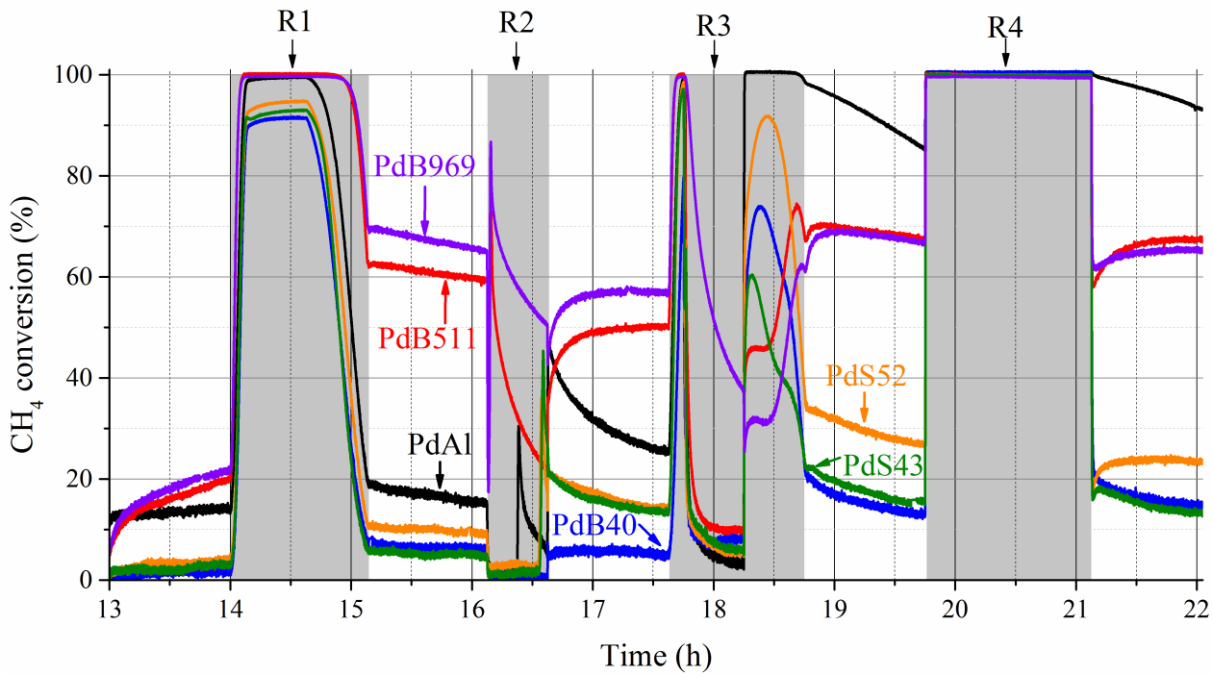

Figure 4.13. Sulfur regeneration sequence for $PdB969_I$ (purple), $PdB511_I$ (red), $PdAl_I$ (black), $PdS52_I$ (orange), $PdB40_I$ (blue) and $PdS43_I$ (green). White areas represent wet reaction mixture (500 ppm CH_4, 8 vol.% O_2 and 5 vol.% H_2O) at 450˚C. Grey areas from left to right represent regeneration step 1-4 (R1-R4), respectively. Detailed descriptions of R1-R4 are found in Table 4.2. Note that the image is the continuation of Figure 4.12.

4.3 Hydrothermal aging

It is known that hydrothermal aging, *i.e.* treatment at high temperature and in the presence of water vapor, of Pd/zeolites may cause formation of ion-exchanged Pd species and/or Pd agglomeration and that this is highly dependent on the type of zeolite used [82, 83]. How this affects the CH_4 oxidation activity is however not well studied. Hydrothermal aging is also likely to result in degradation of the zeolite support. However, it has recently been shown that zeolite LTA has a very high hydrothermal stability [86, 87]. Therefore, the effect of hydrothermal aging at temperatures up to 900°C on the CH_4 oxidation activity over Pd/LTA was studied together with a reference sample of Pd/γ-Al_2O_3 (PdAl) in **Paper III**. The samples were degreened at 600°C and the aging was performed at 700, 800 and 900°C in the presence of water vapor and O_2. The wet CH_4 oxidation activity was evaluated before and after the aging.

4.3.1 Impact on the Pd species and zeolite support material

In order to understand the catalytic performance, the Pd and support material were characterized with XRD, N_2 physisorption and NO-DRIFTS before (*i.e.* after degreening) and after the hydrothermal aging at 900°C. Note that the samples used for characterization were cooled in water vapor and O_2 after the degreening and after the aging to ensure oxidized samples and similar hydroxyl coverage.

Support material

The support materials were evaluated regarding surface area, pore volume and XRD pattern to see how well they were able to sustain the 900°C hydrothermal aging. Table 4.3 shows that the aging only caused minor decrease in surface area and pore volume of the samples.

Table 4.3. Sample information (**Paper III**) regarding Pd content and Si/Al ratio measured by ICP-SFMS together with BET surface area, t-plot micropore volume and BJH pore volume from N_2 physisorption measurements.

	Pd content (wt.%)	Si/Al molar ratio (-)		BET surface area (m^2/g)	Micropore volume (t-plot, cm^3/g)	Pore volume (BJH, cm^3/g)
PdLTA *(Pd/H-LTA)*	2.12	44	Degreened (600°C)	499.8	0.18	0.35
			Aged (900°C)	463.7	0.17	0.32
PdAl *(Pd/γ-Al_2O_3)*	2.21	-	Degreened (600°C)	169.8	0.00	0.50
			Aged (900°C)	123.2	0.00	0.44

The XRD patterns in Figure 4.14 did not show any degradation of the crystalline LTA structure after the 900°C hydrothermal aging. On the contrary, the peak intensity increased slightly meaning that the aging resulted in additional crystallization of the LTA zeolite. Hence, the LTA zeolite exhibited extraordinarily good hydrothermal stability in agreement with previous reports [86, 87]. By comparison, zeolite SSZ-13, which also is known for high hydrothermal stability, has been reported to severely degrade during hydrothermal aging at temperatures > 850°C [84]. Considering the Al_2O_3 support, some changes due to Al_2O_3 phase transition after the aging can

be recognized in the XRD patterns. However, it can be concluded that most of the Al_2O_3 remained in the γ-phase even after 900°C hydrothermal aging.

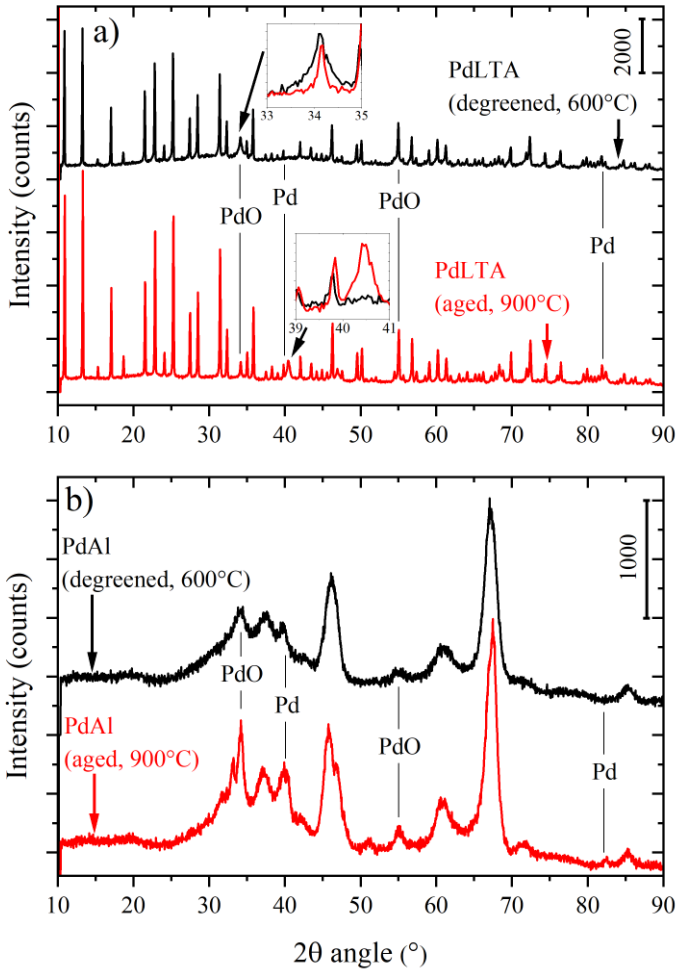

Figure 4.14. XRD patterns of a) PdLTA and b) PdAl. Black lines represent the degreened samples (before aging) and red lines show the 900°C hydrothermally aged samples.

Pd species

The XRD patterns in Figure 4.14 also give information about the crystalline Pd content. For PdAl, both the PdO peaks (2θ=34° and 2θ=55° [60]) and the metallic Pd peak (2θ=40° [60]) increased in intensity and became sharper after 900°C aging, which suggests sintering into larger Pd particles. Some signs of sintering were also found for the PdLTA sample, where a clear peak at 2θ=40.4°, corresponding to metallic Pd, appeared after the aging. Further evidence of Pd sintering upon aging of PdLTA was given by the STEM images in Figure 4.15. Prior to the aging, the particles in PdLTA were about 1-20 nm together with a few larger particles. By contrast, the particle diameter was generally in the range 10-35 nm, in addition to a low number of larger and smaller particles, after the aging. The Pd in PdAl became severely sintered during the aging, based on the STEM images in Figure 4.15. Prior to the aging the Pd particles were about 2-6 nm whereas their diameter increased to 20-60 nm during the 900°C hydrothermal aging. Hence, evidences of sintering upon 900°C hydrothermal aging was found with XRD and STEM for both PdLTA and PdAl.

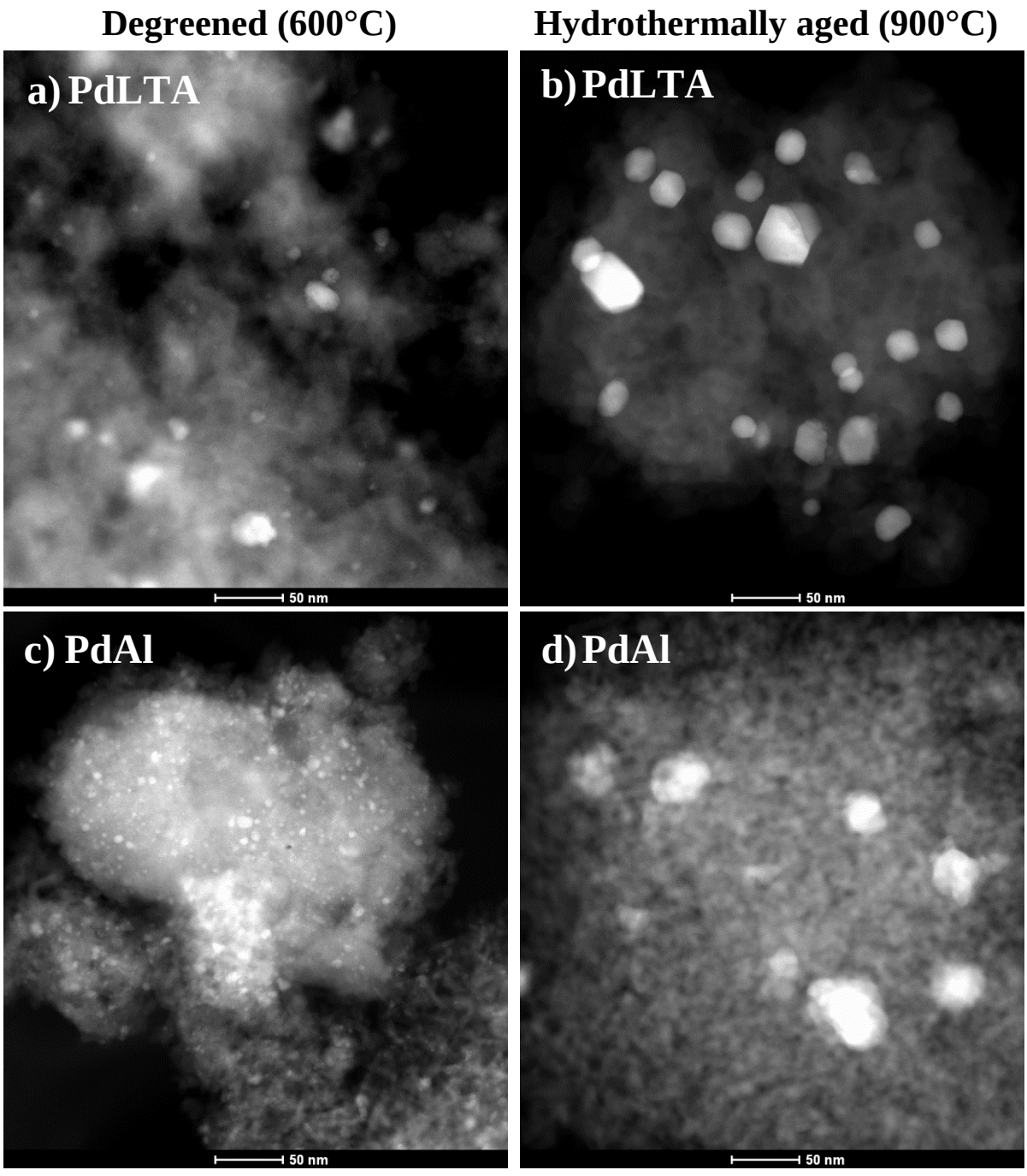

Figure 4.15. STEM images of PdLTA (a, b) and PdAl (c, d). The left column (a, c) represent degreened samples (before aging) and the right column (b, d) show 900°C hydrothermally aged samples.

The formation of ion-exchanged Pd^{2+} was analyzed with NO-DRIFTS. The presence of monoatomic Pd^{2+} species can be confirmed by the formation nitrosyl groups. The spectra in Figure 4.16 clearly show that the aging resulted in significantly increased IR absorbance at the wave numbers 1814 cm^{-1} and 1864 cm^{-1}, which correspond to nitrosyls on isolated Pd^{2+} species [82, 115-118]. Hence, it can be concluded that hydrothermal aging at 900°C caused extensive formation of ion-exchanged Pd^{2+}.

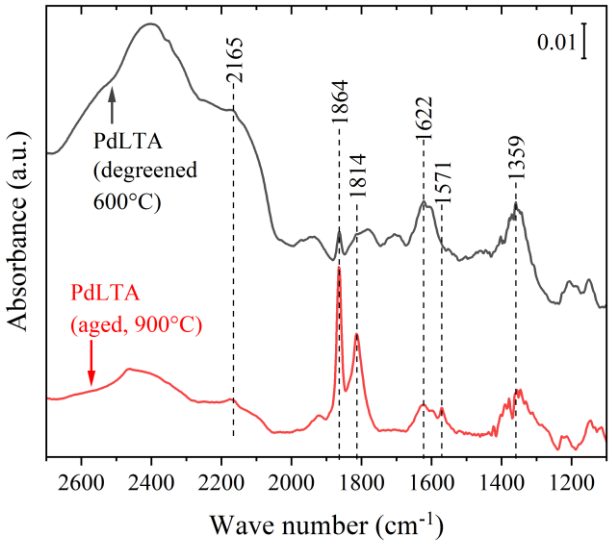

Figure 4.16. DRIFTS spectra of PdLTA acquired after 60 min exposure to NO. The black line represents the degreened samples (before aging) and the red line show the 900°C hydrothermally aged samples.

4.3.2 Methane oxidation activity after hydrothermal aging

The CH_4 oxidation activity was tested before and after hydrothermal aging at and 700, 800 and 900°C which is shown in Figure 4.17. Degreened PdLTA, *i.e.* prior to aging, showed close to 100% CH_4 conversion in the presence of water vapor and no deactivation over time. The activity was still high but slightly decreased, after aging at 700°C. By contrast, the hydrothermal aging at higher temperatures (800°C and 900°C) resulted in significantly lower CH_4 oxidation activity for PdLTA. Since neither the XRD or the N_2 physisorption results showed any major degradation of the LTA support, we suggest that the lower activity and increased sensitivity to water vapor are results of ion-exchanged Pd^{2+} formation and Pd sintering which were observed by XRD, STEM and NO-DRIFTS.

PdAl expressed a close to linear decrease in CH_4 oxidation activity over time. This activity drop is typical for wet CH_4 oxidation over Al_2O_3 supported Pd and occurs due to the accumulation of hydroxyls on the catalyst surface [6] which block active PdO sites [65] and/or decrease oxygen transfer from the support to the Pd [66, 67]. The hydrothermal aging did not impact the CH_4 oxidation activity of PdAl much. Only a slight deactivation could be seen, which may result from Pd sintering and/or that some of the Al_2O_3 underwent phase transition (Figure 4.14-4.15).

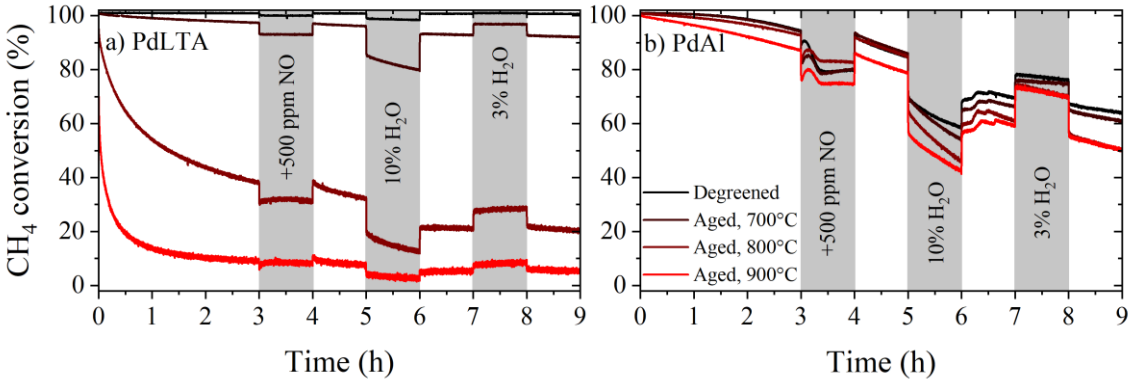

Figure 4.17. Isothermal activity test at 450˚C for a) PdLTA and b) PdAl after degreening and aging at 700, 800 and 900°C. White areas represent wet reaction mixture (500 ppm CH_4, 8 vol.% O_2 and 5 vol.% H_2O). Grey areas from left to right represent: wet reaction mixture + 500 ppm NO; wet reaction mixture but with 10 vol.% H_2O; wet reaction mixture but with 3 vol.% H_2O.

Pd/H-LTA is a promising catalytic material for CH_4 oxidation based on the characterization and the catalytic activity results shown here. In particular due to the high hydrothermal stability of the LTA zeolite. The CH_4 oxidation activity in the presence of water vapor of PdLTA was excellent when treated at temperatures ≤ 700°C. However, one major challenge for zeolite supported Pd is Pd rearrangement during hydrothermal aging, which was prominent at temperatures ≥ 800°C for PdLTA. This resulted in Pd sintering and formation of ion-exchanged Pd^{2+} species which decreased the CH_4 oxidation activity and increased the sensitivity against water vapor. It should be noted that similar concurrent formation of large Pd particles and ion-exchanged Pd^{2+} during hydrothermal aging also has been reported to occur for Pd/SSZ-13 [82, 83]. For zeolites with larger pores, such as beta and ZSM-5, hydrothermal aging seems to primarily result in Pd sintering [83]. Hence, deactivating Pd rearrangement appears to be a general challenge for hydrothermally aged Pd/zeolite materials.

5 Barium promoted Pd/Al_2O_3 for complete CH_4 oxidation

This section concerns Ba promoted Pd/Al_2O_3 samples. Previous studies have shown that it is possible to enhance the CH_4 oxidation activity by the addition of alkali and alkaline earth metal promoters to the catalytic material [60, 128]. This was evaluated in **Paper IV** by the addition of 0.5-2 wt.% of Ba to Pd/Al_2O_3. The main focus was to elucidate the possible promoting effect and how the tolerance to water vapor was affected by the Ba addition. Note that the samples were degreened and pre-treated prior to the characterization and the activity test. To simplify, Pd/Al_2O_3 will hereafter be referred to as "*PdAl*" and Pd/Al_2O_3 modified with 0.5, 1 and 2 wt.% Ba will be denoted "*PdAl-0.5Ba*", "*PdAl-1Ba*" and "*PdAl-2Ba*", respectively.

5.1 Promoting properties of Ba in Pd/Al_2O_3

5.1.1 Influence on the oxidation state of Pd

Alkali metals and alkaline earth metals can serve as electronic promoters in heterogeneous catalysts due to their electron donating properties [53, 58]. Thus, the addition of a proper amount of Ba to Pd/Al_2O_3 may increase the chemisorptive bond strength between the Pd metal and electron accepting adsorbents, such as oxygen, due to an increased electron density on the Pd surface. Since PdO serves as the active phase for CH_4 oxidation, such Ba induced electronic promotion may therefore impact the catalytic performance. In order to examine this possible promoting effect, the oxidation state of the Pd was analyzed with ex-situ XPS and potential changes in the stability of PdO were investigated with TPO and TPR. In addition to this, the CH_4 oxidation activity was evaluated under dry conditions, *i.e.* in the absence of water vapor and other catalyst pollutants in the inlet gas feed.

The acquired XPS spectra are presented in Figure 5.1. It can easily be seen that there were no clear differences in the oxidation state of the Pd amongst the samples. The Pd in all samples existed mainly in its metallic state since all the spectra expressed a doublet peak with maxima at 335.2 eV and 340.45 eV, which correspond to the binding energy of the $3d_{5/2}$ and $3d_{3/2}$ electrons in metallic Pd [129, 130]. However, the slight asymmetry of the peaks towards higher energies demonstrated the presence a small fraction of Pd^{2+}, which $3d_{5/2}$ electrons have a binding energy of 336.7 eV [129, 131]. In general, electronic promotion from the Ba would have been reflected by shifted binding energies of the Pd3d electrons either towards higher energies due higher fraction of Pd^{2+} [60], *i.e.* larger ratio of PdO/Pd, or towards lower energies

as strong electronic promotion could increase the electron density around PdO with a resulting decrease of the binding energy [61, 132].

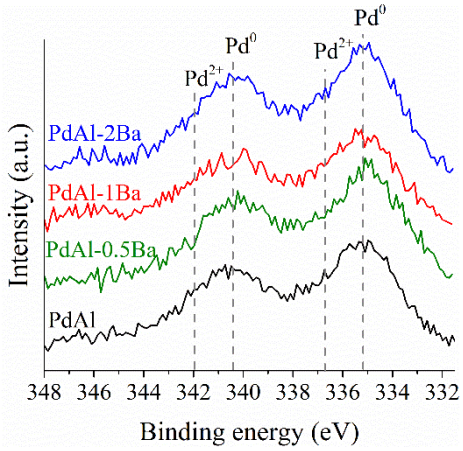

Figure 5.1. XPS specta for Pd3d. From bottom to top: PdAl (black), PdAl-0.5Ba (green), PdAl-1Ba (red) and PdAl-2Ba (blue). The catalyst powders were degreened and O_2 pre-treated prior to analysis.

Further insights in how the Ba addition influences the stability of the PdO were gained from the TPO and TPR analysis. It can be observed in the TPO patterns in Figure 5.2a, that the maximum O_2 consumption, corresponding to the oxidation of the metallic Pd, occurred at around 339˚C for all samples. Hence, no differences between the samples could be demonstrated with TPO. Neither could any clear differences be observed in the TPR patterns, presented in Figure 5.2b. The first CH_4 consumption peak, corresponding to the reduction of PdO, occurred at approximately 203˚C for all samples. Thus, the TPR and TPO analysis showed no evidences for that the addition of Ba would influence the chemisorptive bond strength in Pd-O. It should also be clarified that the steady decrease in CH_4 concentration at temperatures >350˚C in the TPR patterns is associated to the steam reforming reaction, water gas shift reaction and coke formation.

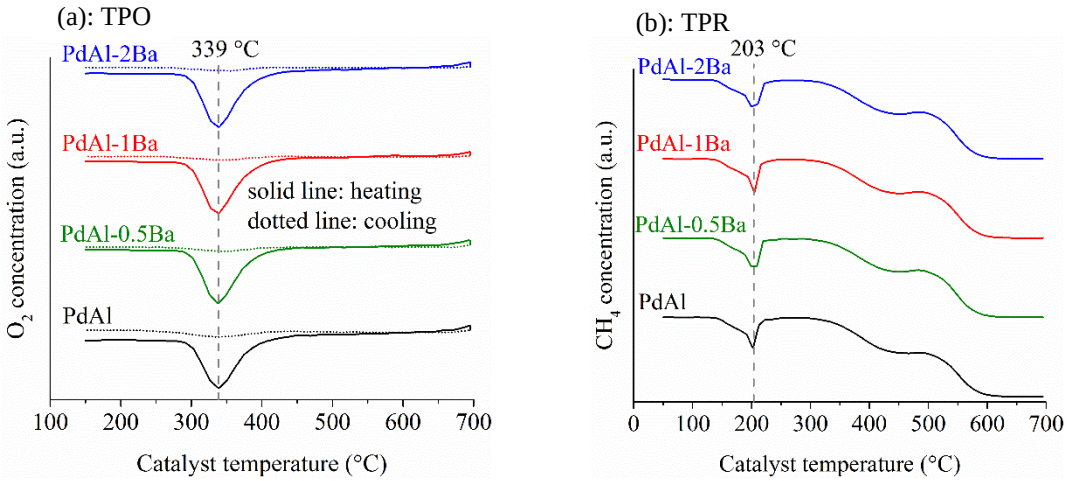

Figure 5.2. Temperature programmed oxidation (TPO) (a) and temperature programmed reduction (TPR) (b). From bottom to top: PdAl (black), PdAl-0.5Ba (green), PdAl-1Ba (red) and PdAl-2Ba (blue). The solid lines represent heating and dotted lines cooling.

In summary, none of the used characterization techniques (XPS, TPO and TPR) showed any signs of Ba induced electronic promotion of the Pd. There are a few examples in the literature,

where electronic promotion by Ba has been demonstrated [59-61, 132]. Thevenin et al. [60] could demonstrate this effect using Pd/Al_2O_3 modified with 3 wt.% Ba (*i.e.* slightly higher Ba loading than the samples analyzed in **Paper IV**), but only after thermal treatment at 1000˚C and not after gentler treatment at 500˚C. Moreover, other studies where electronic promotion was observed are based on samples with higher Ba loading (4 wt.% or more) [61, 132]. Thus, the reason for that no electronic promotion could be demonstrated for the samples studied in **Paper IV** may be that the samples were not treated at sufficiently high temperature and/or that a Ba loading of 2 wt.% was not high enough to provide this effect.

5.1.2 Influence on the Pd particle size

Potential structural changes of the Pd particle size due to the addition of Ba was further investigated with STEM. The samples were degreened at high temperature (700˚C), under alternating rich and lean conditions and in the presence of water vapor, prior to the STEM analysis (see Section 3.3.3). Most certainly, this treatment resulted in some degree of Pd particle sintering. The STEM images in Figure 5.3, reveal that the Pd particle morphology was similar for all samples, despite the addition Ba promoter. The average Pd particle diameter was estimated to around 8-9 nm for all samples, *i.e.* it appears that the addition of Ba did not influence the degree of Pd sintering. This also agrees well with previously reported observations [60]. Moreover, also the Ba distribution in the promoted samples was analyzed with EDX. However, only very little Ba could be detected although several areas were analyzed. Hence, it appears that the Ba was well dispersed in the catalytic material.

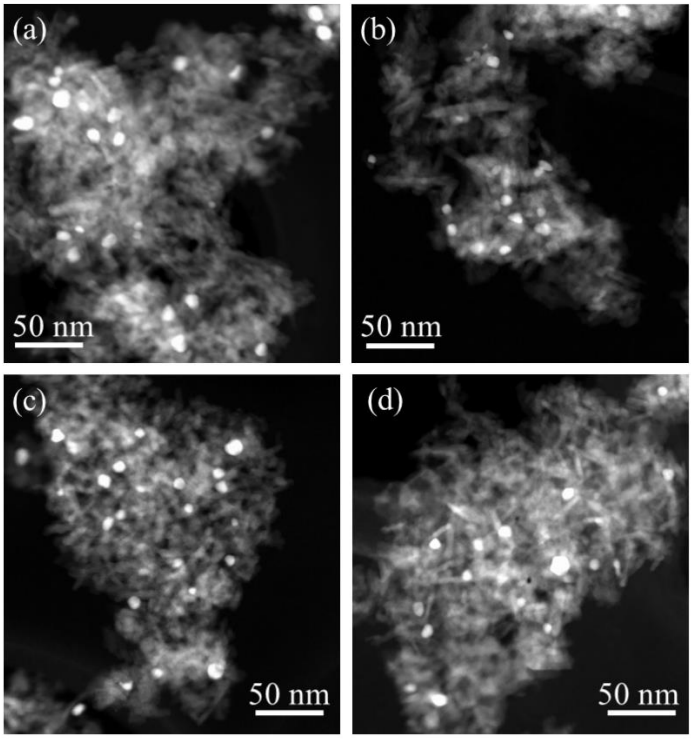

Figure 5.3. STEM images of degreened and O_2 pre-treated catalyst powder of a) PdAl, b) PdAl-0.5Ba, c) PdAl-1Ba and d) PdAl-2Ba.

5.1.3 Methane oxidation activity in the absence of water vapor

The CH_4 oxidation activity was tested in dry reaction mixture (500 ppm CH_4 and 8 vol.% O_2) in order to study the effect of the Ba addition in the absence of catalyst poisons. All samples were first degreened, then pre-treated in O_2 at 700˚C and subsequently cooled in Ar to 150˚C prior to the activity test. Thereafter, the dry reaction mixture was introduced to the reactor while the temperature was ramped (5˚C/min) up to 700˚C. After temperature stabilization at 700˚C, the reactor was cooled (5˚C/min) to 150˚C, also in dry reaction mixture. This heating-cooling cycle was repeated two times.

The CH_4 conversion data corresponding the temperature programmed reaction cycles for PdAl and PdAl-2Ba are presented in Figure 5.4. In general, no noteworthy differences could be distinguished between the two samples. The small hysteresis between the heating and cooling ramp in first cycle is most likely associated to small differences in the oxidation state of Pd, which also has been suggested previously [14]. However, this hysteresis effect leveled out in the second cycle, where the activity was about the same during heating and cooling. These results demonstrate that no enhanced catalytic activity was provided from the Ba under dry conditions. Hence, this agrees well with the previously presented characterization results, *i.e.* that the addition of up to 2 wt.% Ba to Pd/Al_2O_3 does not provide any electronic promotion and, consequently, does not impact the catalytic activity under dry conditions.

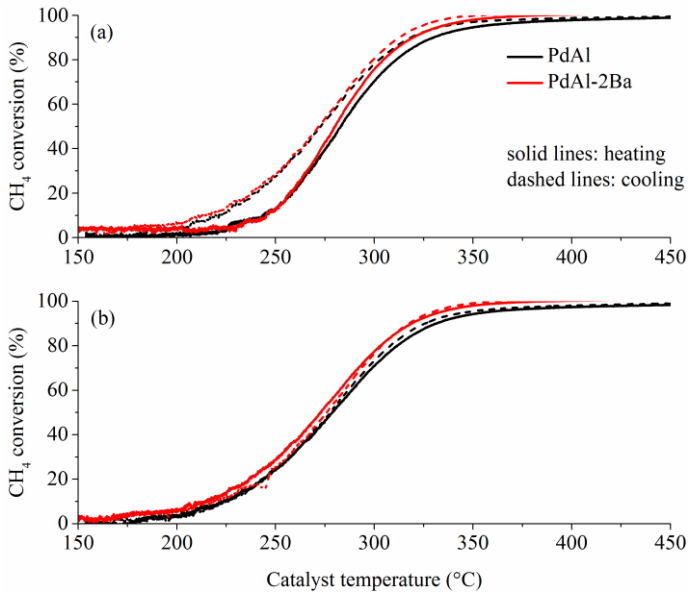

Figure 5.4. Temperature programmed catalytic activity test in dry reaction mixture (500 ppm CH_4 and 8 vol.% O_2), a) first cycle and b) second cycle. The black lines represent PdAl and the red PdAl-2Ba. The CH_4 conversion at heating is shown with solid lines and dashed lines are used for cooling.

5.2 Impact of water vapor on Ba promoted Pd/Al_2O_3

It is well known that the presence of water vapor severely deactivates Pd-based catalysts for CH_4 oxidation [6]. Water vapor is an unavoidable component in the exhaust gases generated

from combustion of CH_4-based fuels and is normally found within the concentration range of 10-15% [6]. Consequently, it is necessary to develop catalytic systems that can resist water deactivation. Another desirable property, next to native low levels of water deactivation, is the feasibility of occasional regeneration of the catalytic activity after the exposure to water vapor containing exhaust gases. The optimal gaseous conditions for efficient regeneration of water deactivated Pd catalysts are not clear based on previous literature. For instance, it has been reported that regeneration in air is more efficiently than regeneration in inert N_2 [69], but also the opposite has been observed [133]. However, it is commonly accepted that the degree of catalytic recovery increases with higher regeneration temperatures [68-70], due to more hydroxyl desorption. The influence on the tolerance to water vapor and the possibility for catalytic activity regeneration by an addition of Ba to Pd/Al_2O_3 were investigated with flow reactor experiments and by studying the water adsorption/desorption with DRIFTS.

5.2.1 Methane oxidation activity in the presence of water vapor

The CH_4 oxidation activity over the Ba promoted samples (PdAl-0.5Ba, PdAl-1Ba and PdAl-2Ba) and the PdAl reference sample was tested isothermally at 450˚C in wet reaction mixture for 3 h. This was followed by a wet regeneration step by heating the catalyst to 700˚C in Ar, exposing the catalyst at to O_2 and H_2O for 15 min at 700˚C and thereafter cooling the catalyst to 450˚C, also in O_2 and H_2O. This cycle of activity test followed by a regeneration step was repeated three times, however, the regeneration temperature was 600˚C and 500˚C for the second and third cycle, respectively. Finally, the CH_4 oxidation activity was tested once again at 450˚C in wet reaction mixture[4].

By observing the CH_4 conversion in Figure 5.5, corresponding to the experimental scheme described above, it becomes clear that the Ba addition had a significant impact on the CH_4 oxidation activity when water vapor was present in the gas feed. The catalytic activity dropped for all the samples during the first 3 h of the exposure to the wet reaction mixture due to the formation of surface hydroxyls. However, the Ba promoted samples expressed much lower degree of water deactivation than the PdAl sample. The same trend of less water deactivation for the Ba promoted samples was also expressed in the following parts of the experiment. Hence, an addition of Ba to Pd/Al_2O_3 can improve the tolerance to water vapor. These results are different to what was observed for the activity test in the dry reaction mixture (Section 5.1.3). In the absence of water vapor, no change in catalytic activity could be associated to the addition of Ba. From this observation together with the results from XPS, TPO, TPR and TEM, discussed in Section 5.1, it was concluded that the addition of Ba does not result in electronic promotion, altered PdO/Pd ratio or changed morphology of the Pd particles. Hence, other phenomena must cause the enhanced catalytic performance of the Ba promoted samples under wet conditions seen in Figure 5.5.

It can also be seen in Figure 5.5 that the possibility to regenerate the catalytic activity after water deactivation was influenced by the addition of Ba promoter. In general, treatment at

[4] Entire experimental scheme: Activity test 450˚C- Wet regeneration 700˚C - Activity test 450˚C - Wet regeneration 600˚C - Activity test 450˚C - Wet regeneration 500˚C - Activity test 450˚C.

higher temperatures resulted in higher degree of activity recovery, as expected [68-70], due to more hydroxyl desorption. It should also be emphasized that the heating ramp in Ar, *i.e.* in the absence of water vapor, during the regeneration step most likely resulted in more hydroxyl desorption. Regeneration at 700˚C resulted in close to complete recovery of the activity for all the samples, whereas regeneration at lower temperatures, *i.e.* 600˚C and 500˚C, was not as efficient. However, for the samples with highest Ba loading (PdAl-1Ba and PdAl-2Ba) the regeneration at 500˚C was almost as efficient as regeneration at 600˚C. This was very different from the sample with the lowest Ba loading (PdAl-0.5Ba) and the PdAl reference, which almost showed no activity recovery after the regeneration at 500˚C. Hence, the addition of Ba to Pd/Al_2O_3 does not only suppress the water deactivation, but it also facilitates the regeneration of the catalytic activity after water deactivation, especially using lower regeneration temperatures.

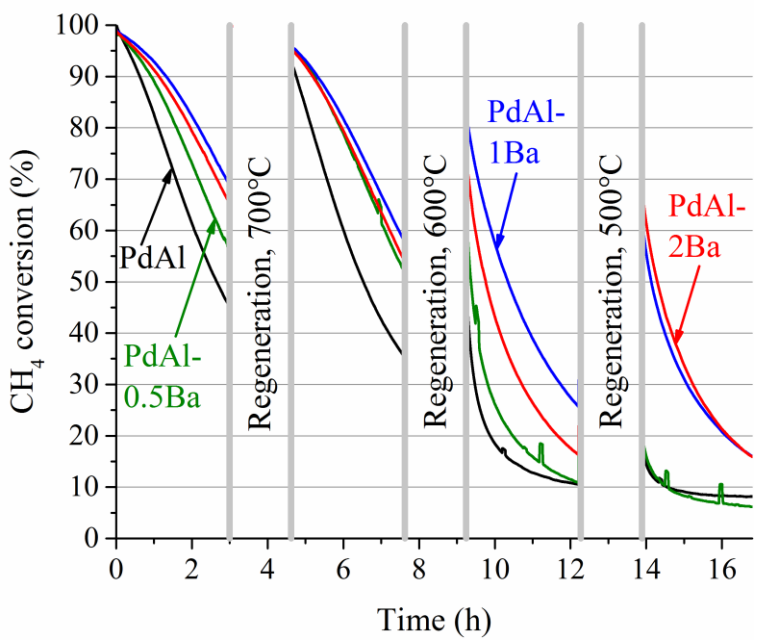

Figure 5.5. Methane oxidation activity test in wet reaction mixture (500 ppm CH_4, 5 vol.% H_2O and 8 vol.% O_2) in steps of 3 hours alternated with wet regeneration steps (5 vol.% H_2O and 8 vol.% O_2) at 700, 600 and 500˚C. It should be noted that the heating ramps in the regenerations were performed in Ar only.

5.2.2 Water adsorption and desorption for Ba promoted Pd/Al_2O_3

More information about the hydroxyl formation on the catalyst surface was obtained by studying the water adsorption/desorption with DRIFTS. This was accomplished by exposing the PdAl-2Ba and PdAl samples to H_2O and O_2 for 2 h at 550˚C and thereafter remove the H_2O from the gas for another 3 h at 550˚C. Note that the samples were degreened and pre-treated in the flow reactor prior to the DRIFTS experiment and then pre-treated once again in O_2 at 550˚C in the DRIFTS cell in order to ensure completely oxidized samples before the introduction of the H_2O. The background spectrum for respective sample was acquired at the end of this O_2 pre-treatment step.

The bottom spectra displayed in Figure 5.6 represent the hydroxyl build up on the catalyst surface of PdAl-2Ba and PdAl, whereas the topmost spectra show the water desorption in the water vapor free gas feed. The presence of surface hydroxyl species is reflected by the absorbance in the wave number region of 2500-3800 cm^{-1}. This feature was rapidly evolved upon the exposure of the water vapor containing gas feed. Indeed, the major part of the surface hydroxylation occurred already during the first 10 min, for both samples. When the water vapor was removed from the gas feed after 120 min, the absorbance in this region decreased gradually during about 90 min. Hence, the formation of surface hydroxyls was much faster than the desorption at the same temperature, for both samples.

Absorbance peaks at around 3732, 3699 and 3549 cm^{-1} have previously been ascribed to terminal, bridged and multi-bound hydroxyl species, respectively, on PdO and its interfaces towards the alumina support [69, 133, 134]. These absorbance bands agree well with the peaks shown in Figure 5.6. Hence, the common peaks for both samples at 3728 cm^{-1} and 3690 cm^{-1} are ascribed to terminal and bridged hydroxyls, respectively. The broader and more intense feature, at around 3549 cm^{-1} for PdAl-2Ba and 3534 cm^{-1} for PdAl, is associated to multi-bound hydroxyl species. Absorbance by the hydroxyls formed on the Al_2O_3 support may also contribute to the spectra, however, some authors have reported that these are more difficult to distinguish due to much lower intensity [69, 134]. In either case, the PdAl-2Ba and PdAl samples can be expected to express common features for the hydroxyls formed on the PdO and its interfaces as well as on the bare Al_2O_3 support whereas differences in the DRIFTS spectra may originate from hydroxyls formed on the Ba or its interface towards the Al_2O_3 and/or PdO. However, no obvious differences are distinguishable by comparison of the acquired spectra. One possible reason for this is that only a relatively small part of the total number of hydroxyl species on the catalyst surface are formed on the Ba or on its interfaces, which therefore could be difficult to recognize in the DRIFTS spectra. This means that the formation of for instance $Ba(OH)_2$ cannot be excluded.

Although, no clear difference in the adsorption/desorption rate of water or the type of formed hydroxyls could be pinpointed with the DRIFTS analysis, the fact that an addition of Ba to Pd/Al_2O_3 can enhance both the tolerance to water deactivation and the regeneration of the catalytic activity remains. However, it cannot be excluded that the hydroxyls are formed on or in connection to the Ba, which might influence the surface chemistry and affect the mechanism of water deactivation.

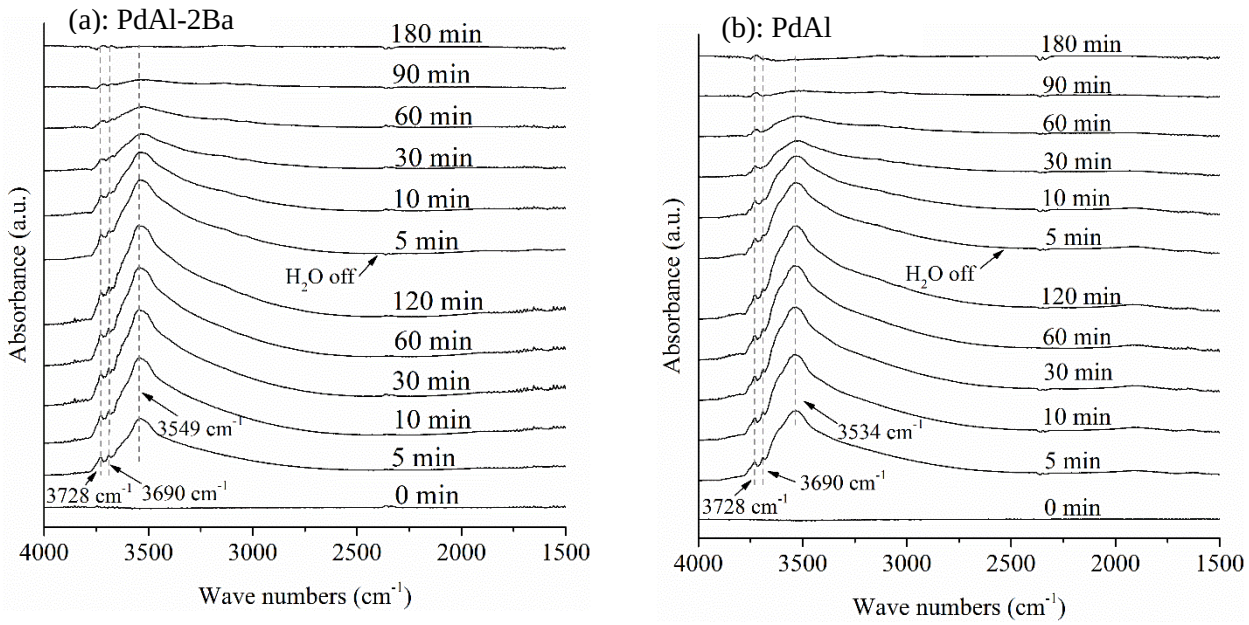

Figure 5.6. DRIFTS spectra showing water adsorption/desorption on a) PdAl-2Ba and b) PdAl. The spectra were collected during 120 min exposure to 1 vol.% H_2O and 2 vol.% O_2 (bottom spectra) followed by 180 min of 2 vol.% O_2 at 550˚C. The shown spectra were corrected by the background spectrum of oxidized samples at 550˚C.

6 Methane oxidation over Pd/Al_2O_3 under stoichiometric conditions

The catalytic behavior of CH_4 oxidation over Pd/Al_2O_3 under lean conditions has been extensively investigated. The catalytic performance using lower O_2 levels is less well investigated. Knowledge about this is however important in order to efficiently clean the exhaust gases from engines operated at stoichiometric lambda values. This section gives an overview of the catalytic performance of Pd/Al_2O_3 using a feed gas with stoichiometric CH_4 and O_2 concentrations, *i.e.* $1CH_4{:}2O_2$ relation. This was studied in **Paper V** by isothermal activity tests at different temperatures using different gas compositions.

6.1 Stoichiometric methane oxidation in the presence of water vapor

The CH_4 conversion of Pd/Al_2O_3 tested at constant temperature of 425, 450 and 500°C is shown in Figure 6.1. During the first 5 hours, a gas feed consisting of 500 ppm CH_4, 1000 ppm O_2 and 5 vol.% water vapor (stoichiometric reaction mixture) was used. The progressive loss of catalytic activity during this period is due to accumulation of OH species on the catalyst surface. After 5 hours of catalyst testing, the water vapor concentration was altered in steps of 1, 3, 7 and 9 vol.%. This resulted in immediate responses of enhanced and inhibited CH_4 oxidation activity when the water vapor concentration was decreased and increased, respectively. This illustrates the rapid adsorption of H_2O and formation of OH which has been described as one of the two routes of water inhibition for Pd-based catalysts. The second route is the slow accumulative water deactivation route [17, 71]. It is also noteworthy that both these water deactivation routes were severer at lower temperatures, which also has been reported previously [65]. In the consecutive parts of the experiment it can be observed that an increased O_2 content enhanced the activity, which agrees with previously reported results [14], and that higher CH_4 conversion was obtained when decreasing the CH_4 concentration. The latter observation is probably a result of that the decreased CH_4 concentration resulted in a lean gas mixture and that the lower number of CH_4 molecules may have matched the number of active PdO sites better.

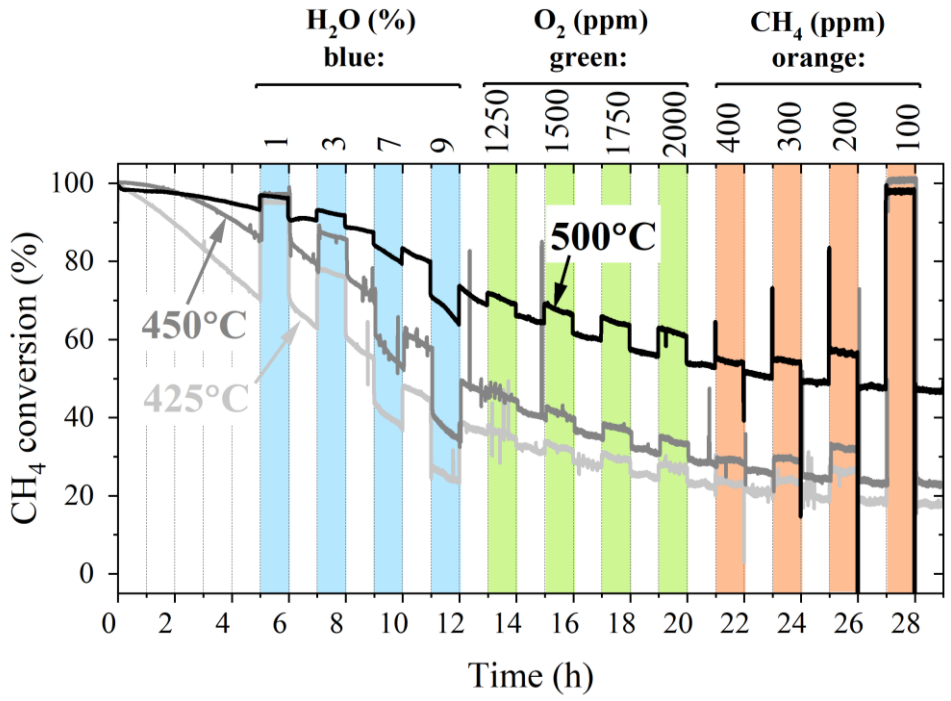

Figure 6.1. Isothermal methane oxidation activity over 3.8 wt.% Pd/Al_2O_3 at 425, 450 and 500°C. White areas represent stoichiometric reaction mixture (500 ppm CH_4, 1000 ppm O_2 and 5 vol.% H_2O) and the colored areas correspond to stoichiometric reaction mixture with the modifications given on top of the figure.

Another similar isothermal CH_4 oxidation experiment was performed, however, the sequence of modified O_2, CH_4 and H_2O concentrations was different compared to the experiment shown in Figure 6.1. The results are displayed in Figure 6.2 and the tested temperatures were 450, 500 and 550°C. Here, the typical activity loss due to accumulative OH formation was also observed during the first 5 hours in the stoichiometric reaction mixture. After 5 hours, the O_2 level was decreased to 500 ppm giving a rich feed gas composition. This resulted in a rapid increase to 100% CH_4 conversion for all tested temperatures. It is known that a low O_2 content generally gives lower CH_4 oxidation activity [14, 26, 135]. However, the reason for the opposite results shown here may be large CH_4 consumption in the steam reforming reaction. In complete absence of O_2, the steam reforming reaction typically occurs at >~ 350°C [13, 14], hence it is reasonable that it occurs at temperatures ≥ 450°C under $1CH_4$:$1O_2$ conditions. When the O_2 level was changed back to 1000 ppm after 6 hours of the experiment, the activity dropped to ca. 10-20% at 500-550°C and to ca. 55-60% at 450°C. Hence, the activity was considerably lower after the rich step than before. This indicates substantial loss of active PdO sites. We suggest that this significant deactivation is due to PdO reduction during the rich step, resulting in metallic Pd with low activity [12]. The PdO reduction is less efficient at lower temperatures which explains the milder deactivation observed at 450°C. The PdO reduction for Pd/Al_2O_3 has been reported to occur at ca. 500°C in stoichiometric feed gas (1300 ppm CH_4, 7000 ppm CO, 1600 ppm NO and 5300 ppm O_2) [136], which is close to the temperatures used for this experiment in Figure 6.2. It has also been demonstrated that the re-oxidation of metallic Pd is poor under stoichiometric conditions [136], which explains why the activity remains at about the same low level for the rest of the experimental sequence. However, surface hydroxyls may

also have contributed to the poor activity. This observed deactivation due to PdO reduction is normally not a problem under lean conditions as the PdO then is stable at temperatures up to ca. 700°C and metallic Pd is easily re-oxidized at lower temperatures [137].

The samples tested at 500-550°C gave very mild responses to the consecutive steps of different CH_4 and H_2O concentrations, which probably was due to the already poor activity. However, the sample tested at 450°C was not as deactivated which made it slightly more sensitive to the changes in CH_4 and water vapor concentration and the responses were similar to those seen Figure 6.1.

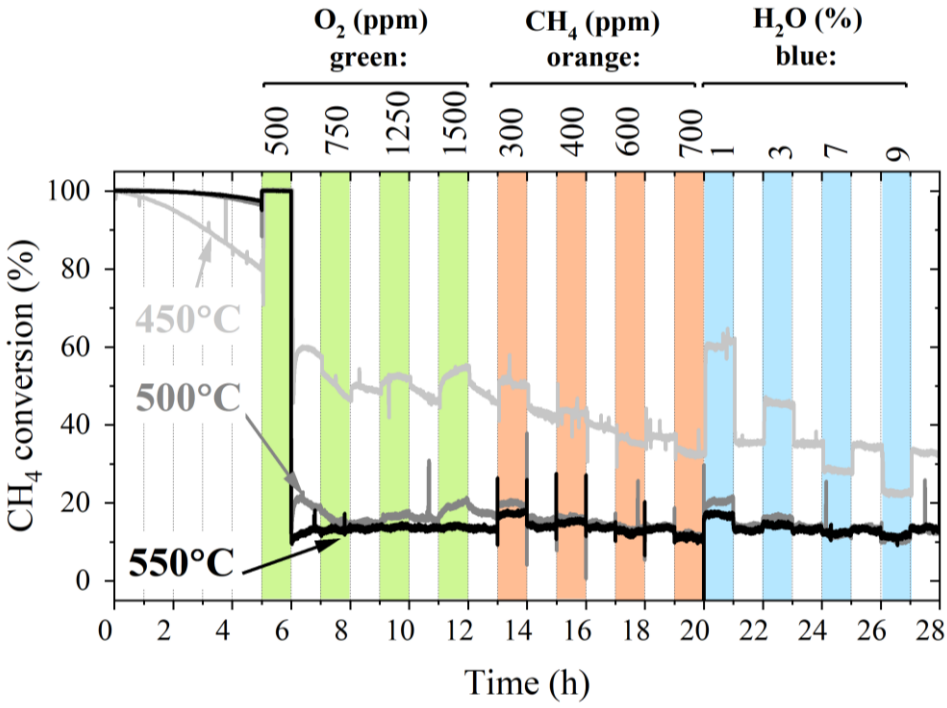

Figure 6.2. Isothermal methane oxidation activity over 3.8 wt.% Pd/Al_2O_3 at 450, 500 and 550°C. White areas represent stoichiometric reaction mixture (500 ppm CH_4, 1000 ppm O_2 and 5 vol.% H_2O) and the colored areas correspond to stoichiometric reaction mixture with the modifications given on top of the figure.

6.2 Stoichiometric methane oxidation in the presence of water vapor and SO_2

Similar isothermal experiments with stepwise modified gas feed were also performed with steps of 10, 25 and 50 ppm SO_2 exposure in the beginning of the sequence. The results of the first sequence including SO_2 exposure are shown in Figure 6.3 and was conducted at 500°C. The general trend was that the higher SO_2 concentration, the faster and severer deactivation was observed. After the execution of all SO_2 containing steps, the remaining CH_4 oxidation activity was no higher than ca. 5% CH_4 conversion. It can also be noted that the detected outlet concentration of SO_2 got higher for each SO_2 step. This is addressed to the higher SO_2 inlet concentration and that the catalyst surface gradually became saturated with surface sulfates resulting in larger SO_2 slip to the exhaust. It is however clear that the addition of SO_2 to the stoichiometric reaction mixture had a strong deactivating effect. It is possible that the co-

exposure of SO_2 and water vapor accelerated the deactivation as the formation of surface hydroxyl influences the spillover of sulfates between the Pd and the Al_2O_3 support [75, 81]. In the subsequent step, the water vapor concentration was changed from 5 vol.% to 1 vol.% which resulted in a CH_4 conversion increase from 13% to 43%. This means that the low activity was caused by both hydroxyls and sulfates on the catalyst surface. When the O_2 and CH_4 concentration was changed in the second half of the experiment, the activity was affected in similar way as reported for the two previous experiment in Figure 6.1 and Figure 6.2.

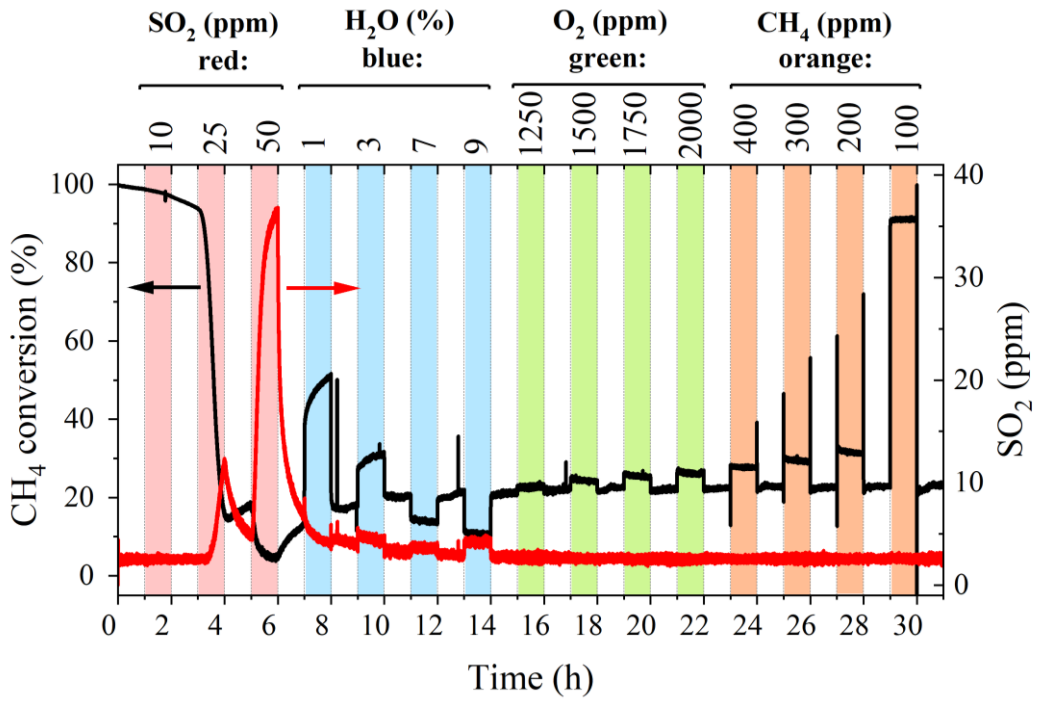

Figure 6.3. Isothermal methane oxidation activity in the presence of SO_2 over 3.8 wt.% Pd/Al_2O_3 at 500°C. White areas represent stoichiometric reaction mixture (500 ppm CH_4, 1000 ppm O_2 and 5 vol.% H_2O) and the colored areas correspond to stoichiometric reaction mixture with the modifications given on top of the figure.

The final isothermal experiment was also conducted at 500°C with SO_2 steps in the beginning of the sequence, hence the procedure was identical during the first 7 hours in Figure 6.3 and Figure 6.4 which yielded very similar results. Thereafter, the O_2 level was decreased from 1000 ppm to 500 ppm in Figure 6.4. This sudden change resulted in increased CH_4 conversion from ca. 10% to ca. 45-70%. By comparison with the results in Figure 6.2, where the similar change resulted in 100% CH_4 conversion, it appears that the presence of sulfates on the catalyst surface inhibited the rate of the steam reforming reaction. The CH_4 conversion decreased again when the O_2 was changed back to the stoichiometric level of 1000 ppm. The activity remained low in the remaining parts of the experiment which probably was a combined effect of hydroxyls and sulfates on the catalyst surface and PdO reduction into metallic Pd during the rich step which was also seen in Figure 6.2. The response to the changes in the CH_4 and O_2 level in the last part of the experiment was mild as the activity already was very low. However, the CH_4 conversion was increased when the water vapor level was changed to 1%. This proves that some of the deactivation was caused by surface hydroxyls.

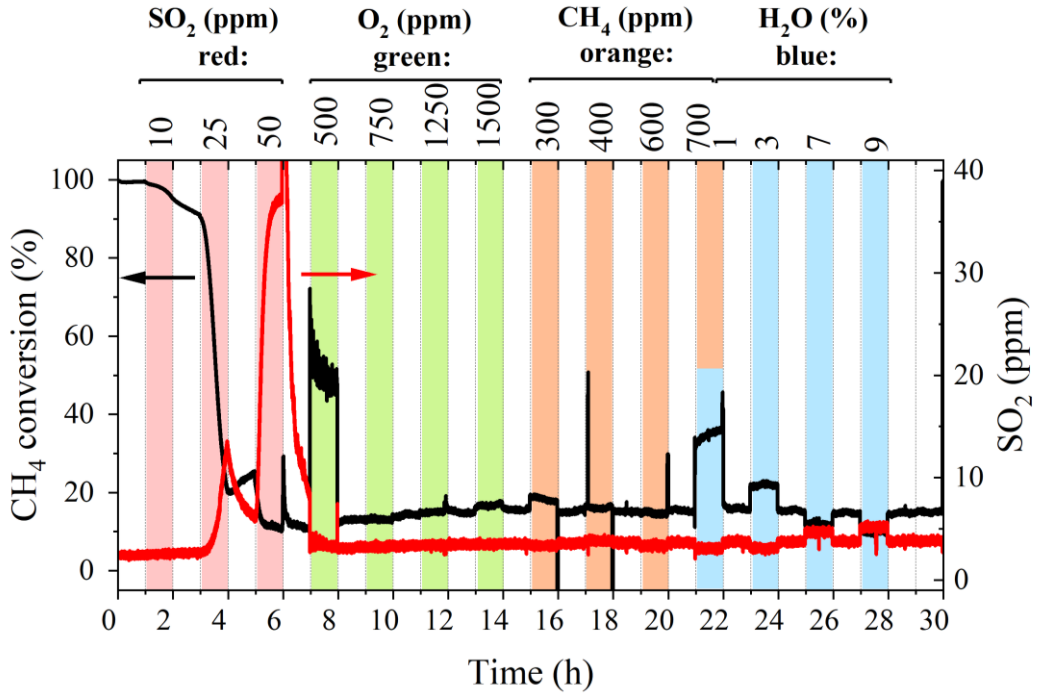

Figure 6.4. Isothermal methane oxidation activity in the presence of SO_2 over 3.8 wt.% Pd/Al_2O_3 at 500°C. White areas represent stoichiometric reaction mixture (500 ppm CH_4, 1000 ppm O_2 and 5 vol.% H_2O) and the colored areas correspond to stoichiometric reaction mixture with the modifications given on top of the figure.

The results presented in Figure 6.1-6.4 show that water vapor and SO_2 cause substantial deactivation also under stoichiometric conditions. Another deactivation mechanism is reduction of active PdO into less active metallic Pd under rich conditions. It is possible that a stoichiometric O_2 level is not high enough to efficiently regenerate the catalytic activity due to poor re-oxidation at the examined temperatures. This is an important aspect for CH_4 combustion with low O_2 levels and in connection with for instance rich regeneration procedures, as occasional re-oxidation in O_2 excess then may be necessary.

7 Concluding remarks

The general objective of this thesis was to fundamentally study how the performance of Pd-based catalysts is influenced by the use of different support materials and by treatment under various thermal and gaseous conditions including exposure to catalyst poisons. The catalytic activity data is supported by detailed characterization in order to understand the underlying factors impacting the catalytic performance.

Paper I-III concerned zeolite supported Pd catalysts which were tested under wet and dry conditions and in the presence of SO_2. A general conclusion from these three studies is that stabilization of dispersed Pd particles on the zeolite supports is crucial for achieving high activity, both under dry and wet conditions. One major deactivation mechanism for Pd/zeolite materials is the formation of ion-exchanged Pd^{2+} species and/or Pd sintering which appears to be facilitated using zeolites with high Al content and large pore size. The conditions the catalyst is being treated under are also important for the Pd speciation. High temperature and presence of water vapor facilitate the formation of Pd^{2+} species and/or Pd sintering. By using highly siliceous zeolites as support material, the formation of monodispersed Pd^{2+} species can be avoided, which is positive for the CH_4 oxidation activity. In addition, the high hydrophobicity of zeolites with low Al content significantly enhances the CH_4 oxidation under wet conditions, which most likely relates to limited hydroxyl formation on the zeolite support. By the comparison of zeolite beta and SSZ-13, it appears that the SAR of the zeolite is more important for maintaining high activity under wet conditions than the type of zeolite framework.

Hydrothermal aging was evaluated for Pd/LTA. Although the performance was excellent when treated at temperatures up to 700°C, severe deactivation was observed after aging at 800-900°C. This deactivation was addressed to the formation of ion-exchanged Pd^{2+} and large Pd particles whereas the structure of the LTA zeolite was well preserved at all tested temperatures (up to 900°C). Deactivating Pd rearrangement appears to be one major challenges for Pd/zeolite materials when treated at high temperatures and in the presence of water vapor.

Compared to Pd/Al_2O_3, zeolite supported Pd becomes more rapidly deactivated by SO_2. The reason for this is less SO_2 adsorption on the zeolite than on the Al_2O_3 support. The use of support materials with high sulfur storage capacity impedes the formation of $PdSO_4$, which is less active

than PdO and suggested to be the main reason for sulfur deactivation. However, it appears that Pd/zeolites can be regenerated more easily after SO_2 poisoning, at least when using highly siliceous zeolites. The reason for this is also the low sulfur storage capacity of zeolites, and thus limited sulfur spill-over from the zeolite support to the Pd and consequently low formation of $PdSO_4$ upon the regeneration.

In **Paper IV**, the catalytic performance of Ba doped Pd/Al_2O_3 was investigated. Based on dry activity data and characterization results, it can be concluded that an addition of up to 2 wt.% Ba to Pd/Al_2O_3 does not provide any electronic promotion of the Pd. However, the Ba doping was shown to mitigate and delay the water deactivation. It was also observed that an addition of Ba to Pd/Al_2O_3 facilitates the regeneration of the catalytic activity after water deactivation. No clear differences in the adsorption/desorption rate of water or in the type of formed surface hydroxyl species could be observed by DRIFTS. However, it should be noted that small differences in hydroxyl formation may be difficult to distinguish with DRIFTS due to the generally high hydroxyl coverage. Nevertheless, the results clearly show that the support material highly impacts the tolerance to water vapor and that this can be improved by an addition of Ba.

Whilst most research concerning CH_4 oxidation catalysts has been performed under lean conditions, **Paper V** focused on stoichiometric CH_4 oxidation over Pd/Al_2O_3. It was concluded that the water deactivation under stoichiometric conditions occurred according to the same two routes as for the lean case, *i.e.* (*i*) immediate deactivation due to rapid OH formation and (*ii*) slow deactivation over time due to OH accumulation on the catalyst surface. In addition, it was demonstrated that SO_2 severely deactivates Pd-based catalysts also under stoichiometric conditions. Treatment under rich conditions at 450-550°C resulted in deactivation which is ascribed to PdO reduction into less active metallic Pd. This deactivation was severer at higher temperatures, due to the more efficient PdO reduction. The activity could not be recovered when the O_2 was reintroduced, which indicates poor Pd re-oxidation under stoichiometric conditions at the examined temperatures. This is an important aspect for the exhaust gas aftertreatment system when engines are operated at low lambda values and it is combined with for instance rich regeneration procedures.

7.1 Outlook

In this thesis it was shown that the support material greatly influences the performance of Pd-based catalysts, either by the type of support material or through the addition of promoters. Hence, there is a great potential in improving CH_4 oxidation catalysts by optimizing the support material. Future CH_4 oxidation catalysts may be based on traditionally used metal oxides or on alternative materials, such as zeolites.

Using metal oxides, such as Al_2O_3, the major challenge is to achieve stable and high activity in the presence of water vapor and SO_2. This remains challenging although it has been the topic of numerous research studies. Examples of strategies to improve the tolerance to catalysts poisons of metal oxide supported Pd are addition of promoters, as shown herein, or by combining different types of metal oxides.

Zeolite-based Pd catalysts are promising candidates for future CH_4 oxidation catalysts, above all due to the possibility to achieve high water vapor tolerance and facilitated regeneration after SO_2 poisoning. One major challenge is to stabilize dispersed Pd particles which appears to be crucial for achieving high activity. This can be done by using highly siliceous zeolites, however, there are most likely other approaches for managing with this as well. Another challenge is to mitigate SO_2 deactivation of Pd/zeolite materials. Based on the results from this thesis, it may be possible to compensate for the high sensitivity to SO_2 by applying efficient SO_2 regeneration procedures since Pd/zeolites appear to be rather easily regenerated after sulfur poisoning. In comparison to Pd/Al_2O_3, zeolite-based Pd catalysts have been much less investigated. More studies are needed in order to fully understand the complexity of Pd/zeolites and considerations must be taken to that different gaseous and thermal conditions may have a high influence on the properties of these materials.

8 References

[1] I. Chorkendorff, J.W. Niemantsverdriet, Concepts of modern catalysis and kinetics, Wiley-VCH Verlag GmbH & Co. KGaA, Weinheim, 2007.
[2] R. van Basshuysen, Natural Gas and Renewable Methane for Powertrains- Future Strategies for a Climate-Neutral Mobility, Springer International Publishing, Switzerland, 2015.
[3] A. Wellinger, J.D. Murphy, D. Baxter, R. Braun, Biogas Handbook : Science, Production and Applications, Elsevier Science & Technology, Cambridge, 2013.
[4] T. Korakianitis, A.M. Namasivayam, R.J. Crookes, Natural-gas fueled spark-ignition (SI) and compression-ignition (CI) engine performance and emissions, Prog. Energy Combust. Sci., 37 (2011) 89-112.
[5] IPCC, 2014: Climate Change 2014: Synthesis Report, Geneva, Switzerland, 2014.
[6] R. Gholami, M. Alyani, K.J. Smith, Deactivation of Pd catalysts by water during low temperature methane oxidation relevant to natural gas vehicle converters, Catal., 5 (2015) 561-594.
[7] J.K. Lampert, M.S. Kazi, R.J. Farrauto, Palladium catalyst performance for methane emissions abatement from lean burn natural gas vehicles, Appl. Catal. B: Environ., 14 (1997) 211-223.
[8] M. Lyubovsky, L. Pfefferle, Methane combustion over the alpha-alumina supported Pd catalyst: Activity of the mixed Pd/PdO state, Appl. Catal. A: Gen., 173 (1998) 107-119.
[9] J. Nilsson, P.A. Carlsson, S. Fouladvand, N.M. Martin, J. Gustafson, M.A. Newton, E. Lundgren, H. Gronbeck, M. Skoglundh, Chemistry of supported palladium nanoparticles during methane oxidation, ASC Catal., 5 (2015) 2481-2489.
[10] S.W. Yang, A. Maroto-Valiente, M. Benito-Gonzalez, I. Rodriguez-Ramos, A. Guerrero-Ruiz, Methane combustion over supported palladium catalysts I. Reactivity and active phase, Appl. Catal. B: Environ., 28 (2000) 223-233.
[11] R. Burch, F.J. Urbano, Investigation of the active state of supported palladium catalysts in the combustion of methane, Appl. Catal. A: Gen., 124 (1995) 121-138.
[12] M. Lyubovsky, L. Pfefferle, Complete methane oxidation over Pd catalyst supported on alpha-alumina. Influence of temperature and oxygen pressure on the catalyst activity, Catal. Today, 47 (1999) 29-44.
[13] N. Sadokhina, G. Smedler, U. Nylén, M. Olofsson, L. Olsson, The influence of gas composition on Pd-based catalyst activity in methane oxidation - inhibition and promotion by NO, Appl. Catal. B: Environ., 200 (2017) 351-360.
[14] O. Mihai, G. Smedler, U. Nylén, M. Olofsson, L. Olsson, The effect of water on methane oxidation over Pd/Al2O3 under lean, stoichiometric and rich conditions, Catal. Sci. Technol., 7 (2017) 3084-3096.

[15] Y.H. Chin, M. Garcia-Dieguez, E. Iglesia, Dynamics and Thermodynamics of Pd-PdO Phase Transitions: Effects of Pd Cluster Size and Kinetic Implications for Catalytic Methane Combustion, J. Phys. Chem. C, 120 (2016) 1446-1460.
[16] J. Fernandez, P. Marin, F.V. Diez, S. Ordonez, Coal mine ventilation air methane combustion in a catalytic reverse flow reactor: Influence of emission humidity, Fuel Process. Technol., 133 (2015) 202-209.
[17] N. Sadokhina, F. Ghasempour, X. Auvray, G. Smedler, U. Nylén, M. Olofsson, L. Olsson, An Experimental and kinetic modelling study for methane oxidation over Pd-based catalyst: Inhibition by water, Catal. Lett., 147 (2017) 2360-2371.
[18] G. Groppi, W. Ibashi, E. Tronconi, P. Forzatti, Structured reactors for kinetic measurements in catalytic combustion, Chem. Eng. J., 82 (2001) 57-71.
[19] G. Groppi, W. Ibashi, M. Valentini, P. Forzatti, High-temperature combustion of CH4 over PdO/Al2O3: kinetic measurements in a structured annular reactor, Chem. Eng. Sci., 56 (2001) 831-839.
[20] P. Hurtado, S. Ordonez, H. Sastre, F.V. Diez, Development of a kinetic model for the oxidation of methane over Pd/Al2O3 at dry and wet conditions, Appl. Catal. B: Environ., 51 (2004) 229-238.
[21] R.E. Hayes, S.T. Kolaczkowski, P.K.C. Li, S. Awdry, The palladium catalysed oxidation of methane: reaction kinetics and the effect of diffusion barriers, Chem. Eng. Sci., 56 (2001) 4815-4835.
[22] S. Specchia, F. Conti, V. Specchia, Kinetic Studies on Pd/CexZr1-xO2 Catalyst for Methane Combustion, Ind. Eng. Chem. Res., 49 (2010) 11101-11111.
[23] R. Burch, M.J. Hayes, C-H bond activation in hydrocarbon oxidation on solid catalysts, J. Mol. Catal. A: Chem., 100 (1995) 13-33.
[24] K. Fujimoto, F.H. Ribeiro, M. Avalos-Borja, E. Iglesia, Structure and reactivity of PdOx/ZrO2, catalysts for methane oxidation at low temperatures, J. Catal., 179 (1998) 431-442.
[25] P. Gelin, M. Primet, Complete oxidation of methane at low temperature over noble metal based catalysts: a review, Appl. Catal. B: Environ., 39 (2002) 1-37.
[26] R. Burch, P.K. Loader, Investigation of Pt/Al2O3 and Pd/Al2O3 catalysts for the combustion of methane at low concentrations, Appl. Catal. B: Environ., 5 (1994) 149-164.
[27] M. Lyubovsky, L.L. Smith, M. Castaldi, H. Karim, B. Nentwick, S. Etemad, R. LaPierre, W.C. Pfefferle, Catalytic combustion over platinum group catalysts: fuel-lean versus fuel-rich operation, Catal. Today, 83 (2003) 71-84.
[28] J.H. Chen, H. Arandiyan, X. Gao, J.H. Li, Recent Advances in Catalysts for Methane Combustion, Catal. Surv. Asia, 19 (2015) 140-171.
[29] K. Narui, H. Yata, K. Furuta, A. Nishida, Y. Kohtoku, T. Matsuzaki, Effects of addition of Pt to PdO/Al2O3 catalyst on catalytic activity for methane combustion and TEM observations of supported particles, Appl. Catal. A: Gen., 179 (1999) 165-173.
[30] K. Persson, K. Jansson, S.G. Jaras, Characterisation and microstructure of Pd and bimetallic Pd-Pt catalysts during methane oxidation, J. Catal., 245 (2007) 401-414.
[31] P. Castellazzi, G. Groppi, P. Forzatti, Effect of Pt/Pd ratio on catalytic activity and redox behavior of bimetallic Pt-Pd/Al2O3 catalysts for CH4 combustion, Appl. Catal. B: Environ., 95 (2010) 303-311.
[32] N.M. Kinnunen, J.T. Hirvi, M. Suvanto, T.A. Pakkanen, Methane combustion activity of Pd-PdOx-Pt/Al2O3 catalyst: The role of platinum promoter, J. Mol. Catal. A: Chem., 356 (2012) 20-28.
[33] G. Lapisardi, L. Urfels, P. Gelin, M. Primet, A. Kaddouri, E. Garbowski, S. Toppi, E. Tena, Superior catalytic behaviour of Pt-doped Pd catalysts in the complete oxidation of methane at low temperature, Catal. Today, 117 (2006) 564-568.

[34] R. Strobel, J.D. Grunwaldt, A. Camenzind, S.E. Pratsinis, A. Baiker, Flame-made alumina supported Pd-Pt nanoparticles: Structural properties and catalytic behavior in methane combustion, Catal. Lett., 104 (2005) 9-16.
[35] H. Yamamoto, H. Uchida, Oxidation of methane over Pt and Pd supported on alumina in lean-burn natural-gas engine exhaust, Catal. Today, 45 (1998) 147-151.
[36] N. Sadokhina, G. Smedler, U. Nylén, M. Olofsson, L. Olsson, Deceleration of SO2 poisoning on PtPd/Al2O3 catalyst during complete methane oxidation, Appl. Catal. B: Environ., 236 (2018) 384-395.
[37] D. Ciuparu, M.R. Lyubovsky, E. Altman, L.D. Pfefferle, A. Datye, Catalytic combustion of methane over palladium-based catalysts, Catal. Rev.-Sci. Eng., 44 (2002) 593-649.
[38] T.V. Choudhary, S. Banerjee, V.R. Choudhary, Catalysts for combustion of methane and lower alkanes, Appl. Catal. A: Gen., 234 (2002) 1-23.
[39] H. Arai, M. Machida, Thermal stabilization of catalyst supports and their application to high-temperature catalytic combustion, Appl. Catal. A: Gen., 138 (1996) 161-176.
[40] Y. Yazawa, H. Yoshida, N. Takagi, S. Komai, A. Satsuma, T. Hattori, Acid strength of support materials as a factor controlling oxidation state of palladium catalyst for propane combustion, J. Catal., 187 (1999) 15-23.
[41] H. Yoshida, T. Nakajima, Y. Yazawa, T. Hattori, Support effect on methane combustion over palladium catalysts, Appl. Catal. B: Environ., 71 (2007) 70-79.
[42] S. Kulprathipanja, Zeolites in Industrial Separation and Catalysis, Wiley-VCH Verlag GmbH & Co. KGaA, Weinheim, 2010.
[43] R.W. Broach, D.Y. Jan, D.A. Lesch, S. Kulprathipanja, E. Roland, P. Kleinschmit, Zeolites, Ullmann's Encyclopedia of Industrial Chemistry, Wiley-VCH Verlag GmbH & Co. KGaA 2012.
[44] K. Okumura, E. Shinohara, M. Niwa, Pd loaded on high silica beta support active for the total oxidation of diluted methane in the presence of water vapor, Catal. Today, 117 (2006) 577-583.
[45] J. Lee, Y. Ryou, S.J. Cho, H. Lee, C.H. Kim, D.H. Kim, Investigation of the active sites and optimum Pd/Al of Pd/ZSM-5 passive NO adsorbers for the cold-start application: Evidence of isolated-Pd species obtained after a high-temperature thermal treatment, Appl. Catal. B: Environ., 226 (2018) 71-82.
[46] H.K. Beyer, Dealumination Techniques for Zeolites, Molecular Sieves, 3 (2002) 203-255.
[47] M. Bjorgen, S. Kolboe, The conversion of methanol to hydrocarbons over dealuminated zeolite H-beta, Appl. Catal. A: Gen., 225 (2002) 285-290.
[48] M.R. Apelian, A.S. Fung, G.J. Kennedy, T.F. Degnan, Dealumination of zeolite beta via dicarboxylic acid treatment, J. Phys. Chem., 100 (1996) 16577-16583.
[49] S. Krijnen, P. Sanchez, B.T.F. Jakobs, J.H.C. van Hooff, A controlled post-synthesis route to well-defined and active titanium Beta epoxidation catalysts, Microporous Mesoporous Mat., 31 (1999) 163-173.
[50] M. Muller, G. Harvey, R. Prins, Comparison of the dealumination of zeolites beta, mordenite, ZSM-5 and ferrierite by thermal treatment, leaching with oxalic acid and treatment with SiCl4 by H-1, Si-29 and Al-27 MAS NMR, Microporous Mesoporous Mat., 34 (2000) 135-147.
[51] D.M. Roberge, H. Hausmann, W.F. Holderich, Dealumination of zeolite beta by acid leaching: a new insight with two-dimensional multi-quantum and cross polarization Al-27 MAS NMR, Phys. Chem. Chem. Phys., 4 (2002) 3128-3135.
[52] R. Srivastava, N. Iwasa, S. Fujita, M. Arai, Dealumination of Zeolite Beta Catalyst Under Controlled Conditions for Enhancing its Activity in Acylation and Esterification, Catal. Lett., 130 (2009) 655-663.

[53] C.G. Vayenas, S. Bebelis, C. Pilangos, S. Brosda, D. Tsiplakides, Electrochemical activation of catalysis: Promotion, electrochemical promotion, and metal-support interactions, Kluwer Academic/Plenum Publishers, New York, 2001.
[54] P. Panagiotopoulou, D.I. Kondarides, Effects of alkali additives on the physicochemical characteristics and chemisorptive properties of Pt/TiO(2) catalysts, J. Catal., 260 (2008) 141-149.
[55] J. Benziger, R.J. Madix, The effects of carbon, oxygen, sulfur and potassium adlayers on CO and H2 adsorption on Fe(100), Surf. Sci., 94 (1980) 119-153.
[56] D. Heskett, The interaction range in alkali metal-promoted systems, Surf. Sci., 199 (1988) 67-86.
[57] E.L. Garfunkel, J.E. Crowell, G.A. Somorjai, The strong influence of potassium on the adsorption of CO on platinum surfaces. A thermal desorption spectroscopy and high-resolution electron energy loss spectroscopy study, J. Phys. Chem., 86 (1982) 310-313.
[58] A. de Lucas-Consuegra, New Trends of Alkali Promotion in Heterogeneous Catalysis: Electrochemical Promotion with Alkaline Ionic Conductors, Catal. Surv. Asia, 19 (2015) 25-37.
[59] H. Shinjoh, N. Isomura, H. Sobukawa, M. Sugiura, Effect of alkaline addition on hydrocarbon oxidation activities of palladium three-way catalyst, Stud. Surf. Sci. Catal., 116 (1998) 83-91.
[60] P.O. Thevenin, E. Pocoroba, L.J. Pettersson, H. Karhu, I.J. Vayrynen, S.G. Jaras, Characterization and activity of supported palladium combustion catalysts, J. Catal., 207 (2002) 139-149.
[61] X.Y. Zhang, E.Y. Long, Y.L. Li, L.J. Zhang, J.X. Guo, M.C. Gong, Y.Q. Chen, The effect of CeO2 and BaO on Pd catalysts used for lean-burn natural gas vehicles, J. Mol. Catal. A: Chem., 308 (2009) 73-78.
[62] B. Mirkelamoglu, G. Karakas, The role of alkali-metal promotion on CO oxidation over PdO/SnO2 catalysts, Appl. Catal. A: Gen., 299 (2006) 84-94.
[63] B.H. Yue, R.X. Zhou, X.M. Zheng, W.C. Lu, Promotional effect of Ca on the Pd/Ce-Zr/Al2O3 catalyst for low-temperature catalytic combustion of methane, Fuel Process. Technol., 89 (2008) 728-735.
[64] C.H. Bartholomew, Mechanisms of catalyst deactivation, Appl. Catal. A: Gen., 212 (2001) 17-60.
[65] R. Burch, F.J. Urbano, P.K. Loader, Methane combustion over palladium catalysts: The effect of carbon dioxide and water on activity, Appl. Catal. A: Gen., 123 (1995) 173-184.
[66] W.R. Schwartz, L.D. Pfefferle, Combustion of methane over palladium-based catalysts: Support interactions, J. Phys. Chem. C, 116 (2012) 8571-8578.
[67] W.R. Schwartz, D. Ciuparu, L.D. Pfefferle, Combustion of methane over palladium-based catalysts: Catalytic deactivation and role of the support, J. Phys. Chem. C, 116 (2012) 8587-8593.
[68] D. Roth, P. Gelin, M. Primet, E. Tena, Catalytic behaviour of Cl-free and Cl-containing Pd/Al2O3 catalysts in the total oxidation of methane at low temperature, Appl. Catal. A: Gen., 203 (2000) 37-45.
[69] K. Persson, L.D. Pfefferle, W. Schwartz, A. Ersson, S.G. Jaras, Stability of palladium-based catalysts during catalytic combustion of methane: The influence of water, Appl. Catal. B: Environ., 74 (2007) 242-250.
[70] M. Monai, T. Montini, C. Chen, E. Fonda, R.J. Gorte, P. Fornasiero, Methane Catalytic Combustion over Hierarchical Pd@CeO2/Si-Al2O3: Effect of the Presence of Water, ChemCatChem, 7 (2015) 2038-2046.

[71] P. Velin, M. Ek, M. Skoglundh, A. Schaefer, A. Raj, D. Thompsett, G. Smedler, P.-A. Carlsson, Water Inhibition in Methane Oxidation over Alumina Supported Palladium Catalysts, J. Phys. Chem. C, 123 (2019) 25724-25737.
[72] A.W. Petrov, D. Ferri, O. Kröcher, J.A. van Bokhoven, Design of Stable Palladium-Based Zeolite Catalysts for Complete Methane Oxidation by Postsynthesis Zeolite Modification, ASC Catal., 9 (2019) 2303-2312.
[73] A.W. Petrov, D. Ferri, F. Krumeich, M. Nachtegaal, J.A. van Bokhoven, O. Kröcher, Stable complete methane oxidation over palladium based zeolite catalysts, Nat. Commun., 9 (2018) 2545.
[74] F. Arosio, S. Colussi, G. Groppi, A. Trovarelli, Regeneration of S-poisoned Pd/Al2O3 catalysts for the combustion of methane, Catal. Today, 117 (2006) 569-576.
[75] D.L. Mowery, R.L. McCormick, Deactivation of alumina supported and unsupported PdO methane oxidation catalyst: the effect of water on sulfate poisoning, Appl. Catal. B: Environ., 34 (2001) 287-297.
[76] S. Ordonez, P. Hurtado, H. Sastre, F.V. Diez, Methane catalytic combustion over Pd/Al2O3 in presence of sulphur dioxide: development of a deactivation model, Appl. Catal. A: Gen., 259 (2004) 41-48.
[77] P. Gelin, L. Urfels, M. Primet, E. Tena, Complete oxidation of methane at low temperature over Pt and Pd catalysts for the abatement of lean-burn natural gas fuelled vehicles emissions: influence of water and sulphur containing compounds, Catal. Today, 83 (2003) 45-57.
[78] P. Hurtado, S. Ordonez, H. Sastre, F.V. Diez, Combustion of methane over palladium catalyst in the presence of inorganic compounds: inhibition and deactivation phenomena, Appl. Catal. B: Environ., 47 (2004) 85-93.
[79] L.J. Hoyos, H. Praliaud, M. Primet, Catalytic combustion of methane over palladium supported on alumina and silica in presence of hydrogen-sulfide, Appl. Catal. A: Gen., 98 (1993) 125-138.
[80] M. Honkanen, J.G. Wang, M. Karkkainen, M. Huuhtanen, H. Jiang, K. Kallinen, R.L. Keiski, J. Akola, M. Vippola, Regeneration of sulfur-poisoned Pd-based catalyst for natural gas oxidation, J. Catal., 358 (2018) 253-265.
[81] D.L. Mowery, M.S. Graboski, T.R. Ohno, R.L. McCormick, Deactivation of PdO-Al2O3 oxidation catalyst in lean-burn natural gas engine exhaust: aged catalyst characterization and studies of poisoning by H2O and SO2, Appl. Catal. B: Environ., 21 (1999) 157-169.
[82] Y. Ryou, J. Lee, S.J. Cho, H. Lee, C.H. Kim, D.H. Kim, Activation of Pd/SSZ-13 catalyst by hydrothermal aging treatment in passive NO adsorption performance at low temperature for cold start application, Appl. Catal. B: Environ., 212 (2017) 140-149.
[83] J. Lee, Y. Ryou, S. Hwang, Y. Kim, S.J. Cho, H. Lee, C.H. Kim, D.H. Kim, Comparative study of the mobility of Pd species in SSZ-13 and ZSM-5, and its implication for their activity as passive NOx adsorbers (PNAs) after hydro-thermal aging, Catal. Sci. Technol., 9 (2019) 163-173.
[84] K. Leistner, A. Kumar, K. Kamasamudram, L. Olsson, Mechanistic study of hydrothermally aged Cu/SSZ-13 catalysts for ammonia-SCR, Catal. Today, 307 (2018) 55-64.
[85] J.H. Kwak, D. Tran, S.D. Burton, J. Szanyi, J.H. Lee, C.H.F. Peden, Effects of hydrothermal aging on NH3-SCR reaction over Cu/zeolites, J. Catal., 287 (2012) 203-209.
[86] A.Y. Wang, P. Arora, D. Bernin, A. Kumar, K. Kamasamudram, L. Olsson, Investigation of the robust hydrothermal stability of Cu/LTA for NH3-SCR reaction, Appl. Catal. B: Environ., 246 (2019) 242-253.
[87] T. Ryu, N.H. Ahn, S. Seo, J. Cho, H. Kim, D. Jo, G.T. Park, P.S. Kim, C.H. Kim, E.L. Bruce, P.A. Wright, I.S. Nam, S.B. Hong, Fully Copper-Exchanged High-Silica LTA Zeolites as Unrivaled Hydrothermally Stable NH3-SCR Catalysts, Angew. Chem.-Int. Edit., 56 (2017) 3256-3260.

[88] J.S. McEwen, T. Anggara, W.F. Schneider, V.F. Kispersky, J.T. Miller, W.N. Delgass, F.H. Ribeiro, Integrated operando X-ray absorption and DFT characterization of Cu-SSZ-13 exchange sites during the selective catalytic reduction of NOx with NH3, Catal. Today, 184 (2012) 129-144.
[89] L. Olsson, K. Wijayanti, K. Leistner, A. Kumar, S.Y. Joshi, K. Kamasamudram, N.W. Currier, A. Yezerets, A multi-site kinetic model for NH3-SCR over Cu/SSZ-13, Appl. Catal. B: Environ., 174 (2015) 212-224.
[90] S. Brunauer, P.H. Emmett, E. Teller, Adsorption of gases in multimolecular layers, J. Am. Chem. Soc., 60 (1938) 309-319.
[91] G. Leofanti, M. Padovan, G. Tozzola, B. Venturelli, Surface area and pore texture of catalysts, Catal. Today, 41 (1998) 207-219.
[92] M. Beller, A. Renken, R.A. van Santen, Catalysis, Wiley-VCH Verlag & Co. KGaA, Weinheim, 2012.
[93] K. Leistner, K.P. Xie, A. Kumar, K. Kamasamudram, L. Olsson, Ammonia Desorption Peaks Can Be Assigned to Different Copper Sites in Cu/SSZ-13, Catal. Lett., 147 (2017) 1882-1890.
[94] N.-Y. Topsøe, K. Pedersen, E.G. Derouane, Infrared and temperature-programmed desorption study of the acidic properties of ZSM-5-type zeolites, J. Catal., 70 (1981) 41-52.
[95] F. Lónyi, J. Valyon, On the interpretation of the NH3-TPD patterns of H-ZSM-5 and H-mordenite, Microporous Mesoporous Mat., 47 (2001) 293-301.
[96] M. Ogura, M. Hayashi, S. Kage, M. Matsukata, E. Kikuchi, Determination of active palladium species in ZSM-5 zeolite for selective reduction of nitric oxide with methane, Appl. Catal. B: Environ., 23 (1999) 247-257.
[97] D.B. Williams, C.B. Carter, Transmission Electron Microscopy, Springer Science+ Business Media, New York, 2009.
[98] P. van der Heide, X-ray photoelectron spectroscopy An introduction to principles and practices, John Wiley & Sons, Inc., New Jersey, 2012.
[99] C. Suryanarayana, M. Grant Norton, X-Ray Diffraction A Practical Approach, Springer Science + Business Media, New York, 1998.
[100] B. Imelik, J.C. Vedrine, Catalyst Characterization, Physical Techniques for Solid Materials, Springer Science+ Business Media, New York, 1994.
[101] J. Bokhoven, C. Lamberti, X-Ray Absorption and X-Ray, Emission Spectroscopy, Theory and Applications, John Wiley & Sons, Ltd., Chichester, 2016.
[102] S. Calvin, XAFS for Everyone, Taylor & Francis Group, New York, 2013.
[103] O. Muller, M. Nachtegaal, J. Just, D. Lutzenkirchen-Hecht, R. Frahm, Quick-EXAFS setup at the SuperXAS beamline for in situ X-ray absorption spectroscopy with 10 ms time resolution, J. Synchrot. Radiat., 23 (2016) 260-266.
[104] A.H. Clark, J. Imbao, R. Frahm, M. Nachtegaal, ProQEXAFS: a highly optimized parallelized rapid processing software for QEXAFS data, J. Synchrot. Radiat., 27 (2020).
[105] B. Ravel, M. Newville, ATHENA, ARTEMIS, HEPHAESTUS: data analysis for X-ray absorption spectroscopy using IFEFFIT, J. Synchrot. Radiat., 12 (2005) 537-541.
[106] G.L. Chiarello, M. Nachtegaal, V. Marchionni, L. Quaroni, D. Ferri, Adding diffuse reflectance infrared Fourier transform spectroscopy capability to extended x-ray-absorption fine structure in a new cell to study solid catalysts in combination with a modulation approach, Rev. Sci. Instrum., 85 (2014) 11.
[107] E. de Hoffmann, V. Stroobant, Mass Spectrometry : Principles and Applications, John Wiley & Sons Ltd., Chichester, 2007.
[108] J.B. Lim, D. Jo, S.B. Hong, Palladium-exchanged small-pore zeolites with different cage systems as methane combustion catalysts, Appl. Catal. B: Environ., 219 (2017) 155-162.

[109] Y. Zheng, L. Kovarik, M.H. Engelhard, Y. Wang, Y. Wang, F. Gao, J. Szanyi, Low-Temperature Pd/Zeolite Passive NOx Adsorbers: Structure, Performance, and Adsorption Chemistry, J. Phys. Chem. C, 121 (2017) 15793-15803.
[110] O. Mihai, L. Trandafilovic, T. Wentworth, F.F. Torres, L. Olsson, The Effect of Si/Al Ratio for Pd/BEA and Pd/SSZ-13 Used as Passive NOx Adsorbers, Top. Catal., 61 (2018) 2007-2020.
[111] K. Okumura, M. Niwa, Control of the dispersion of Pd through the interaction with acid sites of zeolite studied by EXAFS, Top. Catal., 18 (2002) 85-89.
[112] K. Okumura, M. Niwa, Regulation of the dispersion of PdO through the interaction with acid sites of zeolite studied by extended X-ray absorption fine structure, J. Phys. Chem. B, 104 (2000) 9670-9675.
[113] K. Khivantsev, N.R. Jaegers, L. Kovarik, J.C. Hanson, F. Tao, Y. Tang, X.Y. Zhang, I.Z. Koleva, H.A. Aleksandrov, G.N. Vayssilov, Y. Wang, F. Gao, J. Szanyi, Achieving Atomic Dispersion of Highly Loaded Transition Metals in Small-Pore Zeolite SSZ-13: High-Capacity and High-Efficiency Low-Temperature CO and Passive NOx Adsorbers, Angew. Chem.-Int. Edit., 57 (2018) 16672-16677.
[114] B.J. Adelman, W.M.H. Sachtler, The effect of zeolitic protons on NOx reduction over Pd/ZSM-5 catalysts, Appl. Catal. B: Environ., 14 (1997) 1-11.
[115] K. Chakarova, E. Ivanova, K. Hadjiivanov, D. Klissurski, H. Knozinger, Co-ordination chemistry of palladium cations in Pd-H-ZSM-5 as revealed by FTIR spectra of adsorbed and co-adsorbed probe molecules (CO and NO), Phys. Chem. Chem. Phys., 6 (2004) 3702-3709.
[116] H.Y. Chen, J.E. Collier, D.X. Liu, L. Mantarosie, D. Duran-Martin, V. Novak, R.R. Rajaram, D. Thompsett, Low Temperature NO Storage of Zeolite Supported Pd for Low Temperature Diesel Engine Emission Control, Catal. Lett., 146 (2016) 1706-1711.
[117] F. Lonyi, H.E. Solt, J. Valyon, H. Decolatti, L.B. Gutierrez, E. Miro, An operando DRIFTS study of the active sites and the active intermediates of the NO-SCR reaction by methane over In,H- and In,Pd,H-zeolite catalysts, Appl. Catal. B: Environ., 100 (2010) 133-142.
[118] B. Pommier, P. Gelin, On the nature of Pd species formed upon exchange of H-ZSM5 with Pd(NH3)(4)(2+) and calcination in O-2, Phys. Chem. Chem. Phys., 1 (1999) 1665-1672.
[119] J.M. Watson, U.S. Ozkan, Adsorption characteristics of sol-gel Gd-Pd/TiO2 catalysts in reduction of nitric oxide with CH4: DRIFTS and TPD, J. Catal., 210 (2002) 295-312.
[120] Z.K. Zhang, L.Y. Xu, Z.L. Wang, Y.J. Xu, Y.F. Chen, Pd/H beta-zeolite catalysts for catalytic combustion of toluene: Effect of SiO2/Al2O3 ratio, J. Nat. Gas Chem., 19 (2010) 417-421.
[121] R. Roldan, A.M. Beale, M. Sanchez-Sanchez, F.J. Romero-Salguero, C. Jimenez-Sanchidrian, J.P. Gomez, G. Sankar, Effect of the impregnation order on the nature of metal particles of bi-functional Pt/Pd-supported zeolite Beta materials and on their catalytic activity for the hydroisomerization of alkanes, J. Catal., 254 (2008) 12-26.
[122] J.N. Carstens, S.C. Su, A.T. Bell, Factors affecting the catalytic activity of Pd/ZrO2 for the combustion of methane, J. Catal., 176 (1998) 136-142.
[123] M.V.d. Bossche, H. Grönbeck, Methane Oxidation over PdO(101) Revealed by First-Principles Kinetic Modeling, J. Am. Chem. Soc., 137 (2015) 12035-12044.
[124] C.A. Muller, M. Maciejewski, R.A. Koeppel, R. Tschan, A. Baiker, Role of lattice oxygen in the combustion of methane over PdO/ZrO2: Combined pulse TG/DTA and MS study with O-18-labeled catalyst, J. Phys. Chem., 100 (1996) 20006-20014.
[125] C.A. Muller, M. Maciejewski, R.A. Koeppel, A. Baiker, Combustion of methane over palladium/zirconia: effect of Pd-particle size and role of lattice oxygen, Catal. Today, 47 (1999) 245-252.

[126] R.F. Hicks, H.H. Qi, M.L. Young, R.G. Lee, Structure sensitivity of methane oxidation over platinum and palladium, J. Catal., 122 (1990) 280-294.
[127] A. Ali, W. Alvarez, C.J. Loughran, D.E. Resasco, State of Pd on H-ZSM-5 and other acidic supports during the selective reduction of NO by CH4 studied by EXAFS/XANES, Appl. Catal. B: Environ., 14 (1997) 13-22.
[128] X. Auvray, A. Lindholm, M. Miroslawa, L. Olsson, The addition of alkali and alkaline earth metals to Pd/Al2O3 to promote methane combustion. Effect of Pd and Ca loading, Catal. Today, (2017).
[129] K. Otto, L.P. Haack, J.E. Devries, Identification of two types of oxidized palladium on gamma-alumina by X-ray photoelectron spectroscopy, Appl. Catal. B: Environ., 1 (1992) 1-12.
[130] R.J. Bird, P. Swift, Energy calibration in electron spectroscopy and the re-determination of some reference electron binding energies, J. Electron Spectrosc. Relat. Phenom., 21 (1980) 227-240.
[131] D.H. Kim, S.I. Woo, J.M. Lee, O.B. Yang, The role of lanthanum oxide on Pd-only three-way catalysts prepared by co-impregnation and sequential impregnation methods, Catal. Lett., 70 (2000) 35-41.
[132] F. Klingstedt, H. Karhu, A.K. Neyestanaki, L.E. Lindfors, T. Salmi, J. Vayrynen, Barium promoted palladium catalysts for the emission control of natural gas driven vehicles and biofuel combustion systems, J. Catal., 206 (2002) 248-262.
[133] D.N. Gao, S. Wang, C.X. Zhang, Z.S. Yuan, S.D. Wang, Methane Combustion over Pd/Al2O3 Catalyst: Effects of Chlorine Ions and Water on Catalytic Activity, Chin. J. Catal., 29 (2008) 1221-1225.
[134] D. Ciuparu, E. Perkins, L. Pfefferle, In situ DR-FTIR investigation of surface hydroxyls on gamma-Al2O3 supported PdO catalysts during methane combustion, Appl. Catal. A: Gen., 263 (2004) 145-153.
[135] A. Gremminger, J. Pihl, M. Casapu, J.-D. Grunwaldt, T.J. Toops, O. Deutschmann, PGM based catalysts for exhaust-gas after-treatment under typical diesel, gasoline and gas engine conditions with focus on methane and formaldehyde oxidation, Appl. Catal. B: Environ., 265 (2020) 118571-118581.
[136] S.K. Matam, G.L. Chiarello, Y. Lu, A. Weidenkaff, D. Ferri, PdOx/Pd at Work in a Model Three-Way Catalyst for Methane Abatement Monitored by Operando XANES, Top. Catal., 56 (2013) 239-242.
[137] S.K. Matam, M.H. Aguirre, A. Weidenkaff, D. Ferri, Revisiting the Problem of Active Sites for Methane Combustion on Pd/Al2O3 by Operando XANES in a Lab-Scale Fixed-Bed Reactor, J. Phys. Chem. C, 114 (2010) 9439-9443.